Preface

From March 22 through 27, 2004, again one of the traditional Workshops on Nuclear Astrophysics was held at the Ringberg Castle near Munich. This year's workshop, the twelfth in a series which began in May 1981, was a very special one, as the workshop was also organized to honor Wolfgang Hillebrandt on the occasion of his 60's birthday. Therefore for the first time in the series the workshop program also included 10 invited talks by renowned colleagues of Wolfgang, highlighting his scientific interests and achievements in nuclear and stellar astrophysics since the early beginnings in Darmstadt in the 1970's.

Because of the special occasion the workshop was attended by an unusally large number of 55 participants from 12 countries plus many additional participants from the Munich area attending on a day-by-day basis. This large crowd could just barely be handled by the seating and dining facilities at the Ringberg Castle, and 10 participants had to be accommodated in a hotel in Rottach-Egern.

The workshop program was somewhat more weighted towards astrophysics, but according to the good tradition of the workshop series also consisted of several talks on theoretical and experimental developments in nuclear physics relevant to nuclear astrophysics. Continuing another good tradition of the series, again several students had an opportunity to present, for the fist time, their work to an international audience in a benevolently and friendly atmosphere. The talks often stimulated intense discussions, and the relaxed atmosphere of the Castle together with ample time for discussions between the sessions provided optimum conditions for a successful workshop.

Concerning the weather the workshop was also a very special one, as snowfall lasting from Monday afternoon to Friday night turned the Castle and the surrounding landscape into a winter fairyland. After a couple of days the cars on the parking lot of the Castle were covered by about three feet of snow. The extreme weather conditions also caused a severe accident on late Friday afternoon when the MPA bus seated with seven participants and driven by Ewald Müller came off the road and made a full 360 degree overturn into a small creek besides the road. Fortunately nobody was seriously injured, but the bus had to be scrapped.

The following Proceedings (an electronic version with colour figures is available at `www.mpa-garching.mpg.de/mpa/publications/proceedings`) contain a collection of extended abstracts of most of the contributions which were presented at the Twelfth Nuclear Astrophysics workshop. PDF files of the talks of several participants are posted on the workshop webpage (`www.mpa-garching.mpg.de/hydro/NucAstro/final-prog.html`).

The success of the workshop, of course, also depended on the financial support by the Max-Planck-Gesellschaft via the Dr. Ernst Rudolf Schloesmann foundation and, needless to say, on the enormous efficiency and friendliness of Mr. Hörmann and his crew.

Garching, August 2004

Ewald Müller H.-Thomas Janka

Figure 1: Wolfgang testing his new toy; for his observations he, of course, uses much larger instruments.

Figure 2: Wolfgang at work!

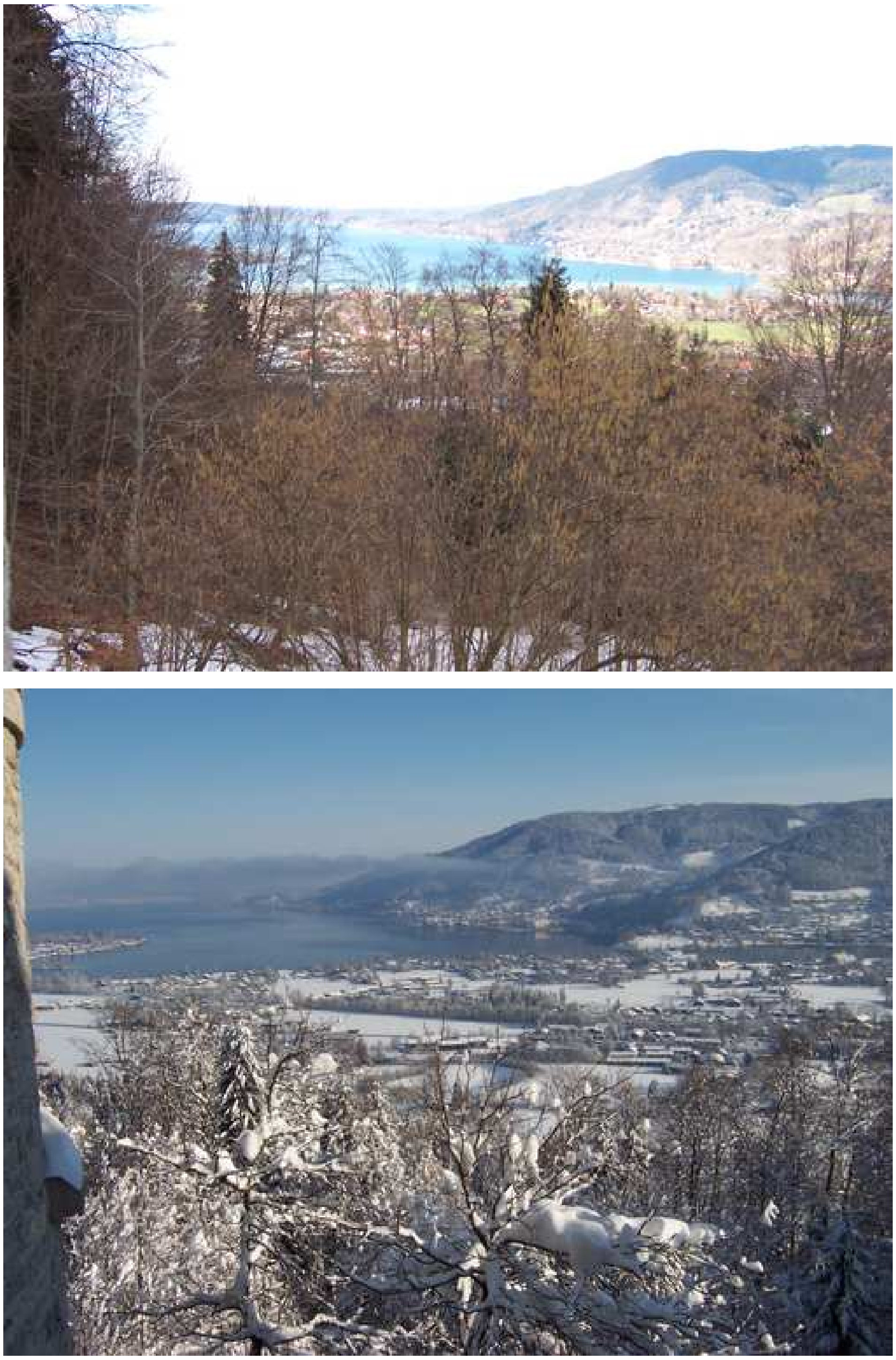

Figure 3: View to lake Tegernsee on Monday afternoon (top) and on Saturday morning after five days of snow fall (bottom).

Figure 4: Snow, snow, and more snow!

Acknowledgement: The photos were kindly provided by John Cowan; check his homepage `www.nhn.ou.edu/~cowan` for more snapshots.

List of participants	**Institute**
Carlos Abia	Universidad de Granada
Jean Audouze	Institute d'Astrophysique, Paris
Isabelle Baraffe	Ecole Normale Superieure, Lyon
Edward Brown	Michigan State University
Adam Burrows	University of Arizona, Tucson
Alan Calder	University of Cicago
Ramon Canal	University of Barcelona
Gilles Chabrier	Ecole Normale Superieure, Lyon
Cesare Chiosi	University of Padua, I
John Cowan	University of Oklahoma, Norman
Roland Diehl	MPE, Garching
Mounib ElEid	American University, Beirut
Roberto Gallino	University of Turino
Joachim Goerres	University of Notre Dame
Dieter Hartmann	Clemson University
Alexander Heger	Los Alamos National Laboratory
Michael Heil	Forschungszentrum Karlsruhe
Ebs Hilf	Universität Oldenburg
Wolfgang Hillebrandt	MPA Garching
Luigi Iapichino	MPA Garching
Inese Ivans	CALTEC, Pasadena
Thomas Janka	MPA Garching
Jordi Jose	IEEC-CSIC, Barcelona
Konstantinos Kifonidis	MPA Garching
Gunther Korschinek	TU München
Kei Kotake	University of Tokyo
Karl-Ludwig Kratz	Universität Mainz
Karlheinz Langanke	University of Aarhus
Norbert Langer	University of Utrecht
Jim Lattimer	University of New York, Stony Brook
Bruno Leibundgut	ESO Garching
Matthias Liebendoerfer	CITA, Toronto

List of participants	**Institute**
Gabriel Martinez-Pinedo	IEEC-CSIC, Barcelona
Akira Mizuta	Osaka University
Ewald Mueller	MPA Garching
Dimitrij Nadyozhin	ITEP, Moskow
Jens Niemeyer	Universität Würzburg
Kenichi Nomoto	University of Tokyo
Igor Panov	ITEP, Moskow
Francesca Primas	ESO Garching
Georg Raffelt	MPI f. Physik, München
Rene Reifarth	Los Alamos National Laboratory
Martin Reinecke	MPA Garching
Fritz Roepke	MPA Garching
Pilar Ruiz Lapuente	University of Barcelona
Katsuhiko Sato	University of Tokyo
Leonhard Scheck	MPA Garching
Wolfram Schmidt	MPA Garching
Matthias Steinmetz	Astrophys. Inst. Potsdam
Norbert Straumann	Universitẗ Zürich
Friedel Thielemann	Universität Basel
Claudia Travaglio	Osserv. Astronomico di Torino
Jim Truran	University of Cicago
Achim Weiss	MPA Garching
Stan Woosley	University of California, Santa Cruz

Contents

Presentations available as PDF files at

www.mpa-garching.mpg.de/hydro/NucAstro/final-prog.html

Flavor oscillations of SN neutrinos
Georg Raffelt

The role of the exclusion principle for atoms to stars: a historical account
Norbert Straumann

Type Ia supernova modeling
Stan Woosley

A neutron source for activation measurements in a stellar spectrum close to $kT = 8\,\mathbf{keV}$

M. Heil[1], *S. Dababneh*[1], *F. Käppeler*[1], *R. Plag*[1], *A. Juseviciute*[1], *R. Reifarth*[2], *S. O'Brien*[3]

[1] Forschungszentrum Karlsruhe, Institut für Kernphysik, Postfach 3640, D-76021 Karlsruhe, Germany
[2] Los Alamos National Laboratory, Los Alamos, New Mexico, 87545, USA
[3] University of Notre Dame, Physics Department, Notre Dame, IN 46556, USA

Introduction

Activation measurements with the ^{7}Li(p,n)^{8}Be reaction [1] as a neutron source have been successfully used to determine Maxwellian averaged neutron capture cross sections (MACS) corresponding to a thermal energy of kT = 25 keV. The superior sensitivity of this method compared to time of flight (TOF) experiments allowed to measure extremely small cross sections or to perform measurements, where the sample mass is limited to a few nanograms [2]. The classical model of the s process, assuming a constant temperature and an exponential neutron exposure, fits the observed abundance distribution best with kT = 29 keV, or T_8 = 3.3 K [3]. Experimental values obtained at kT = 25 keV could easily be extrapolated to the desired value of kT = 29 keV. Present stellar models [4] suggest that the main component of the s process takes place in TP-AGB stars at temperatures of kT = 8 keV and kT = 25 keV where the neutrons are produced via ^{13}C(α,n)^{16}O and ^{22}Ne(α,n)^{25}Mg reactions, respectively. An extrapolation of the measured values at kT = 25 keV down to kT = 8 keV is in principle possible but requires assumptions on the energy dependence of the capture cross section which may introduce significant uncertainties. Therefore it would be highly desirable to measure the MACS close to the relevant thermal energy of kT = 8 keV. In this contribution we describe the use of the ^{18}O(p,n)^{18}F reaction for activation measurements at lower stellar energies of kT = 5 keV and illustrate its first application at the example of the ^{138}Ba(n,γ)^{139}Ba cross section.

Activation with ^{18}O(p,n)^{18}F as neutron source

The neutron energy distribution of the ^{18}O(p,n)^{18}F reaction was investigated by a time-of-flight (TOF) experiment. The neutron spectrum was determined by means of a movable ^{6}Li glass detector for measuring the angular distribution from 0° to 80° in steps of 10°. Located at a distance of 222 mm from the target, this detector covered an angle of 9.8° with respect to the ^{18}O target. A stationary neutron monitor detector was positioned 300 mm from the target at an angle of 40°. This detector served for normalizing the individual spectra taken with the movable detector. The pulsed proton beam was provided by the Karlsruhe 3.7 MV Van de Graaff accelerator. The beam energy was calibrated via the threshold of the ^{18}O(p,n)^{18}F reaction at 2574 keV. The target consisted of an 0.2 mm thick tantalum disk with an oxide layer about 2 μ in thickness, which was produced by electrolysis of water with 95% enrichment in ^{18}O. The TOF measurements at different angles were first corrected for the neutron efficiency of the ^{6}Li glass detector assuming a 1/v behavior of the efficiency in the considered energy range below 40 keV. After correction for solid angle and normalizing to the flux measured by the monitor detector the spectra were added to the angle-integrated neutron spectrum shown by the histogram in Fig. 5. The dashed line in Fig. 5 indicates a Maxwellian fit of the form

$$\Phi = cE_n \mathrm{e}^{-E_n/kT}, \tag{1}$$

where E_n, kT, and c denote neutron energy, thermal energy, and a normalization constant, respectively. The best fit of the measured spectrum was obtained for a thermal energy of $kT = 5.1 \pm 0.3$ keV.

In astrophysics, the main nuclear physics input for stellar s-process models are the MACS

$$\frac{<\sigma v>}{v_T} = \frac{2}{\sqrt{\pi}} \frac{\int_0^\infty \sigma(E_n) E_n \exp(-E_n/kT) \mathrm{d}E_n}{\int_0^\infty E_n \exp(-E_n/kT) \mathrm{d}E_n}. \tag{2}$$

Here, $\sigma(E_n)$ is the differential capture cross section, E_n the total kinetic energy in the center of mass system, and $v_T = \sqrt{2kT/m}$ the mean thermal velocity with the reduced mass m. The quality of the fit can be illustrated by comparing the astrophysically relevant MACS for a cross section following the 1/v law. The difference between the MACS obtained with the experimental spectrum and with an ideal Maxwellian spectrum is only 2%. This difference becomes negligible in practical applications, since all activations will be carried out relative to gold as a standard by the concomitant activation of gold foils attached to the sample. In this way, the 2% deviation is common to al .

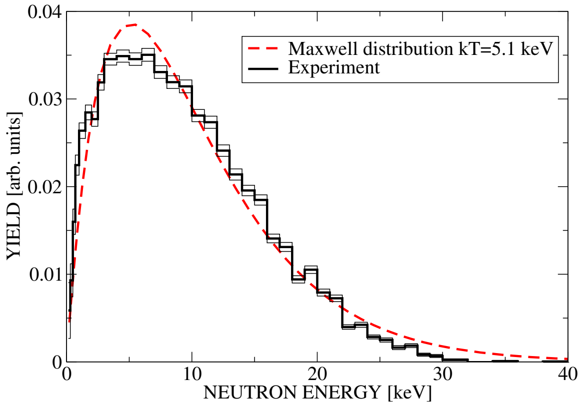

Figure 5: Neutron energy spectrum of the $^{18}O(p,n)^{18}F$ reaction after integration of the entire neutron field up to the maximal emission angle. The dashed line represents the best fit of a Maxwellian spectrum with a thermal energy of $kT = 5.1$ keV.

The ^{138}Ba(n,γ)^{139}Ba cross section

As a first application we present the measurement of the MACS of ^{138}Ba at a thermal energy of $kT = 5.1$ keV. As a neutron magic isotope the capture cross section of ^{138}Ba may well deviate from the 1/v law, which would imply large uncertainties in extrapolating the measured MACS from $kT = 25$ keV [1] to the required value at $kT = 8$ keV. The proposed neutron spectrum can be validated by comparison with the MACS obtained in a recent TOF measurement [5].
The sample was prepared from barium carbonate powder pressed into pellets 20 mm in diameter and 1.5 mm in thickness. Immediately after pressing, the samples were enclosed in 0.1 mm thick aluminum cans to prevent material losses during activation. The $BaCO_3$ was 98.04% enriched in ^{138}Ba. For the determination of the absolute neutron flux the samples were sandwiched between two 0.06 mm thick gold foils of the same diameter.

The neutron field for the activation measurements was produced with the method described above. The samples were placed 4.7 mm in front of the neutron production target to ensure they were completely inside the neutron cone. Throughout the irradiations the neutron flux was monitored

in steps of 5 s by means of a ^{6}Li glass detector at 1 m distance from the target. This information is required for off-line corrections due to variations in the neutron flux and for the decay of activated nuclei during the irradiations. The induced activities in the barium sample and the gold foils were measured using a system of two Clover type HPGe detectors placed face-to-face in close geometry.
With 50 μA proton beam current a neutron flux of 10^5 s^{-1} cm^{-2} was obtained with the ^{18}O(p,n)^{18}F reaction, a factor of about 10^4 lower than the flux produced with the ^{7}Li(p,n)^{8}Be reaction [6]. This drawback can partly be compensated by measuring the induced activities with high-efficiency detection systems. The gold cross section is well known for neutron energies above 2.7 keV [7, 8] and is, therefore, used as a standard for activation measurements with the ^{7}Li(p,n)^{7}Be neutron source.
To evaluate the average for activations at $kT = 5.1$ keV the energy-dependent capture cross section of ^{197}Au is also needed for lower energies down to 0.1 keV. Since no reliable experimental data are presently available in this energy region, the evaluated cross section of the ENDF/B database was used in the full energy region, but was normalized to reproduce the measured MACS of 582±9 mb at $kT = 30$ keV [8]. With the normalization factor of 0.954 the resulting MACS of ^{197}Au at $kT = 5.1$ keV is 2028 mb. We note, however, that an accurate measurement at lower neutron energies is urgently needed to establish the gold cross section as a standard also for activation measurements at $kT = 5.1$ keV.

The Maxwellian average neutron capture cross section of ^{138}Ba was obtained as the weighted average of the activations performed so far. The preliminary value at $kT = 5.1$ keV is $\frac{\langle\sigma v\rangle}{v_T}(^{138}Ba) = 12.5 \pm 1.0$ mb, in good agreement with the value of 13.6 ± 0.5 mb measured via the TOF method [5]. Since only the resonant part is considered by the uncertainty of the TOF result, an additional 3% may be necessary to account for the 10% contribution of the DC component to the stellar cross section.
The overall uncertainty of the present result is dominated by counting statistics and the systematic uncertainty of the neutron flux at the sample position. It is planned to reduce both uncertainties in additional activations.

References

[1] H. Beer, and F. Käppeler, Phys. Rev. C**21** (1980) 534

[2] R. Reifarth, C. Arlandini, M. Heil, F. Käppeler, P.V. Sedychev, A. Mengoni, M. Herman, T. Rauscher, R. Gallino, and C. Travaglio, Ap.

J. **582** (2003) 251

[3] F. Käppeler, H. Beer, and K. Wisshak, Rep. Prog. Phys. **52** (1989) 945

[4] C. Arlandini, F. Käppeler, K. Wisshak, R. Gallino, M. Lugaro, M. Busso, O. Straniero, Ap. J. **525** (1999) 886

[5] H. Beer, F. Corvi, P. Mutti, Ap. J. **474** (1997) 843

[6] Reifarth, R. and Käppeler, F. Phys. Rev. C **66** (2002) 054605

[7] R.L. Macklin, private communication to S.F. Mughabghab, (1982)

[8] W. Ratynski, and F. Käppeler, Phys. Rev. C **37** (1988) 595

The stellar (n,γ) cross section of ^{62}Ni

R. Reifarth[1], *A. Heger*[1], *S. Ghelberg*[2], *H. Nassar*[2], *M. Paul*[2] *S. Dababneh*[3], *M. Heil*[3], *F. Käppeler*[3], *R. Plag*[3], *I. Ahmad*[4], *J.P. Greene*[4], *D.J. Henderson*[4], *C.L. Jiang*[4], *R.C. Pardo*[4], *S. Sinha*[4], *T. Pennington*[4], *K.E. Rehm*[4], *R. Scott*[4], *X. Tang*[4], *R. Vondrasek*[4], *H. Koivisto*[5], *D. Berkovits*[6], *M. Bettan*[6], *P. Collon*[7], *S. O'Brien*[7], *N. Patronis*[8], *S.E. Woosley*[9]

[1] Los Alamos National Laboratory, Los Alamos, New Mexico, 87545, USA
[2] Hebrew University Jerusalem, Israel, 91904
[3] Forschungszentrum Karlsruhe, PF 3640, 76201 Karlsruhe, Germany
[4] Argonne National Laboratory, Argonne, IL, 60439, USA
[5] University of Jyvaskyla, FIN-40351, Finland
[6] Soreq NRC, Yavne, Israel
[7] University of Notre Dame, Physics Department, Notre Dame, IN 46556, USA
[8] Department of Physics, The University of Ioannina, 45110 Ioannina, Greece
[9] University of California, Santa Cruz, California, 95064, USA

Introduction

About 50% of the element abundances beyond iron are produced via slow neutron capture nucleosysnthesis (*s* process). Starting at iron-peak seed, the *s*-process mass flow follows the neutron rich side of the valley of stability. The weak *s*-process component is related to helium burning in massive stars of 10 to 25 $M_\odot$ [1]. During the weak *s*-process mainly isotopes with masses between 60 and 90 are produced. Its path is sketched in Fig. 1 for the region around Ni .

The neutron exposure during the weak *s*-process component is not strong enough to reach a local equilibrium. The production rate of neighboring nuclei is the not same, so that the change of of a single neutron capture rate affects not only the abundance of that nucleus, but rather the abundances of all nuclei downstream in the flow. The production of ^{62}Ni in a 25 $M_\odot$ stellar model [2] motivated a closer investigation of the neutron capture rates involved.

The Maxwellian averaged neutron capture cross section (MACS) of ^{62}Ni was only poorly known until this experiment. Even though there were time-of-flight (TOF) measurements available, it was affected by large uncertainties due to the unknown direct capture (DC) component. The most recent estimated values for the MACS at $kT = 30$ keV are 35.5±4 mb [3], 12.5±4 mb

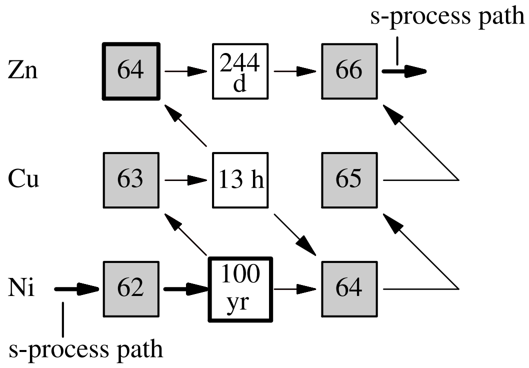

Figure 1: Reaction flow in the Ni-Cu-Zn region during the weak s process. The entire mass flow toward heavier elements passes through ^{62}Ni.

[4], and 35±5 mb [5]. The spread of the estimated neutron capture rate underlines the need for an experimental value.

Measurement

If neutron capture produces an unstable isotope the activation technique provides a powerful tool for cross section measurements. This technique offers two advantages: (i) It does not require isotopically enriched samples since the capture reactions can be identified either via γ-spectroscopy of transitions in the decay of the product nuclei or via the abundance of the product nucleus. (ii) It allows to measure the sum of the direct and the resonant capture components. ^{63}Ni decays via β^- with a rather long half-life of $t_{1/2} = 100 \pm 2$ yrs without emitting γ-rays. The end point energy of the β^--spectrum is only 66 keV. A detection of the induced activity during the neutron activation is therefore extremely difficult. Therefore, a combination of neutron activation and accelerator mass spectrometry, where the activation products themselves are identified and counted (and not their activity), was applied for the first time to measure a (n,γ) cross section in the keV-region.

Activation with stellar neutrons

A 36.8 mg Ni metal sample, enriched to 95% in ^{62}Ni, was activated at the Karlsruhe 3.7 MV Van de Graaff accelerator using the ^{7}Li$(p,n)^7$Be reaction for neutron production. Before each run, the accelerator was operated in

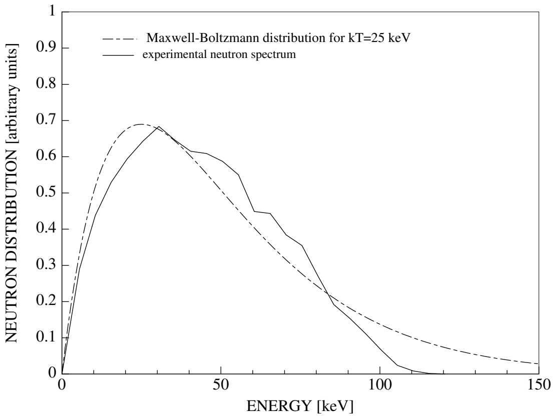

Figure 2: The neutron spectrum used for the activations at the Van de Graaff accelerator. The experimental spectrum (solid line) represents a good approximation of a thermal spectrum for $kT = 25$ keV (dashed line).

pulsed mode with a repetition rate of 1 MHz and a pulse width of 10 ns. This allowed to define the neutron spectra via time of flight (TOF) by means of a ^{6}Li glass monitor located 1 m downstream of the neutron target. For the activations, the accelerator was switched to direct current mode for achieving beam currents around 100 μA. In this mode, the ^{6}Li glass monitor was used to record the neutron yield in regular intervals. The resulting time history was used to evaluate the proper corrections for the decays during activation [6].

A quasi-stellar distribution corresponding to a thermal energy of $kT = 25$ keV was used in these activations. This is a typical temperature of the stellar He-burning sites. The spectrum was obtained by bombarding thick metallic lithium targets with a proton beam of $E_p = 1912$ keV, just above the neutron production threshold at 1881 keV. With this choice, all neutrons are emitted in a forward cone of 120° opening angle. The angle-integrated spectrum provides a good approximation of the thermal case, but is truncated at 106 keV [6, 7], as illustrated in Fig. 2. The proper proton energy is verified via the 106 keV cut-off in the TOF run with the ^{6}Li glass monitor.

The samples were sandwiched between thin gold foils determining the neutron exposure, since both the stellar neutron capture cross section of ^{197}Au [7] and the parameters of the ^{198}Au decay [8] are accurately known. With a typical neutron flux of $\Phi = 3 \cdot 10^9$ cm^{-2}s^{-1} a time-integrated flux of $\Phi_t = 3.9 \cdot 10^{15}$ cm^{-2} could be achieved after an irradiation time of several days.

Analysis of the ^{63}Ni/^{62}Ni ratio using AMS

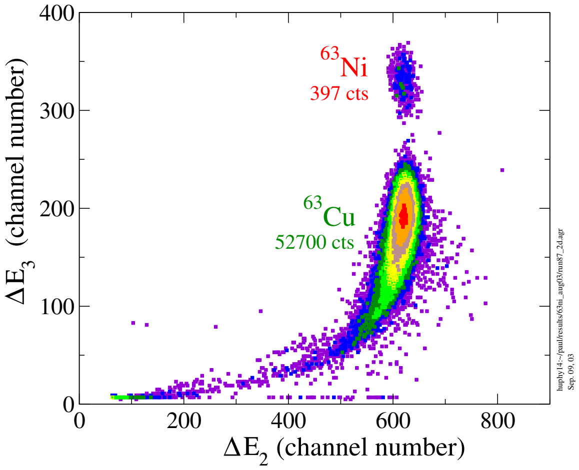

Figure 3: Two dimensional plot of the events detected in the multi-anode ionization chamber. The ^{63}Ni group is clearly separated from its ^{63}Cu isobars.

The measurement of the ratio $R_{\rm AMS} = {}^{63}\rm Ni/{}^{62}Ni$ was performed using accelerator mass spectrometry (AMS). The velocity-averaged cross section was then extracted using:

$$\frac{\langle \sigma v_T \rangle}{v_T}(^{62}{\rm Ni}(n,\gamma)) \quad = \quad \frac{R_{\rm AMS}}{\Phi_t}.$$

The AMS measurement was performed at the Argonne ATLAS facility, using the ECR ion source and the gas-filled magnetic spectrograph technique to separate the extremely intense isobaric ^{63}Cu component [9]. Ni is fed into the ECR source in gas phase using high vapor pressure organo-metallic nickelocene, a technique, which was shown to reduce the ^{63}Cu contaminant by a factor of 100 in comparison with solid sample feed. In our experiment, activated and natural Ni samples (100-150 mg) were converted to nickelocene at the University of Jyvaskyla [10]. $^{63}\rm Ni^{15+}$ ions extracted from the ECR were accelerated to 9.2 MeV/A without further stripping. The setup of the ATLAS accelerator and the ion transmission were determined using a guide beam of $^{84}\rm Kr^{20+}$, having the same mass to charge ratio. The two ions have nearly the same m/q ratio (δ(m/q)/(m/q)=6.4 10^{-5}). The transmission of the accelerator was periodically measured during the experiment, using the $^{84}\rm Kr^{20+}$ guide beam. The Enge magnetic spectrograph, filled with N_2 at

20 Torr, separated the ^{63}Ni group in the focal plane from the ^{63}Cu isobaric beam and from the residual ^{84}Kr, which were then blocked before entering the detector. Further ion identification in a multi-anode ionization chamber placed along the focal plane of the spectrograph led to the unambiguous detection of ^{63}Ni (see Fig. 3)

The ^{63}Ni count rate, corrected for ion transmission and normalized to the Ni ion intensity from the ECR source, defines the ^{63}Ni/^{62}Ni ratio to be used for the cross section determination. In order to reduce systematic uncertainties, measurements were performed also with Ni activated with thermal neutrons from the Soreq nuclear reactor, using the known thermal ^{62}Ni(n,γ)^{63}Ni cross section ($\sigma_{thermal} = 14.2 \pm 0.3$ b).

The ^{62}Ni(n,γ)^{63}Ni cross section at stellar temperatures of $kT = 25$ keV was determined to $\sigma_{stellar} = 22.6 \pm 2.4$ mb. A comparison with previous estimates is given in Fig. 4.

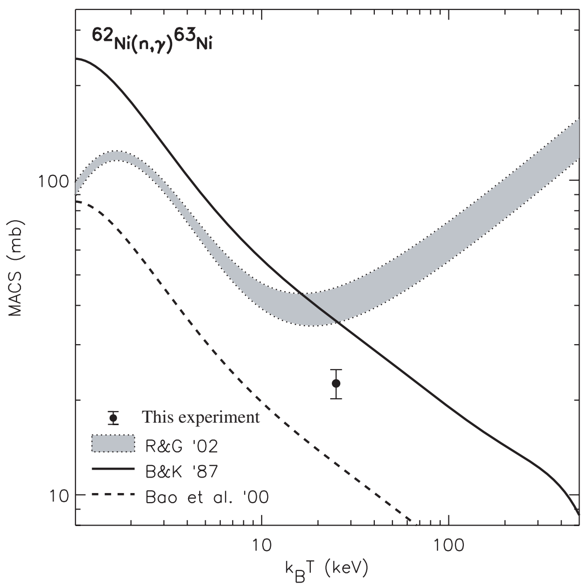

Figure 4: Comparison of the present measurement with previous prediction. The different curves refer to the values mentioned in Sect. . 'R&G 02' means [5], 'B&K 87' means [3] and 'Bao et al. 00' means [4].

Astrophysical implications

The weak s-process component is sensitive to the (n,γ) cross sections of individual nuclei along the s-path, in particular to the cross sections of the

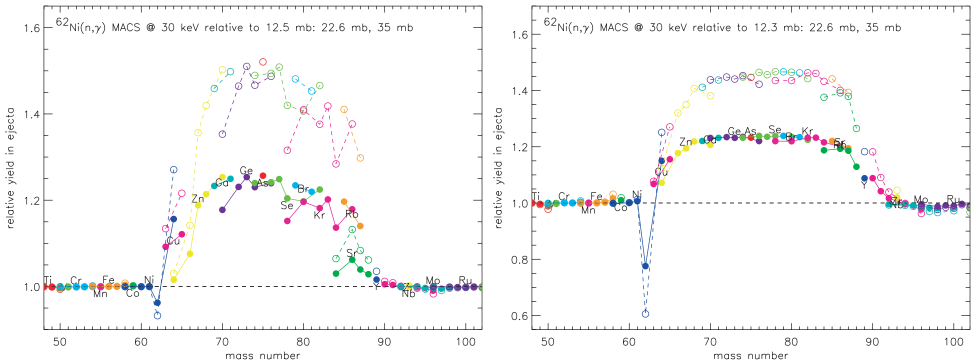

Figure 5: Comparison of nucleosynthesis calculations for a 15 $M_\odot$ (left) and a 25 $M_\odot$ (right) star carried out with different values for the ^{62}Ni(n,γ) cross section. The set of filled circles shows the yield ratio for 22.6 mb (this measurement) to 12.5 mb [4]. The set of open circles shows the yield ratio for 35 mb [3, 5] to 12.5 mb [4].

seed nuclei in the Fe group. Fig. 5 shows the results of stellar evolution simulations for a 15 and a 25 $M_\odot$ star.

Each star was simulated with 3 different values for the ^{62}Ni(n,γ) cross section. Except for this cross section the simulations were identical to [2]. A change to the ^{62}Ni(n,γ) MACS at kT = 30 keV from 12 mb to 22.3 mb results in a overall increase of for the weak s-process yield by 20%, while the production of ^{62}Ni is decreased due to the increased destruction. This has to be compensated by a decreased neutron exposure. The overproduction of ^{62}Ni in the 25 $M_\odot$ star, however, remains considerable. If an equilibrated s-process flow would be responsible for the production of ^{62}Ni, one would expect that the resulting abundance is inversely proportional to its (n,γ) cross section. In this 25 $M_\odot$ star, however, most of the ^{62}Ni is made in the α-rich freeze-out and not much affected by the change of the (n,γ) cross section.

References

[1] C.M. Raiteri et al., Ap. J. **419** (1993) 207.

[2] T. Rauscher et al., Ap. J. **576** (2002) 323.

[3] Z.Y. Bao and F. Käppeler, Atomic Data Nucl. Data Tables **36** (1987) 411.

[4] Z.Y. Bao et al., Atomic Data Nucl. Data Tables **76** (2000) 70.

[5] T. Rauscher and K.H. Guber, Phys. Rev. C **66** (2002) 028802.

[6] H. Beer and F. Käppeler, Phys. Rev. C **21** (1980) 534.

[7] W. Ratynski and F. Käppeler, Phys. Rev. C **37** (1988) 595.

[8] R.L. Auble, Nucl. Data Sheets **40** (1983) 301.

[9] M. Paul et al., Nucl. Inst. Meth. A **277** (1989) 418.

[10] H. Koivisto et al., Nucl. Inst. Meth. B **94** (1994) 291.

The fission rate calculations and consequences for r-process abundances

I.V. Panov[1,2], *E. Kolbe*[2], *B. Pfeiffer*[3], *T. Rauscher*[2], *K.-L. Kratz*[3], *F.-K. Thielemann*[2]

[1] State scientific center-Institute for Theoretical and Experimental Physics, B.Cheremushkinskaya 25, Moscow, 117259, Russia.

[2] University of Basel, Klingelbergstr. 82, CH-4056 Basel, Switzerland

[3] Institute fur Kernchemie, Fritz-Strassman-Weg 2, D-55128 Mainz, Germany

Introduction

Fission plays an important role in the r-process which is responsible not only for the yields of transuranium isotopes, but may have a strong influence on the formation of the majority of heavy nuclei due to fission recycling. We present calculations of beta-delayed and neutron-induced fission rates, taking into account different fission barriers predictions and mass formulae.

The fission barriers, used in the past for fission rate calculations [1] were probably underestimated. Recent calculations [2, 3] predict higher fission barriers, sometimes significantly. Therefore, a recalculation of fission rates is important as well as an evaluation of their sensitivity on nuclear data. We consider all fission channels, but first discuss beta-delayed and neutron-induced fission.

Here we want to emphasize that, besides neutron-induced fission and beta-delayed fission rates, the mass-distribution of fission yields is important as well as it was discussed earlier [4]. Although the mass distribution of fission products is known rather well for long-lived transactinide nuclei, the mass distribution after fission of neutron-rich heavy elements is an open question. The r-process yields in the mass region of $80 < A < 120$ can be affected by the mass distribution of fissioning nuclei, and triple or ternary [5] fission can play an important role in some cases.

Beta-delayed fission rates differ very strongly due to difficulties to predict reliable beta-strength functions for very neutron-rich and especially for deformed nuclei as well as reliable fission barriers for such nuclei. The degree of difference depends either on the r-process model used. In the case of the classical model of the r-process, the path of the r-process lies along nuclei with neutron separation energy $S_n \approx$ 2MeV, and the r-process stops at mass numbers A≈260. Both of the data sets [8, 10] yield the maximum values of $P_{\beta f}$ for these nuclei. That is why the previously used approximation of 100% instantaneous fission in the vicinity of A$\sim$260 [6], [7], [9] was a fairly good approximation. But when considering extreme r-process paths in the framework of the classical model ($S_n \sim 3$ MeV or $S_n \sim 1$ MeV) or with a calculation of the heavy element abundances in a very high neutron density environment, the difference in the results with utilization of different beta-delayed fission rates can be large.

The statistical approach to fission rates

As in previous approaches [8, 10, 16], we have applied the statistical Hauser-Feshbach formalism for the calculation of fission rates. It has been shown [12] that the statistical model is very well applicable for the astrophysical neutron-induced rate calculations, as long as there is a high density of excited states, which is the case for heavy nuclei. Of course, just near the neutron drip-line the systematic errors of the approach in neutron-induced fission rate calculations can rise, underlining that reliable mass predictions are absolutely necessary for r-process applications far from stability. Early r-process calculations made use of the mass predictions by Hilf et al. [11] and the fission barriers of ref. [1] for fission rate evaluations. For a consistent treatment of fission rates, however, the neutron separation energies, reaction Q-values and fission barrier heights should be used from the same mass model.

In our calculations of beta-delayed fission we used the new approach for the beta-strength function [13], based on the approach [14], applying the QRPA formalism to deformed nuclei. The model combines calculations within the quasi-particle RPA for the Gamow-Teller part with an empirical spreading of quasi-particle strength and the gross theory for the first-forbidden part of β-decay.

To calculate β-decay Q-values and neutron separation energies the experimental ground-state masses were used where available, otherwise calculated masses (ETFSI [15], Thomas-Fermi [2] or Howard and Möller [1]).

It has to be noted that for very neutron rich nuclei the possibility of fission after delayed neutron emission could be rather high and, that in principle, such a fission mode also should be calculated. In order to evaluate the role of secondary fission on the base of new data this process can be investigated by iterating the SMOKER-code: if neutron emission leads to an excited level of the residual nucleus, we again calculate the branching ratios for the subsequent decay with the statistical model including the fission channel. Thus the probability for fission in the second decay step is essentially given by multiplication of the branching ratios for neutron emission and fission of the residual nucleus. Note that this is done by keeping track of energies, angular momenta and parities of the excited states, and the final probability for (β^-, nf)-decays is obtained by summing up the contributions from all quantum mechanically allowed partial waves.

Since the amount of excitation energy in the system is significantly reduced with every particle emission and eventually drops below the particle emission thresholds or fission barrier, we found that the cascade, could practically be terminated after two emission steps, contrary to neutrino-induced fission [17] when some consequent emissions of different particles can occur. Thus, the residual daughter nuclei after two iterations were assumed to be in their ground state.

Results

When the r-process approaches the actinide region, fission channels appear. Beta-delayed fission competes with beta-delayed neutron emission and pure beta-decay. Also the well known process of neutron induced fission has to be included. This process, discussed earlier [9] for uranium isotopes has not yet been included in r-process calculations. Neutron-induced fission rates can be very high [9], [18], [20] for isotopes of transuranium elements and exceed beta-decay rates by orders of magnitude even near the neutron drip-line. This is mainly the case for very high neutron densities n_n as the product $< \sigma_{nf} v > n_n$ competes with beta-delayed fission rates $\lambda_{\beta df}$. The recycling timescale, measuring the time until the neutron capture on fission products leads again to the formation of actinides can be significantly less than the duration time of the r-process.

For the neutron-star merger scenario [21, 22] or polar jets in supernova [19] such conditions are maintained for a long time ($\sim 1s$). However, as already pointed out above, the fission barriers of Howard and Möller [1] are very likely underestimated.

The calculation of rates for neutron-induced fission and beta-delayed fission made use of the statistical model code SMOKER, extended by including fission channels [9, 16] as discussed in section 2.

Simultaneous consideration of beta-delayed fission and neutron-induced fission in our calculation, and spontaneous fission in an other approach [23] give very similar results (see Section 6), at least within the calculation accuracy. However, neutron-induced and beta-delayed fission should be faster and consequently more important in the r-process than spontaneous fission, which can play, however, an important role during cooling in the final de-

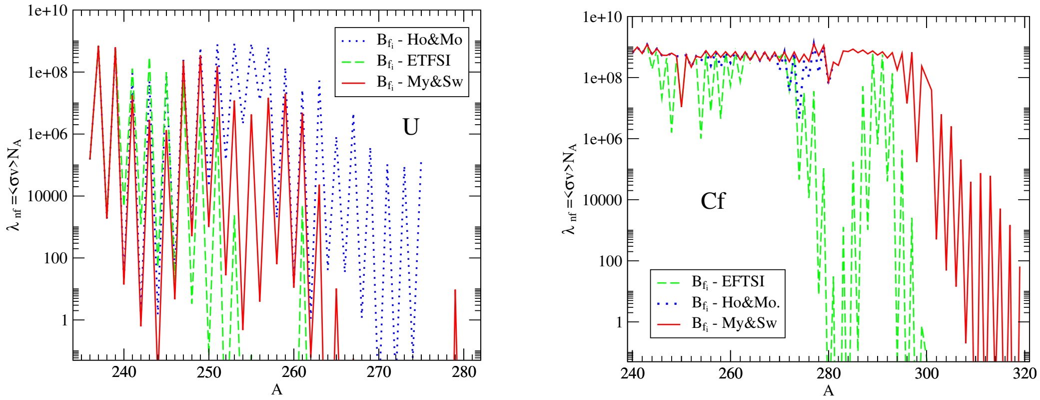

Figure 1: Neutron-induced fission rates for U (left) and Cf (right) isotopes for different fission barriers as well as for different mass formulae.

cay of the r-process products. But for a consistent inclusion of fission in the r-process, especially for the calculation of final abundances, the specific scenarios of the r-process considered the regions and conditions where spontaneous fission could be important should be considered.

In 1, the neutron-induced fission rates λ_{nf} derived with the barriers of ref. [1] and mass predictions of [11] are compared with consistent calculations when all mass and fission barriers predictions were made on the base of approaches [24], [25]. The results show that for uranium isotopes with atomic masses A<260 the rates using Thomas-Fermi predictions [2] are also rather high whereas the rates calculated on the base of ETFSI predictions [26] for atomic masses greater 250 become too small compared to beta-decay and neutron capture rates. The latter can not interrupt the formation of new transuranium elements in r-process nucleosynthesis. As mentioned above the comparison was made for very high neutron environments with $\rho Y_n = 1$. As Z increases the rate values go up and all approaches give very high values of neutron-induced fission rates already for Cf isotopes, with the exception of the ETFSI approach in the vicinity of neutron shell N=184 (1), where $S_n << B_f$. But the heights of barriers [26] for these nuclei seem to be overestimated [27].

The first extended results for beta-delayed fission probabilities (2) for the majority of neutron-rich isotopes of some chemical elements show that for fission barriers of refs. [2], [26], which are significantly higher then previously

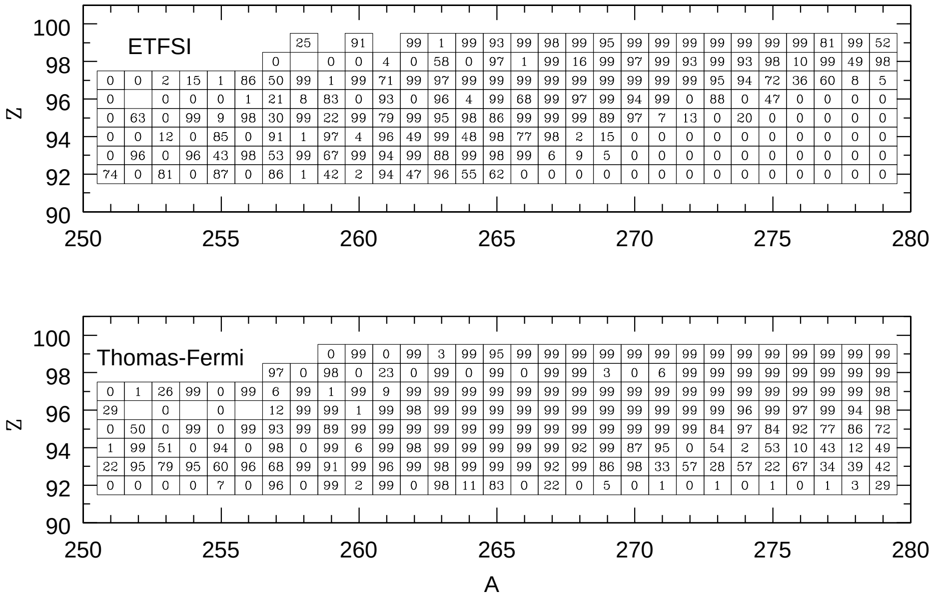

Figure 2: ETFSI and Thomas-Fermi beta-delayed fission probabilities

used [1], the values of $P_{\beta df}$ are still high for very neutron rich isotopes. For majority of them this applies in the case when mass model [2] was used and for part of them when the model based on ETFSI [3] was used.

Calculations of fission rates in the framework of the statistical model(see [8] and Section 2 of the present work) for both self-consistent approaches [2], [26] show similar results when the maximum values are reached for isotopes with atomic mass numbers A$\approx 255 - 265$. But with increasing Z the region of isotopes with high values of $P_{\beta df}$ close to 100% expands and in case of data set [2] the majority of isotopes attain close to maximum values above Z=95 and in case of [26] above Z=98. The suppression in $P_{\beta df}$ values for californium for the ETFSI barriers is explained by very high fission barriers in the vicinity of nuclei with number of neutrons close to 184.

In the Table 1 results of cascade calculations for beta-delayed fission are shown. We choose nuclei with very small values of direct beta-delayed fission probability for the calculations. It turns out, as nevertheless one suppose, that after neutron emission exited nuclei can fission. In our calculations

Table 1: Beta-delayed cascade fission probabilities (in %) for some U isotopes.[1)]

decay	A	$P_{\beta df}$	$P_{\beta n}$	$P_{\beta dnf}$	$\mathbf{P^{tot}_{\beta df}}$	$P^{max}_{n\beta df}$	$P^{min}_{n\beta df}$
U →Np	264	41	59	4	45	86	-
U →Np	266	8	92	69	77	38	-
U →Np	268	1	99	28	29	25	7
U →Np	270	3	96	23	26	44	14
U →Np	272	3	97	8	11	23	10
U →Np	274	4	96	4	8	16	11
U →Np	276	2	98	9	10	31	-

[1)] $\mathbf{P^{tot}_{\beta df}}(Z,A)=P_{\beta df}+P_{\beta dnf}$, $\quad P^{max}_{\beta dnf} \equiv P_{\beta df}(Z+1, A-1)$,

total $P^{tot}_{\beta df}$ increased for all considered nuclei, in some cases in times. That means, that the cascade mechanism can be important for nuclei for which the direct (one step) beta-delayed fission is small and beta-delayed neutron emission is high.

In the last two columns the results of our evaluations are presented. The first ($P^{max}_{\beta dnf}$) shows the fission contribution during beta-decay of daughter nucleus. The second one ($P^{min}_{\beta dnf}$) shoes the same but in assumption that compound nucleus does not changed during all the steps of cascade. It was calculated as probability of delayed fission of daughter nucleus but with reduced β-strength function of the mother nucleus $S_\beta(U)$ where $U = E - S_n$ as in [28]. Different mass and barrier predictions for U [1] and Cf [26] were used.

Discussion and conclusions

The new calculations of fission rates considered two consistent approaches. The calculations showed that, on a whole, the new rates based on fission barriers of [2, 26] are lower than the ones previously used [8, 18, 20]. However, taking into account a cascade model of fission after beta-delayed neutron emission, the total value of fission rates can increase in some cases, especially when beta-delayed fission of the mother nucleus is low and primary beta-delayed neutron emission is high. For such nuclei the addition to delayed fission after neutron emission can be significant and the total value of beta-delayed fission can increase strongly.

Unfortunately, the agreement of different calculations (used in different mass and fission barrier predictions) have not converged yet, especially for very neutron rich nuclei in the region with N $\sim$ 184.

The extended calculations of fission rates taking into account Thomas-Fermi [2] and ETFSI [26] fission barriers have not been finished yet. A detailed comparative analysis of the influence of fission modes on the results of nucleosynthesis was made in full network calculations [20, 29] using the mass relations [11] and fission barriers [1], used for years in many astrophysical applications. An evaluation of the relative contribution of neutron-induced and β-delayed fission on the formation of r-elements under conditions of high neutron densities ($10^{20} < n_n < 10^{30}$) was made. Our present calculations of fission rates should not change significantly our previous conclusions concerning competition of beta-delayed fission and neutron induced fission but the resulting changes in r-process abundances can be significant.

When considering dynamical r-process models at extremely high neutron densities, in which fission occurs strongly, the path of the r-process lies close to neutron drip-line, and the efficiency of beta-delayed fission depends strongly on fission rates for the group of nuclei close to the neutron shell N$\approx$184. In particular, in the scenario realized in the model of neutron star mergers [21], [22]), r-process nucleosynthesis proceeds mainly along the neutron drip-line [30] due to very high neutron densities. In this case, the role of neutron-induced fission will be comparatively more important than beta-delayed fission. For realistic fission barriers [2, 26] and mass predictions [24, 25], nuclei with masses as large as A$\sim$300 could be formed. In this case the predicted abundance curve for nuclei below $A \sim 130$ should also consider triple (ternary) fission.

The probability of triple (or ternary) fission [31, 32] is highly uncertain but for nuclei with $A > 260$ near the neutron drip-line, fission into 3 fragments is energetically possible and could occur. Present [32] and forthcoming [33] experiments should clarify the probabilities of such a processes.

After extended calculations of both beta-delayed fission probabilities and neutron-induced fission rates for all nuclei involved in the r-process, we hope to clarify the question of the role of fission rates at different stages of nucleosynthesis for more specific astrophysical conditions. Due to our new results, it seems that fission will affect the r-process, but further detailed studies are ahead.

The acknowledgements. The authors thanks F. Gönnenwein, S. Goriely, C. Wagemans and all colleagues, especially participants of the Conferences: Nuclei in the Cosmos (Tokyo, 2002), Seminar on Fission (Pont d'Oye, 2003), Nucleus-2003 (Moscow 2003) for discussions on fission data, especially mass

distribution of fission fragments.

This work supported by grant 20-68031.02 of the Swiss National Science Foundation and partially supported by grant 04-02-16793-a of Russian Foundation of Basic Research (RFBR).

References

[1] W.M. Howard, P. Möller. ADNDT, 25 (1980) 219.

[2] W.D. Myers, W.J.Swiatecki, Phys. Rev. C 60 (1999) 014606-1.

[3] A. Mamdouh, J.M. Pearson, M. Rayet, F. Tondeur, Nucl. Phys. A 644 (1998) 389.

[4] I.V. Panov, C. Freiburghaus, F.-K. Thielemann, Nucl. Pnys. A 688 (2001) 587.

[5] H Diehl, W. Greiner. Nucl. Pnys. A 229 (1974) 29.

[6] J.J. Cowan, B. Pfeiffer, K.-L. Kratz, F.-K. Thielemann, C. Sneden, S. Burles, D. Tytler, T.C. Beers, Astrophys. J. 521 (1999) 194.

[7] T. Rauscher, J.H. Applegate, J.J. Cowan, F.-K. Thielemann, M. Wiescher. Astrophys. J. 429 (1994) 499.

[8] F.-K. Thielemann, J. Metzinger, H.V. Klapdor-Kleingrothaus, Zt. Phys. A 309 (1983) 301.

[9] F.-K. Thielemann, A.G.W. Cameron, J.J. Cowan, Proc. of Int. Conf. 50 years with Nuclear Fission, 1989, ed. J. Behrens, A.D. Carlson, p. 592.

[10] A. Staudt, H.V. Klapdor-Kleingrothaus. Nucl. Phys. A 549 (1992) 254.

[11] E.R. Hilf, H.V. Groote, K. Takahashi. Proc. 3 Int. Conf. on Nucl. far from Stability, 1976, CERN-76-13, 142.

[12] T. Rauscher, F.-K. Thielemann, K.-L. Kratz, Nucl. Phys. A 621 (1997) 331c.

[13] P. Moller, B. Pfeiffer, K.-L. Kratz, Phys. Rev. C 67 (2003) 055802.

[14] J.Krumlinde, P.Möller, Nucl. Phys. A 417 (1984) 419.

[15] J.M. Pearson. R.C. Nayak, S. Goriely, Phys. Lett. B 387 (1996) 455.

[16] J.J. Cowan, F.-K. Thielemann, J.W. Truran, Phys. Reports, 208 (1991) 267.

[17] A. Hektor, E. Kolbe, K. Langanke, J. Toivanen. Phys. Rev. C, 61 (2000) 055803.

[18] I.V. Panov, F.-K. Thielemann, Astronomy Lett. 29 (2003) 510.

[19] A.G.W. Cameron, Astrophys. J. 587 (2003) 327.

[20] I.V. Panov, F.-K. Thielemann, Nucl. Phys. A 718 (2003) 647.

[21] C. Freiburghaus, S. Rosswog, F.-K. Thielemann, Astrophys. J. 525 (1999) L121.

[22] S. Rosswog, M. Liebendorfer, F.-K. Thielemann, M.B. Davis, W. Benz, T. Piran, Astron. Astrophys, 341 (1999) 499.

[23] S. Goriely, B. Clerbaux, Astron. Astrophys. 346 (1999) 798.

[24] W.D. Myers, W.J.Swiatecki. Nucl. Phys. A 601 (1996) 141

[25] Y. Aboussir, J.M. Pearson, A.K. Dutta, F. Tondeur. ADNDT 61 (1995) 127

[26] A. Mamdouh, J.M. Pearson, M. Rayet, F. Tondeur Nucl. Phys. A 679 (2001) 337.

[27] S. Goriely, M. Samyn, P.-H. Heenen, J.M. Pearson, F. Tondeur, Phys. Rev. C 66 (2002) 024326.

[28] Yu.S. Lyutostansky, I.V. Panov, V.K. Sirotkin. Phys. Lett. B 161 (1985) 9.

[29] I.V. Panov, F.-K. Thielemann, Astronomy Letters, 30 (2004) 8.

[30] I.V. Panov, Astronomy Letters, 29 (2003) 163.

[31] V.P. Perelygin et al., Nucl. Phys. A 127 (1969) 577.

[32] I. Tsekhanovich et al., Phys.Rev. C67 (2003) 034610.

[33] Yu.N. Kopach, M. Mutterer, D. Schwalm, P. Thirolf, F. Gënnenwein, Phys. Rev. C 65 (2002) 04461.

The nuclear reaction waiting points ^{22}Mg, ^{26}Si, ^{30}S and ^{34}Ar and bolometrically double peaked type I X-ray bursts

J.Lund Fisker[1], *F.-K. Thielemann*[1] *and M. Wiescher*[2]

[1]Department für Physik und Astronomie, University of Basel, Klingelbergstr. 82, CH-4056 Basel, Switzerland
[2]Department of Physics, University of Notre Dame, IN 46556, USA

Abstract

Type I X-ray bursts with a double peak in the bolometric luminosity have been observed from several sources. The separation between the two peaks are on the order of a few seconds. We propose a nuclear waiting point impedance in the thermonuclear reaction flow to explain these observations. Nuclear structure information suggests the potential waiting points: ^{22}Mg, ^{26}Si, ^{30}S and ^{34}Ar, which arise in conditions, where a further reaction flow has to await a beta-decay, because the (α, p)-reaction is too weak to overcome the target Coulomb barrier and the (p, γ)-reaction is quenched by photo-disintegration at the burst temperature. he (α, p)-reaction is too weak to overcome the target Coulomb barrier and the (p, γ)-reaction is quenched by photo-disintegration at the burst temperature. The conclusion is that the effects of the experimentally unknown ^{30}S$(\alpha, p)^{33}$Cl and ^{34}Ar$(\alpha, p)^{37}$K might be directly visible in the observation of X-ray burst light curves.

References

[1] J.L. Fisker, F.-K. Thielemann, M. Wiescher, Ap.J.Lett. **608, 61 (2004).**

Nucleosynthesis Studies with Cosmic Gamma-Rays

Roland Diehl

Max Planck Institut für extraterrestrische Physik, D-85741 Garching, Germany

Gamma-Rays and Cosmic Nucleosynthesis

Gamma-rays provide one of the most direct observational proofs of ongoing nucleosynthesis in the universe through radioactive decay of a few specific isotopes produced along with the bulk of fresh nucleosynthesis products. SN1987A and interstellar ^{26}Al have demonstrated this nucleosynthesis connection. In the past decades, efforts have concentrated on supernova studies through radioactive ^{56}Ni decay products and ^{44}Ti, search for ^{60}Fe from supernovae and ^{22}Na from Galactic novae, and mapping of the Galaxy in diffuse radioactivities from ^{26}Al and positron annihilation emission at 511 keV.

The calibration of the energy source of **thermonuclear supernovae** through ^{56}Ni decay products has not been achieved despite dedicated long observations to the only two events which were sufficiently nearby, SN1991T and SN1998bu: A 3 σ detection for the bright SN1991T [11] event contrasts with an upper limit for SN1998bu [3] which falls below expectations for this rather normal SN.

^{44}Ti radioactivity is expected from **core-collapse supernovae**, and has been seen from Cas A, not only by COMPTEL [4], but also by the BeppoSAX mission [21]. ^{44}Ti decay at τ ~89 y occurs through ^{44}Sc to excited ^{44}Ca, which emits the gamma-rays at 1157 keV seen by COMPTEL. BeppoSAX has detected K_α emission from ^{44}Sc, which occurs in a relatively less background-contaminated region. Yet, both measurements are not significant enough by themselves to allow a good determination of ^{44}Ti mass, furthermore ionization in the supernova remnant is important for such interpretation, in both cases, though for different reasons. Therefore one of INTEGRAL's main objectives is a detection of the ^{44}Ti radioactive-decay lines at 68 and 78 keV from excited ^{44}Sc, and their spectroscopy. No other young supernova remnant has been seen in the Galaxy in ^{44}Ti emission ($\tau \sim 100$ y) yet; the Galactic core collapse frequency is probably $\simeq 1/30\ y^{-1}$, so a few objects should be seen, preferentially in the inner Galaxy where young stars are abundant. The detection of Cas A at 3.4 kpc distance and an age of $\simeq$ 335 years confirms that such detection is possible; yet it may be misleading, if Cas A is a very non-typical core collapse event.

Diffuse radioactivity from ^{26}Al has been mapped along the plane of the Galaxy, and provides us with the best tracer of massive-star activity on a coarse ($\simeq$ degrees) scale in our Galaxy. Presolar grains have revealed signatures of ^{26}Al from grains which can be attributed from their isotopic signatures undoubtedly to each of the event types of supernovae, novae, and AGB stars. So, the relative contributions of all these candidate sources to the total interstellar ^{26}Al mass as seen in the 1809 keV gamma-rays remains an open question. Interesting studies of localized ^{26}Al emission such as in the Cygnus [12, 7] and Orion [2] regions have confirmed a dominating contribution from massive stars, and suggest that the Wolf Rayet phase of massive stars is the major contributor. ^{26}Al emission is relatively bright; interestingly, source models suggest that the same sources should produce also interstellar ^{60}Fe gamma-rays from radioactivity as well as positron annihilation emission at 511 keV, both at intensities in the vicinity of 10% of the ^{26}Al gamma-ray sky brightness. For positrons, other even brighter sources must exist at least in the central region of the Galaxy, because annihilation flux from the GC region has been measured by several experiments to be $\simeq 10^{-3}$ph cm^{-2}s^{-1}. ^{60}Fe, on the other hand, may only come from cc-SNe, or maybe also from rare SNIa subclasses which would be apparent as single bright point sources. Detection and mapping of such emission is the goal of present and future gamma-ray missions, to advance massive-star nucleosynthesis research.

So far, gamma-ray line spectroscopy, i.e. line identifications and analysis of line shapes in terms of velocity or thermal broadening has been sporadic, based on short-duration balloon experiments or space missions. With INTEGRAL this new dimension of observational data was made broadly accessible.

INTEGRAL and its Spectrometer

The INTErnational Gamma-Ray Astrophysics Laboratory (INTEGRAL) of ESA has been launched on October 17, 2002 from Baikonur into an excentric 3-day orbit spending most of its time outside the radiation belts. The INTEGRAL mission's nominal duration was 2 years; after its successful first phase now it is even approved until 2008. A Core Program of 25% is aimed mainly at the inner Galaxy, while most of the observing time is available to the "Open Program" for complementary or specific and deeper studies, selected from $\simeq$ annual proposal evaluation cycles.

The spectrometer SPI on INTEGRAL[20, 15] is based on 19 hexagonal Ge detector modules, each one 7 cm thick and 5.5 cm wide, arranged in a densely packed detector plane of 500 cm^2 total. It is illuminated through a 127-element coded mask made of tungsten, defining a field-of-view of 16 degrees opening angle. The Ge detector temperature needs to be maintained at $\simeq$ 90 K, done by stirling coolers. During "annealings" the camera is warmed up to $\simeq$ 105 C for $\simeq$ 1.5 days to cure the accumulated damage from cosmic-ray bombardement which leads to $\simeq$ 10% degradation of spectral resolution. The spectral resolution is thus being maintained at $\simeq$ 3 keV at 2 MeV, suitable for a previously unavailable level of cosmic gamma-ray spectroscopy.

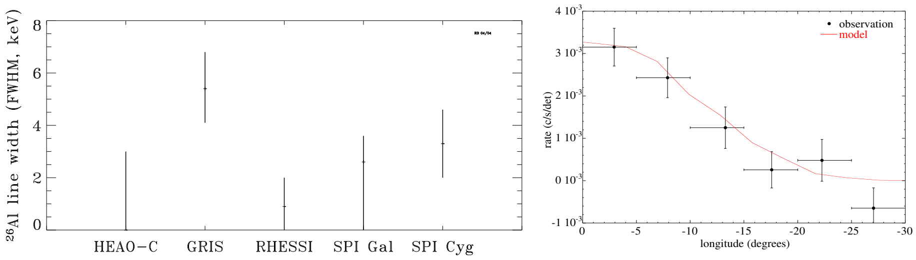

Figure 1: *Left:* The line width results for ^{26}Al from different experiments for the inner Galaxy show that the GRIS result appears as an outlier, and the line probably is as narrow as expected; however, for the Cygnus region, SPI finds a modest broadening, suggestive of increased interstellar energy input from young stars. *Right:* The 511 keV line from positron annihilation appears rather symmetric around the center of the Galaxy, a disk component cannot be found (yet). The model shown here is a symmetric 2D Gaussian with a FWHM width of 10 deg and traces measured count rates.

New Results, Remaining Issues

Determination of instrumental background lines, which underly and contaminate cosmic gamma-ray lines at typically 10–100 times their intensity, is the key to achieving the target line sensitivity of INTEGRAL. This builds on the experience of background variations during the mission, which is being accumulated.

^{44}Ti studies on Cas A and SN1987A have begun, the 1–2 Ms of exposure are still inadequate for detection or significant limits if the lines are broadened. An upper limit from SPI [22] for GRO0852-4642/RXJ0852-4622 ^{44}Sc lines from ^{44}Ti decay also still leaves this marginally-significant COMPTEL ^{44}Ti source [5, 16] in the grey area of 'candidate' sources. Search for further expected young SNR from the Galaxy with the IBIS instrument [14] confirms their striking absence, or Cas A's peculiarity, as concluded from COMPTEL before[19].

Diffuse radioactivity from ^{26}Al has been detected with SPI both from the inner Galaxy [1] and from the Cygnus region [9]. Spectroscopy tells us that this line is not or only modestly broadened, as expected, but in contrast to an earlier balloon experiment's results (see Fig. 1 a). Emission from ^{60}Fe has not been found, but the achieved sensitivity still would be consistent with RHESSI's flux at 9.7% of the ^{26}Al gamma-ray intensity, detected however at 2.6σ only [18]; it is still unclear if the ^{60}Fe gamma-ray flux can demonstrate a dominating Wolf-Rayet origin of ^{26}Al [13].

Mapping the positron annihilation in the Galaxy is one of the main goals of INTEGRAL. First imaging analysis suggests a surprisingly-symmetric emission morphology [6, 8] (see also Fig. 1 b). Disk emission, as expected from the radioactivities of ^{56}Ni from SNIa and from ^{26}Al, has not been found, in contrast to earlier OSSE results. This had stimulated several speculations about a dark matter origin.

Outlook and Acknowledgements

From these early results, SPI's capabilities for nuclear spectroscopy in space have been demonstrated. Limitations from knowledge of the underlying background are still severe, but will reduce with accumulating mission experience. – It is a pleasure to thank my colleagues in the SPI Team for their efforts to provide an excellent high-resolution gamma-ray spectrometer in space, and for the collaborative analysis of SPI's complex data.

References

[1] Diehl, R., *et al.* (2003), A&A, **411**, 451.

[2] Diehl, R., *et al.* (2002), New Ast.Rev., **46**, 547.

[3] R. Georgii *et al.* (2002), A&A **394**, 517.

[4] A.F. Iyudin *et al.* (1997), ESA **SP-382**, 37.

[5] A.F. Iyudin *et al.* (1998), Nature **369**, 142.

[6] P. Jean *et al.* (2003), A&A, **407**, L55.

[7] J. Knödlseder *et al.* (2002), A&A **390**, 935.

[8] J. Knödlseder *et al.* (2003) A&A, **411**, L457.

[9] J. Knödlseder *et al.* (2004), ESA-SP, *in press.*

[10] K. Kretschmer, Diehl R., Hartmann D.H. (2003), A&A **412**, L47.

[11] D. Morris *et al.* (1997), AIP Conf.Proc. **410**, 1087.

[12] S. Plüschke *et al.* (2002), New Ast.Rev. **46**, 535.

[13] N. Prantzos (2004), A&A **420**, 1033.

[14] M. Renaud *et al.* (2004), ESA-SP, *in press.*

[15] J.-P. Roques *et al.* (2003), A&A **411**, L91.

[16] v. Schönfelder *et al.* (2000), AIP Conf.Proc. **510**, 54.

[17] D. Smith (2003), ApJ **589**, L55.

[18] D. Smith (2004), ESA-SP, *in press.*

[19] L.-S. The *et al.* (2000), AIP Conf.Proc. **510**, 64.

[20] G. Vedrenne, G., Roques, J.-P., Schönfelder, V., *et al.* (2003), A&A **411**, L63.

[21] J. Vink *et al.* (2001), ApJ **560**, 29.

[22] A. von Kienlin *et al.* (2004), ESA-SP, *in press.*

[23] C. Winkler *et al.* (2003), A&A **411**, L1.

Halo Star Abundances and Heavy Element Nucleosynthesis

J. J. Cowan[1], *C. Sneden*[2]

[1] Department of Physics & Astronomy, University of Oklahoma, Norman, OK 73019
[2] Department of Astronomy and McDonald Observatory, University of Texas, Austin, TX 78712

Introduction

Abundance observations of neutron-capture elements in halo stars are providing a wealth of new information on the nature of heavy element nucleosynthesis in evolved stars. In particular these observations provide clues and constraints to the synthesis mechanisms for the n-capture elements, suggestions for the site (or sites) for the r-process and Galactic chemical evolution. We have been obtaining such stellar abundance data both with ground-based telescopes and recently with the Hubble Space Telescope (HST). We present a small sample of the results of our new observations, along with some preliminary analysis, in this short proceedings paper. A more complete listing of the new HST abundance data and more detailed analyses will be forthcoming in Cowan *et al.* [1].

n-Capture Observations and the r-Process

We show in Figure 1 the latest observations of the well-known r-process-rich Galactic halo star CS 22892−052 [2], along with a scaled solar system r-process abundance distribution (solid line). A total of 57 elements (52 detections and five upper limits) have been observed in CS 22892−052 – more than in any other star except the Sun. As has been noted previously, the agreement between the heavier n-capture elements (Ba and above) and the solar r-process abundances is quite striking [3, 4]. This agreement has been expanded and strengthened with our new HST observations of the 3$^{\rm rd}$ r-process peak elements Os and Pt in CS 22892−052. More accurate and reliable abundance determinations have also been obtained for the elements Nd [5] and Ho [6] as a result of new atomic physics data. Ga and Ge are not observable from the ground and necessitated the HST. While attempts to detect these elements in CS 22892−052 were unsuccessful, meaningful upper limits were established (see Figure 1). Those abundance limits fall far below the solar system r-process curve and suggest that the synthesis of Ga and Ge may be different than that (for example) of the rare-earth elements, and may be tied to the (very low) stellar iron abundance.

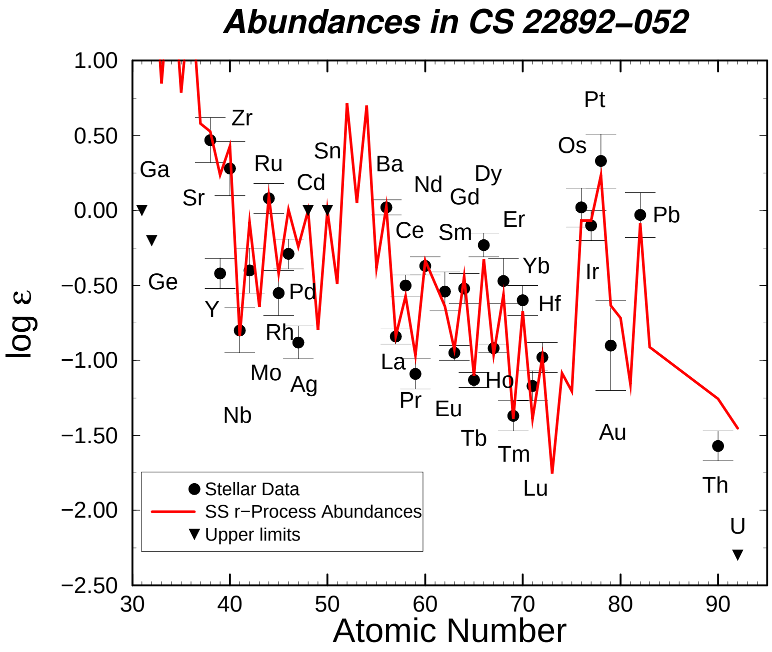

Figure 1: n-capture elemental abundances in CS 22892−052 compared to a (scaled for metallicity) solar system r-process abundance curve (solid line).

The agreement between the solar system r-process curve and the heavy (Z $\geq$ 56) elemental abundances in CS 22892−052 has now been seen in several other halo stars [7], and suggests a robust r-process operating over many billions of years. It also implies a well-defined range of astrophysical conditions (*e.g.*, neutron number densities) and/or that not all supernovae are responsible for the r-process – instead perhaps only a narrow mass range. We note, however, that the well-studied stars showing this pattern are all r-process-rich and much less is know about r-process-poor stars, such as HD 122563.

What has not been as well explored in the halo stars is the elemental abundance regime of Z = 40-50. The new data for CS 22892−052, along with some very sparse data in several other stars, apparently indicate a different abundance pattern between the elements in this regime and those for Ba and above. Thus we see in Figure 1 that the elements from Z =

40-50, in general, fall below the same curve that fits the heavier (upper) end of the n-capture element distribution. This seems to suggest different synthesis sources or origins for the two different ranges of n-capture elements. These results strengthen earlier suggestions of two r-process sites for the lighter and heavier n-capture elements [8]. Those two sites could be different mass ranges or frequencies of supernovae [9] or perhaps a combination of supernovae and neutron-star binary mergers. Alternatively, all of the n-capture elements might be synthesized under different sets of conditions in the same core-collapse supernova (see Cowan and Sneden [6] and references therein for further discussion).

We note in Figure 1 that the elements Sr and Zr appear to lie on the solar r-process curve for CS 22892−052, while Y does not. Extensive observations of these elements versus metallicity in other stars indicates that the nucleosynthetic origin of Sr-Y-Zr is different than heavier elements such as Ba [10]. Furthermore, there is a possibility that a primary process – tentatively identified as a lighter element primary process (LEPP) [10] – might be responsible for some fraction of the synthesis of each of these three elements.

Abundance Trends in Halo Stars

Our new HST abundance observations of a sample of 11 halo stars have provided new information not previously attainable concerning both the very light n-capture elements (such as Ge) and the 3rd r-process peak elements including Pt and Os. While Ge was not detected in CS 22892−052 it was found in many of the other target stars. Zr was also detected in these stars using HST. The results of those observations will be forthcoming [1]. We show here the elemental abundance trends of [Pt/Fe] and [Os/Fe] with respect to [Eu/Fe] in Figure 2. The consistency between the solar system curve and the halo star abundances (for the elements from Ba and above) has, in the past, mostly been predicated on the rare-earth elements detected from the ground. Now with the HST detections of elements such as Os and Pt – with dominant spectral transitions in the near UV – that agreement seems to extend through the 3rd r-process peak. We see a direct comparison of these two latter elements with the r-process element Eu – the abundances of this element were obtained with ground-based observations [11]. It is clear in Figure 2 that the abundances of both Pt and Os seem to be correlated – there is a 45% angle straight-line relationship – with Eu in these metal-poor halo stars. This strongly suggests a similar synthesis origin for all three of those n-capture elements in the halo star progenitors.

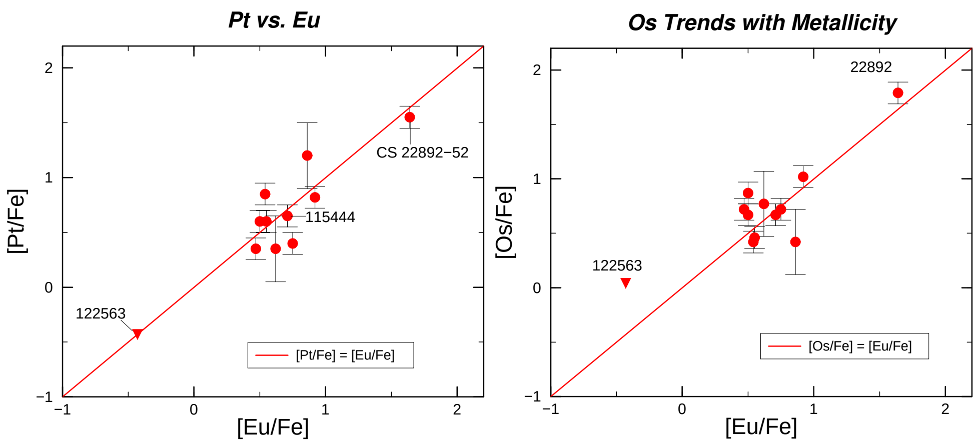

Figure 2: Abundance correlation between [Pt/Fe] (left panel) and [Os/Fe] (right panel) and [Eu/Fe].

Acknowledgments

We thank our collaborators for their contributions to this work. This research has been supported in part by NSF grants AST-9986974 and AST-0307279 (JJC), AST-9987162 and AST-0307495 (CS), and by STScI grants GO-8111 and GO-08342.

References

[1] J.J. Cowan et al., *Ap. J.* (2004) in preparation.

[2] C. Sneden et al., *Ap. J.* **591** (2003) 936.

[3] J.W. Truran, J.J. Cowan, C.A. Pilachowski and C. Sneden, *PASP* **114** (2002) 1293.

[4] C. Sneden and J.J. Cowan, *Science* **299** (2003) 70.

[5] E.A. Den Hartog, J.E. Lawler, C. Sneden and J.J. Cowan, *Ap. J. Supp.* **148** (2003) 543.

[6] J.J. Cowan and C. Sneden, astro-ph/0309802, To appear in *Carnegie Observatories Astrophysics Series, Vol. 4: Origin and Evolution of the Elements*, ed. A. McWilliam & M. Rauch (Cambridge: Cambridge Univ. Press) (2004).

[7] J.E. Lawler, C. Sneden and J.J. Cowan, *Ap. J.* **608** (2004) 850.

[8] G.J. Wasserburg, M. Busso and R. Gallino, *ApJ* **466** (1996) L109.

[9] G.J. Wasserburg and Y.-Z. Qian, *Ap. J.* **529** (2000) L21.

[10] C. Travaglio et al., *Ap. J.* **601** (2004) 864.

[11] J. Simmerer et al., *Ap. J.* (2004) submitted.

s-Process Nucleosynthesis in Massive Stars

Mounib F. El Eid[1], *Bradley S. Meyerd*[2], *and Lih-Sin The*[2]

[1]Department of Physics, American University of Beirut, Bliss Street, Beirut, Lebanon; meid@aub.edu.lb
[2]Department of Physics and Astronomy, Clemson University, Clemson, SC 29634-0978,
tlihsin@clemson.edu; mbradle@clemson.edu

We have reinvestigated the s-process nucleosynthesis in massive stars (the so called weak component of the s-process) under the physical conditions of core helium burning, and also under the more exotic conditions of shell-carbon burning. The characteristics of the s-process is not only sensitive to the reaction rates, but depends also crucially on the underlying stellar models obtained for the phases mentioned above being so relevant for the production of s-process nuclei in this site which are know to lie in the mass range A=60-90. The details of our stellar evolutionary calculations are described in our recent paper(El Eid , Meyer and The, APJ 2004, in press, hereafter referred to as EMT004). We summarize here only the most important features of these calculations

1. We have considered stars of masses of 15,20,25 and 30 $M_\odot$ and of solar-like initial composition. The evolution of these stars was followed beyond central oxygen burning such that we can analyze the characteristics of the weak component of the s-process during the relevant phases of core helium burning and shell-carbon burning.

2. In the evolutionary calculations, we have studied the effects of three important physical parameters which influences remarkably the evolution of massive stars: a) effect of the still unsettled $^{12}C(\alpha,\gamma)^{16}O$ reaction on the evolution during core helium burning and beyond, b) effect of mass loss during the hydrogen and helium burning phases where mass loss is significant, and c) the influence of considering the inhibiting effect of the gradient of the mean molecular weight during shell hydrogen burning by using the Ledoux criterion for convection instead of the Schwarzschild criterion.

3. The thermonuclear reaction rates we have used to perform the s-process calculations have been taken from the compilation of the "NACRE"

collaboration (Angulo et al. 1999) and also from the so called "Non-Smoker" rates according to Rauscher & Thielemann (2000). The s-process in massive stars is strongly affected by the rate of ^{22}Ne$(\alpha,\mathrm{n})^{25}$Mg reaction which is the main she source of neutrons especially during the core helium burning phase. In addition, the reaction ^{16}O$(\mathrm{n},\gamma)^{17}$O seems to have a strong poisoning effect on the s-process.

The reaction rate of ^{12}C$(\alpha,\gamma)^{16}$O, is known to have remarkable effects on the structures of massive stars during the core helium burning phase and beyond. The present situation concerning this rate is depicted in Fig. 1. In our recent evolutionary calculations(EMT004), we have used the NACRE's rate (Angulo et al. (1999) and that obtained by Kunz et al. (2002). Fig. 1 shows that the NACRE's rate is very weakly dependent on temperature in the range T=(1-4)10^8 K relevant to core He-burning in the massive stars. In contrast, the Kunz's rate or that according to Buchmann (1996)are significantly different.

Fortunately, there is no significant effect of utilizing the two different rates as mentioned above on the s-process during core helium burning. However, the Kunz's et al rate being lower all the time during core helium burning, as compared to the NACRE's rate, leads to a larger central mass fraction of ^{12}C (referred to as X$-$12) at the end of this burning phase (0.28 in the first case, but o.236 in the second case and in a 25 $M_\odot$ star). We have found (see details by EMT004) that shell carbon burning is remarkably affected by the value of X_{12} as mentioned above, and this in turns will affect the production of the s-process nuclei in that shell. Details of these results are beyond the scope of this short contribution and will be escribed elsewhere in a forthcoming paper (The, El Eid and Meyer, in preparation). It seems that the production of nuclei like ^{70}Zn, ^{80}Se, ^{86}Kr, 87Rb and ^{96}Zr is rather sensitive to the physical conditions prevailed during shell carbon burning.

The s-process in massive stars is of course sensitive to the release of neutron by the ^{22}Ne$(\alpha,\mathrm{n})^{25}$Mg reaction, especially during core helium burning. Fig.2 illustrates the actual situation concerning the rate of this reaction. The recent NACRE's compilation as compared with that by Caughlan & Fowler (1988) (referred to as CF88), yields a lower rate in the temperature range below T_8=2.5 which comprises the major part of core helium burning in massive stars. However, the NACRE's rate is larger by a factor up to three in the range T_8=(3-6) which is relevant to the ensuing core carbon and shell carbon burning phases. In Fig.2, the rate obtained by Jaeger et al.(2001) is seen to be in close agreement with the NACRE's rate except at relatively lower temperatures, below T_8=2.0, which is fortunately not relevant for our discussion of the s-process in massive stars.

Our calculations of the s-process using the NACRE's rate for $^{22}\mathrm{Ne}(\alpha,\mathrm{n})^{25}\mathrm{Mg}$ show a significantly lower efficiency of the s-process during core helium burning as compared with the rate compiled by CF88. For example, the overproduction factor of ^{80}Kr is 618 in the case of a 25 $M_{\odot}$ star at the end of core helium burning when the CF88 rate is used, while this value is reduced to 174 (by a factor of about 3.6) when the NACRE's rate is utilized. This is in close agreement with the results by Rayet & Hashimoto(2000) showing the smallest overproduction factor for ^{80}Kr found in evolutionary calculations in this mass range. The main reason for this is that in case of the NACRE's rate the neutron exposure is lower, since in the case of the NACRE's $^{22}\mathrm{Ne}(\alpha,\mathrm{n})^{25}\mathrm{Mg}$ rate, high neutron density is obtained only toward the end of core helium burning such that the burning time runs out for the s-process in this phase.

As a conclusion in the context of this short contribution, we can state that the s-process during core helium burning in massive stars is primarily influenced by the $^{22}\mathrm{Ne}(\alpha,\mathrm{n})^{25}\mathrm{Mg}$reaction releasing the neutrons and also to the reaction $^{16}\mathrm{O}(\mathrm{n},\gamma)^{17}\mathrm{O}$ as a neutron-poisoning reaction. It is not very sensitive to the details of the stellar models during this phase. However, the s-process during shell carbon burning is highly dependent on the details of the stellar models during such phase. We will present a detailed analysis of this issue in our forthcoming paper (El Eid, The and Meyer 2004).

Acknowledgments

M.F. EL Eid thanks the URB of the American University of Beirut (AUB) for travel support to the Ringberg meeting . He is grateful to the organizer of the meeting for their help and support.

References

[Angulo et al.(1999)] Angulo, C., et al. 1999, Nucl. Phys. A, 656, 3

[Buchman(1996)] Buchmann, L. 1996, Apj., 468, 127

[CF88(1988)] Caughlan, G. R., & Fowler, W. A. 1988, Atomic Data Nucl. Data Tables 40, 283 (CF88)

[CFHZ85(1985)] Caughlan, G. R., Fowler, W. A., Harris, M., & Zimmermann, B. 1985, Atomic Data Nucl. Data Tables 40, 283 (CFHZ85)

[Jaeger et al.(2001)] Jaeger, M., Kunz, R., Mayer, A., Hammer, J. W., Staudt, G., Kratz, K. L., & Pfeiffer B. 2001, PRL, 87, 202501-1

[Rauscher & Thielemann(2000)] Rauscher, T., & Thielemann, F.-K. 2000, ADNDT, 75, No.1/2, 1.

[Kunz et al.(2002)] Kunz, R., Fey, M., Jaeger, M., Mayer, A., Hammer, J. W., Staudt, G., Harissopulos, S., Paradellis, T. 2002, ApJ, 567, 643

[rayet2000] Rayet, M., Hashimoto, M. 2000, A&A, 354, 740

Can a ”standard” initial mass function explain the metal enrichmernt in clusters of galaxies?

L. Portinari[1], *A. Moretti* [2], *C. Chiosi*[2], *J. Sommer-Larsen*[1]

[1] Theoretical Astrophysics Center, Juliane Maries Vej 30, DK-2100 Copenhagen Ø, Denmark
[2] Department of Astronomy, University of Padova, Vicolo dell'Osservatorio 2, I-35122 Padova, Italy

lportina,jslarsen@tac.dk; moretti,chiosi@pd.astro.it

Abstract

It is frequently debated in literature whether a “standard” Initial Mass Function (IMF) — meaning an IMF of the kind usually adopted to explain the chemical evolution in the local Solar Neighbourhood — can account for the observed metal enrichment and Iron Mass–to–Light Ratio in clusters of galaxies. We address this problem by means of straightforward estimates that should hold independently of the details of chemical evolution models.

It is crucial to compute self–consistently the amount of mass and metals locked–up in stars, by accounting for the stellar mass–to–light ratio predicted by a given IMF. It becomes then clear that a “standard” Solar Neighbourhood IMF cannot provide enough metals to account for the observed chemical properties in clusters: clusters of galaxies and the local environment must be characterized by different IMFs.

Alternatively, if we require the IMF to be universal, in order to explain clusters such an IMF must be much more efficient in metal production than usually estimated for the Solar Vicinity. In this case, substantial loss of metals is required from the Solar Neighbourhood and from disc galaxies in general. This “non–standard” scenario of the local chemical evolution would challenge our present understanding of the Milky Way and of disc galaxy formation.

Summary of the paper by L. Portinari, A. Moretti, C. Chiosi, and J Sommer-Larsen, 2004, ” Can a ”standard” initial mass function explain the metal enrichmernt in clusters of galaxies?”, ApJ, 604, 579-595

Chemical Signatures of the First Stellar Generations. A VLT Observer's Point of View

F. Primas

ESO Garching

The history of the chemical composition of the Galaxy is dominated by the nucleosynthesis occurring in many generations of stars. In each generation, a fraction of the gas will be transformed into metals and returned to the interstellar medium (ISM).

Very metal-poor stars represent one of the main diagnostic tools to probe the earliest phases of the chemical evolution of our Galaxy, as they exhibit the products of nucleosynthesis from the first high-mass, zero-metallicity objects to have evolved and polluted the proto-galaxy. Elemental abundance ratios observed in these low-mass stars allow us to infer important constraints on the ejecta of the earliest supernovae and to determine the nature of the stars and sites of nucleosynthesis that existed during the first epochs of star formation in the Galaxy. Any variation in the elemental abundance ratios observed at different metallicites can then be compared with the yields derived from SNe of different masses to identify which ones have contributed to the Galactic chemical enrichment and when.

The advent of 8-10m class telescopes equipped with very efficient and high resolution spectrographs has significantly impacted the study of chemical patterns in the Galactic halo, allowing us to derive very accurate abundances in large samples of extremely metal-poor stars.

By using the Ultraviolet and Visible Echelle Spectrograph (UVES) at the VLT, Cayrel et al. ([1] and references therein) have focused on the analysis of 65 objects (30 dwarfs and 35 giants), the majority of which has a metallicity lower than 1/1000 solar. One of the most important outcomes of this work is the finding of very well defined abundance trends, with very little dispersion down to the lowest metallicites (cf Fig. 1, where the trend of the α-elements Ca and Ti are shown). Compared to earlier works, these results are in agreement with the trends and slopes already found, but they disagree with the significant scatter previously found in the early Galaxy. This clearly has important implications on the number of SNe that polluted the early Galaxy and the size of the clouds undergoing independent chemical evolution in the first epochs of halo formation. The new abundance trends could imply that these stars have been pre-enriched by single burst events, or that mixing was very efficient already at these early epochs. Another interesting result is the finding of a plateau at the lowest metallicity end in most of the elemental trends when abundances are plotted *vs* magnesium, instead of iron (cf Fig. 13 in [1]). Because these could tell us something about the primordial yields of the first supernovae to go off in the Galaxy, they clearly deserve further investigation, especially on the theoretical side.

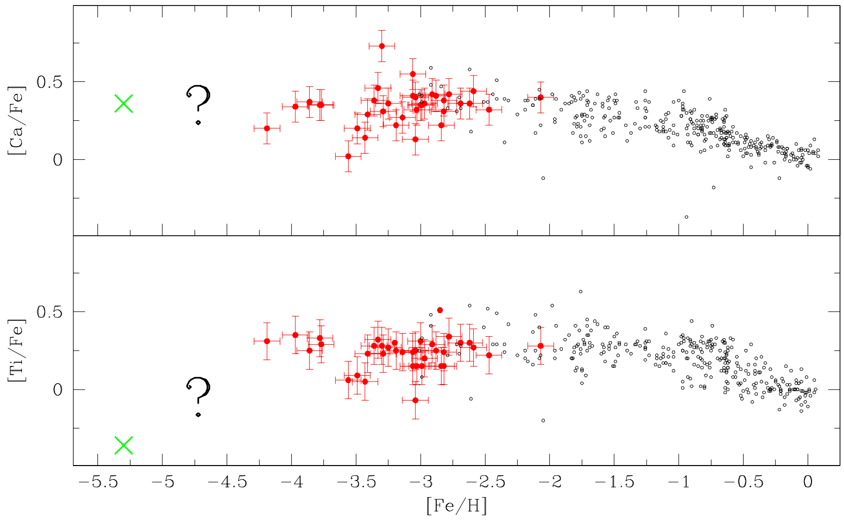

Figure 1: [Ca/Fe] and [Ti/Fe] trends vs [Fe/H] as derived from recent spectroscopic analyses: Cayrel et al. (2004, in red), Christlieb et al. (2004, in green) and a compilation of galactic abundances from the literature (in black).

A second highlight obtained with UVES at the VLT is the detailed chemical analysis of one of the 2 most metal-poor stars ever found, the halo giant HE 0107−5240 ([2] and references therein), with a metal content around 1/200000 solar. The star is characterised by large over-abundances of carbon, nitrogen, and oxygen, but no radial velocity variations have been detected so far. This implies that the mass transfer scenario (in which an AGB star produced the CNO observed today in HE 0107−5240 before evolving to a white dwarf) does not seem to be the most obvious explanation (though it cannot yet be excluded, as the radial velocity monitoring needs to span a longer temporal baseline). The global abundance pattern of the star (in total there are 8 elements detected and 12 upper limits) can be accounted for if pre-enrichment from a zero-metallicity Type II supernova with a progenitor mass around 20-25 $M_{\odot}$ is considered.

Another VLT-based important result is the finding of a new n-capture rich star, in which it has been possible to detect Uranium, for the first time in the stellar atmosphere of an extremely metal-poor star (cf [3]). The star CS 31082-001 was found to be characterised by an enhancement in its heavy element r-process abundances by a factor of 50 with respect to the Sun. Despite these stars represent only a small percentage of the most metal-poor Galactic halo population, they are important diagnostic tools to study heavy elements nucleosynthesis in the early Galaxy.

In summary, with the telescopes and instruments currently available, we can investigate the early chemical evolution of the Galaxy following two main approaches: we can achieve very detailed chemical abundance analyses of single objects for a very large number of chemical species (like in the n-capture rich stars mentioned above, in which we can measure the abundances from the very light elements LiBeB down to the heaviest nuclei like Uranium), and/or we can study in a reasonable amount of telescope time large samples of the most metal-poor stellar population. What is now missing is to find out why objects between [Fe.H]=-4.3 and -5.3 have yet to be found (cf Fig. 1).

Acknowledgements

Excellent meeting, scientific atmosphere and location! Thanks!

References

[1] R. Cayrel, E. Depagne, M. Spite, V. Hill, F. Spite, P. Francois, B. Plez, T.C. Beers, F. Primas, J. Andersen, B. Barbuy, P. Bonifacio, P. Molaro, and B. Nordstroem, A&A **416** (2004) 1117.

[2] N. Christlieb, B. Gustafsson, A. Korn, P.S. Barklem, T.C. Beers, M.S. Bessell, T. Karlsson, and M. Mizuno-Wiedner, ApJ **603** (2004) 708.

[3] R. Cayrel, V. Hill, T.C. Beers, B. Barbuy, M. Spite, F. Spite, B. Plez, J. Andersen, P. Bonifacio, P. Francois, P. Molaro, B. Nordstroem, and F. Primas, Nature **409** (2001) 691.

Supernova Feedback during Galaxy Formation

D.H. Hartmann[1], *J.P. Johnson*[1], *L.-S. The*[1], *and J.M. Myers*[2]

[1] Department of Physics & Astronomy, Clemson University, Clemson, SC29634-0978
[2] Department of Physics & Astronomy, Francis Marion University, Florence, SC29501

The formation and evolution of galaxies is the result of a complex interplay between the physics of stellar and gaseous systems, embedded in an expanding universe. While observations of large scale structure, supernovae, and the cosmic micro-wave background suggest that a concordance model of a universe dominated by dark matter and dark energy is in hand, a sufficient understanding of how the basic building blocks of the baryonic component (diffuse gas, stars, galaxies) evolved is not yet in sight. In particular, the formation of the first stars, the formation and evolution of black holes (over a wide range in mass), the reionization history of the universe, and the assembly of galaxies are all targets of intense study, and in essentially all cases are far from a sufficient understanding.

Deep surveys with ground- and space-based telescopes yield insights into the complex history of galaxies and clusters of galaxies. Most galaxies do not evolve in isolation, so that their merger history may have played a major role in the creation of their present-day structures and dynamic features. Merging introduces many new degrees of freedom, so that a first step along the rocky road to galaxy formation should perhaps focus on understanding isolated galaxies. The Milky Way may qualify as such a test case. In particular, the halo of the Galaxy provides detailed information of early galactic evolution that is hard to obtain even for nearby galaxies. We thus concentrate on the halo of our Galaxy as a test case for early formation of (nearly) isolated galaxies.

We have described our attempts to model proto-galactic collapse with the SPH/N-body code GADGET in [3]. Following earlier work by [5] in which spherical symmetry was assumed and dark matter was ignored, the new simulations with GADGET are significantly more realistic. However, it is not sufficient to model gas-star-dark matter systems in 3D, but one must also be careful about the implementation of the interaction between the gaseous and stellar components. As many groups noted before, we also find that energy feedback from supernovae has essentially no dynamic impact on the hydrodynamics of the collapsing proto-galaxy as long as one assumes that the returned energy is quickly thermalized (e.g., [4]. Efficient cooling mechanisms remove the energy injected into the gas on time scales much shorter than the dynamic time scale. Supernovae (and also pre-SN winds from massive stars) are thus unable to pressurize the ISM and to slow down the collapse. The need for breaking free-fall, and thus preventing over-cooling, is driven by the fact that rapid collapse (the Eggen Lynden-Bell Sandage scenario) does not produce the observed galactic angular momentum distribution and does not match important observational constraints such as the age distribution of globular clusters.

The observed age spread of the halo sub-class of the Galactic globular cluster system (e.g., [7]) indicates that halo formation may have taken several Gyrs, which is much longer than the $\sim 10^8$ yr free- fall time scale of our proto Galaxy. A mechanism to slow down the collapse may thus be required to explain the observed age spread. This argument assumes that cluster formation traced halo hydro-dynamics, which may only partly be right as an extended merger history is a (perhaps favored) alternative to a more or less monolithic collapse. In any case, the question arises whether supernovae and/or other feedback mechanisms can naturally provide a breaking mechanism during the era of halo formation over a period of a few Gyrs. [5] concluded that this is indeed the case. However, their positive answer to this question resulted from at least two overly simplistic assumptions. Their models were spherically symmetric, so that energy returned from supernovae was felt in a full shell rather than just in the vicinity of the explosion. The feedback was communicated too efficiently on large scales. Furthermore, they also assumed that a large fraction of the canonical 10^{51} ergs per explosion was available as pressure, stored in some form of turbulence. Our simulations show that the relaxation of the assumption of spherical symmetry, together with efficient cooling (SN energy is returned in regions of enhanced gas density, due to star formation scaling laws, so that cooling rates are increased as well) renders SN-feedback ineffective.

We also studied a two-reservoir scenario, in which the feedback energy from supernovae and stellar winds is converted to turbulent energy instead of thermal energy. While turbulence plays an important role in the present-day galaxy, and probably also in the young Galaxy (see [1], and [8] for recent reviews), first order estimates and further discussions at this meeting made it clear that this energy reservoir is depleted on time scales comparable to those for thermal losses. Therefore, a simple thermal/turbulence model also does not solve the "problem" of the large halo age spread. Furthermore, it is not even clear that the concept of a "turbulent pressure" is applicable (e.g., [1]). Detailed multi-component ISM models [6] appear to provide an alternate and perhaps more promising road towards realistic galaxy models.

During subsequent discussions at the meeting, Wolfgang Hillebrandt suggested that cosmic rays may provide an alternative. Supernova remnants are believed to be the source for most of the observed cosmic ray (CR) component of our Galaxy, and the energy fraction transferred to CRs is often claimed to be close to 100%. If CR cooling is less efficient than gas cooling and decay of turbulence, it is indeed conceivable that relativistic particles played a major dynamic role in the early Galaxy. This topic needs to be studied in greater detail. Here we just remind ourselves that the present-day CR energy density is of order 0.5 - 1.5 eV/cm^3 with corresponding "pressure" of 3-9 10^{-13} ergs/cm^3 (energetics is dominated by nucleons, with electrons and positrons contributing significantly less), which is comparable to the thermal and magnetic pressures in the ISM ([9]; [2]). CRs diffuse in the Galaxy with a mean lifetime of order 10^7 yrs ([8]), and experience reacceleration near localized shock structures. Whether the CR component can really affect halo collapse requires a self-consistent study of CR production and transport (in space and energy) within the collapsing halo.

The CR component can in turn generate turbulence, and thus provide a non-local energy feedback mechanism. Even if CRs turn out to be unable to solve the "halo age spread problem", it seems likely that realistic scenarios of galaxy formation need to include non-local feedback that follows from star formation and subsequent energy release at a later time and at a different location (stellar dynamics), as well as transport via gas dynamics and particle diffusion (CRs). Modelling galaxy formation appears to be a daunting task, but we are encouraged by progress made in modeling supernovae, which also present a hyper-challenge.

Acknowledgements

It is a pleasure to thank the organizers and the staff of Ringberg castle for a stimulating and enjoyable conference. In particular, we thank Wolfgang Hillebrandt for suggesting the possibility that CRs may have to be taken into account. Thanks, and happy times!

References

[1] B.G. Elmegreen, and J. Scalo 2004, ARAA, in press (astro-ph:0404451)

[2] R. Diehl, E. Parizot, R. Kallenbach, and R. von Steiger 2001, *The Astrophysics of Galactic Cosmic Rays*, (Kluwer Academic Publishers), reprinted from Space Science Reviews 99, No. 1-4, 2001

[3] D.H. Hartmann, J.M. Myers, and L.-S. The, 2003, in *From Twilight to Highlight: The Physics of Supernovae*, eds. W. Hillebrandt and B. Leibundgut, ESO Astrophysics Symposia, Springer Verlag, pp. 384

[4] R.C. Kennicutt 1997, in *The Interstellar Medium in Galxies*, ed. J.M. van der Hulst (Kluwer Academic Publishers), pp. 171

[5] G. Malinie, D.H. Hartmann, and G. Mathews 1991, ApJ **376**, 520

[6] S. Marri, and S.D.M. White 2003, MNRAS, **345**, 561

[7] M. Salaris, and A. Weiss 2002, *A&A* **388**, 492

[8] J. Scalo, and B.G. Elemgreen 2004, ARAA in press, astro-ph/ 0404452

[9] R. Schlickeiser 2002, *Cosmic Ray Astrophysics*, A&A Library, Springer Verlag

Cu/Zn versus Metallicity. Diverse Nucleosynthesis Sources

Gallino, R.[1], *Bisterzo, S.*[1], *Pignatari, M.*[1], *Pompeia, L.*[2], *Cunha, K.*[3], *Smith, V.V.*[4]

[1] Dipartimento di Fisica Generale, Via P. Giuria, 1, 10125 Torino (Italy)
[2] Universidade de Sao Paulo, Sao Paulo, Brazil
[3] Observatorio Nacional, Rio de Janeiro, Brazil
[4] Dept. of Physics, University of Texas in El Paso, El Paso, USA

Abstract

We compare spectroscopic observations of Cu and Zn in different stellar populations with present nucleosynthesis theory. Cu is the best signature of the weak s-component origin in massive stars, with a small primary contribution by explosive nucleosynthesis. Zn needs a more complex description. AGBs contribute little Cu or Zn. No need of extra contributions by SNIa is required.

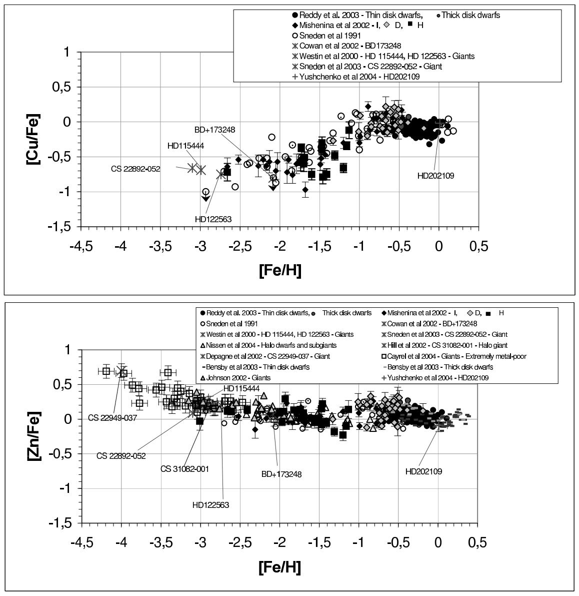

Figure 1: *Top panel.* Collection of spectroscopic observations of [Cu/Fe] versus [Fe/H] for field stars in the Galactic Halo, thick-disk and thin-disk. Different symbols correspond to different classes of objects and/or different authors, as indicated in the inset. *Bottom panel.* The same for [Zn/Fe].

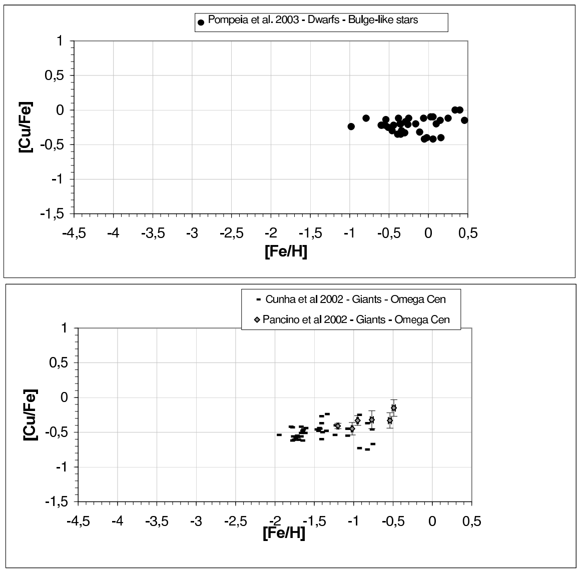

Figure 2: *Top panel.* Spectroscopic observations of [Cu/Fe] versus [Fe/H] for bulge-like stars [8]. *Bottom Panel.* The same for Omega Cen [9, 10].

Copper and Zinc behave strongly differently each other in field stars of various metallicities and stellar populations (Fig. 1). This means that their nucleosynthesis origin is to be ascribed to different astrophysical sources, despite the fact that Cu and Zn ($Z = 29$ and 30, respectively) are situated in the tail of the iron peak. Current hypotheses on the astrophysical origin of both elements are highly debated. In particular it has been advanced that most solar Cu is synthesized in Type Ia Supernovae [1, 2], although standard theory predicts very little contribution to Cu [3]. Our collection of recent spectroscopic observations of [Cu/Fe] and [Zn/Fe] versus [Fe/H] include unevolved stars in the Galactic halo, thick disk and thin disk. Spectroscopic data of [Cu/Fe] in the halo mainly derive from refs. [4, 2] and can be represented by a flat distribution at [Cu/Fe] $= -0.65 \pm 0.15$ for metallicities up to [Fe/H] ~ -1.8, followed by a linear increase in the range $-1.5 <$ Fe/H] < -1. For disk metallicities there is a bending towards a flat distribution. These spectroscopic observations can be understood in the frame of a Galactic Chemical Evolution model (GCE) [5], using SNII yields for different masses and metallicities by [6]. For halo stars, a small primary yield of both ^{63}Cu and ^{65}Cu, of 5 to 10% to solar Cu, may be inferred from the yields by [6]. Under the current assumption that the α-elements like O, Mg, are entirely produced by SNII, while solar iron is contributed by only

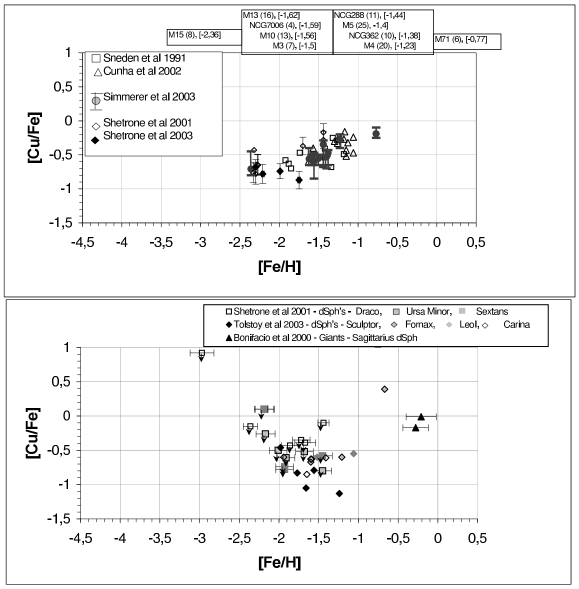

Figure 3: *Top panel.* Collection of spectroscopic observations of [Cu/Fe] versus [Fe/H] for giants of various globular clusters. The range of data for several stars of each globular cluster by [11] are indicated. The name of the clusters and the number of stars observed are reported in the top inset. Other data are from [4, 9, 12, 13]. *Bottom panel.* The same for giant stars belonging to different dwarf Spheroidal systems [12, 14, 15].

1/3 (the residual 2/3 being synthesized in the long-lived SNIa), one would expect in the halo [Cu/Fe] $= -0.6 \pm 0.15$, in strict agreement with spectroscopic observations. One may then ask what is the origin of 90% of solar Cu. Using the yields of ^{63}Cu and its parent unstable nucleus ^{63}Ni, ^{65}Cu and its parent nucleus ^{65}Zn calculated by [6] at [Fe/H] $= -1$ and at solar metallicity and considering their distribution in the various mass zones for a typical 25 $M_{\odot}$, one sees that the larger production of Cu in massive stars derives from the regions having suffered He burning or convective C burning. There, an efficient s-process (the so-called weak s-process) is driven by the activation of the ^{22}Ne(α,n)^{25}Mg reaction. Since ^{22}Ne derives from the original CNO nuclei transmuted into ^{14}N in the ashes of H burning followed by double α-capture on ^{14}N during core He burning, the weak s-process depends linearly on metallicity. The secondary-like production of Cu implies a linear increase of [Cu/Fe] versus [Fe/H] in the interstellar medium. The bending in the [Cu/Fe] in the disk is the result of the linear increase of secondary

Cu with metallicity accompanied by the rapid increase of primary Fe by SNIa. The prediction of the GCE trend of [Cu/Fe] versus [Fe/H] by [5] is a satisfactory fit to the observational trend. The main s-process in AGB stars provides a marginal contribution to solar Cu and Zn, of 5 and 3%, respectively [7]. Summing up, solar copper is mostly the outcome of the weak s-process in massive stars and there is no need of SNIa contribution. Fig. 2 shows the existent spectroscopic data of Cu in bulge-like stars [8] (top panel) and Omega Cen [9, 10] (bottom panel), while Fig. 3 shows Cu data for globular clusters [11, 12, 13, 9, 4] (top panel) and dwarf spheroidal systems [12, 14, 15] (bottom panel). While globular cluster data nicely overlap with Galactic field stars in the same range of metallicity, in both bulge-like and Omega Cen stars this is true only for stars with the lowest metallicity. No enhancement in [Cu/Fe] is shown by the many s-element-rich stars in Omega Cen [9]. There, the most metal-rich stars by [10] show the appearance of the weak s-process. The subsequent flatter distributions most likely reflects a different star formation history in those systems. At the state of the art, dSph systems do not behave so differently from Galactic populations.

Despite the [Zn/Fe] trend versus [Fe/H] in field stars of different populations (see Fig. 1 bottom panel) is much flatter than [Cu/Fe], Zn is an extremely interesting element. To infer its nucleosynthetic origin one needs to consider the composite contribution of its various isotopes. ^{64}Zn (48.6% of solar Zn) receives a little contribution from the weak-s component. It mostly derives from α-rich freezeout in neutrino winds [16], all other Zn isotopes belonging to the weak s-component. Note that there is no apparent departure from the Galactic trend of the very metal-poor and r-process-rich stars labeled in Fig. 1, or of Ba stars enriched in s-process elements (like HD 202109 in Fig. 1 [17]). The recent result by [19] of a linear increase of [Zn/Fe] with decreasing metallicity for [Fe/H] < -3 may indicate a higher efficiency of α-rich freezout in the more massive SNII. The [Zn/Fe] observed in bulge-like stars [18] overlap with spectroscopic observations in disk stars. In dSph systems there are stars with somewhat lower [Zn/Fe] than in the Milky Way [12, 14]. *Acknowledgements.* Work supported by Italian MURST-Cofin2004 Project Nucleosynthesis in the Early Phases of the Universe.

References

[1] Matteucci, F., Raiteri, C., Busso, M., Gallino, R. and Gratton, R. A&A **272** (1993) 421.

[2] Mishenina, T.V. et al. A&A **396** (2002) 189.

[3] Thielemann, F.-K., Nomoto, K. and Yokoi, K. A&A **158** (1986) 17.

[4] Sneden, C., Gratton, R.G. and Crocker, D.A. A&A **246** (1991) 354.

[5] Timmes, F.X., Woosley, S.E. and Weaver, T.A. ApJS **98** (1995) 617.

[6] Woosley, S.E. and Weaver, T.A. ApJS **101** (1995) 181.

[7] Travaglio, C. et al. ApJ **601** (2004) 864.

[8] Pompeia, L., *Copper and Zinc in Bulge-like Stars*, astroph/0305567 (2003).

[9] Cunha, K. et al. AJ **124** (2002) 379.

[10] Pancino, E. et al. ApJ **568** (2002) 101L.

[11] Simmerer, J. et al. AJ **125** (2003) 2018.

[12] Shetrone, M.D., Coté, P. and Sargent, W.L.W. ApJ **548** (2001) 592.

[13] Shetrone, M.D. et al. AJ **125** (2003) 684.

[14] Tolstoy, E. et al. AJ **125** (2003) 707.

[15] Bonifacio, P. et al. A&A **359** (2000) 663.

[16] Woosley, S.E. and Hoffman, R.D. ApJ **395** (1992) 202.

[17] Yuschenko, A.V. et al. A&A **413** (2004) 1105.

[18] Pompeia, L., Barbuy, B. and Grenon, M. ApJ **592** (2003) 1173.

[19] Cayrel, R. et al. A&A **416** (2004) 1117.

Nucleosynthesis in Pop III Stars

A. Heger[1,2], *S.E. Woosley*[3], *R.D. Hoffman*[4], *T. Rauscher*[5]

[1] Theoretical Astrophysics Group, T-6, MS B227, Los Alamos, NM 87545, U.S.A.
[2] Enrico Fermi Institute, The University of Chicago, 5640 S. Ellis Ave, Chicago, IL 60637, U.S.A.
[3] Astronomy Department, University of California, Santa Cruz, CA 95064m U.S.A.
[4] Nuclear Theory & Modeling Group L-414, Lawrence Livermore National Laboratory, Livermore, CA 94551, U.S.A.
[5] Department of Physics and Astronomy, Universität Basel, Klingbergstr. 82, CH-4056 Basel, Switzerland

Extended Abstract

The first stars to form in the universe (Pop III stars) are only composed of the material made by the big bang and are essentially free of any metals, i.e., material other than hydrogen and helium. Due to the different cooling physics during star formation for such a composition, these first stars were likely significantly more massive than present-day stars (e.g., [1, 2]), however, their initial mass function is still very uncertain. Once formed, these Pop III stars probably had small to negligible mass loss (e.g., [3, 4]). In the calculations presented here we therefore neglect any mass loss and due to lack of any better information we assume a "Salpeter" initial mass function [5].

To determine accurate nucleosynthesis from Pop III supernovae we compute a fine grid of 100 initial stellar masses from 10 to 95 solar masses using the KEPLER code [6, 7]. When the stars reach iron core collapse we employ a parametric "piston" model to initial the explosion. The piston is positioned at an entropy of $S = 4$, typically corresponding to the base of the oxygen-burning shell and coinciding with sudden drop in density. The piston movement is adjusted to reproduce a given explosion energy. Ejecta and fallback (what comes out and what goes back in onto the stellar remnant) are determined by following the hydrodynamics of the explosion so that we obtain self-consistency between the ejected mass ("mass cut") and the explosive nucleosynthesis in the supernova shock. However, we assume that mixing processes occur in the ejecta prior to fallback which are adjusted to produce appropriate mixing to reproduce light curves of observed

core collapse supernovae. Details of the calculations and the results will be published in [8].

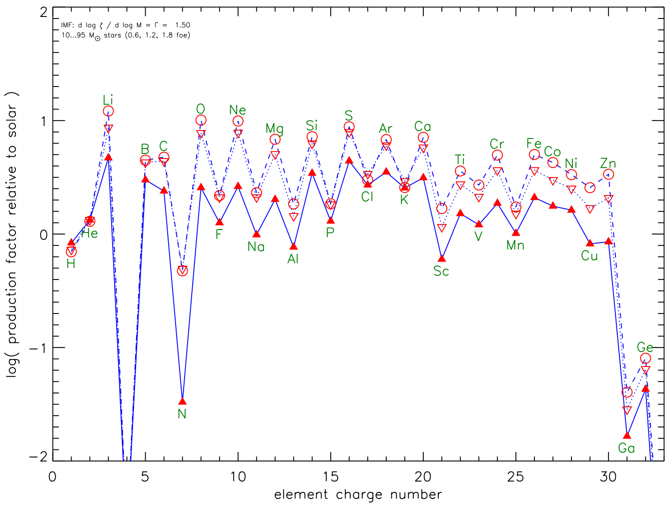

Figure 1: Yield of metal free stars in the mass range 10 - 95 $M_\odot$ integrated over a Salpeter initial mass function (IMF) with $d \ln \zeta / d \ln M = \Gamma = 1.5$. We show the results for explosion energies of 0.6, 1.2, and 1.8 $\times 10^{51}$ erg as solid, dotted and dashed lines.

In Figure 3 we show the remnant masses as a function of assumed supernova explosion energy (final kinetic energy of ejecta for an explosion into vacuum) and compare it to helium and CO core masses. We find that in most cases with large fallback the entire helium core tends to fall back and in some cases that only CO core falls back; only in a fraction of the cases we find significant partial fallback (say, half of the He or CO core falls back). At low explosion energies we seem to obtain a gradual increase of the remnant masses – that is, a almost continuous spectrum of remnant masses – while at high explosion energies the distribution changes rapidly from little fallback to fallback of the entire He core for bigger initial masses.

The resulting nucleosynthesis of these model is shown in Fig. 1 for three different explosion energies: For higher energies the overall production of metals is increased. However, for elements from oxygen to calcium the production of alpha elements (with even charge number) increases more than that of elements with odd mass number and a more pronounced "odd-even" effect results. Not including possible r-process contributions, our models only produce negligible amounts of elements heavier than zinc.

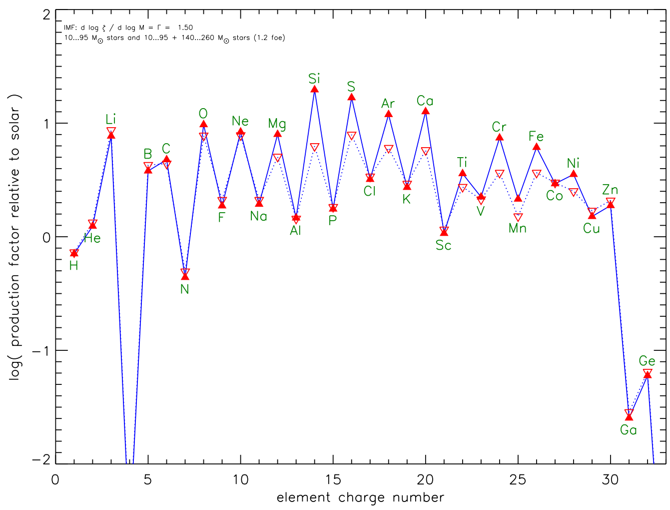

Figure 2: Yields of metal-free stars in the mass range of 10 - 95 $\mathrm{M}_\odot$ integrated over an initial mass function for and explosion enegry of 1.2 $\times 10^{51}$ erg (dotted line; see Fig. 1) and combiend with yield from pair-instability supernovae (mass range of 140 - 260 $M_\odot$), continuing the IMF in this mass range but assuming no ejecta for stars of 100 - 140 $\mathrm{M}_\odot$

When combined with the yields of pair instability supernovae from previous work [9], an even stronger odd-even effect results (Fig. 3). Current surveys of extremely metal poor stars in our galaxy (e.g., [10]) do not show such an abundance pattern, limiting the possible contribution of pristine Pop III pair instability supernovae ejecta material to the initial abundances of there stars. On the other hand, the abundance pattern of some of the metal-poor stars seem to be surprisingly well matched by high-energetic explosions ("hypernovae") of rather massive Pop III stars ($M \sim 30 - 50\,\mathrm{M}_\odot$; e.g., [11, 12]) and assuming significant mixing and fallback. Therefore detailed modeling of such events is needed to better understand the origin of the enrichment of extremely metal-poor stars and possibly place limits on the initial mass function of Pop III stars based on nucleosynthesis constraints.

Acknowledgements

We thank Thomas Janka for extended discussions on the explosion model for supernovae and the location of the "piston" assumed in this work.

AH performed this work under the auspices of the U.S. Department of Energy at the Los Alamos National Laboratory operated by the University of California under contract No. W-7405-ENG-36, in part through support by the Department of Energy under grant B341495 to the Center for Astrophysical Thermonuclear Flashes at the University of Chicago, and by support through a Fermi Fellowship at the University of Chicago. SEW is supported by the NSF (AST 02-06111), NASA (NAG5-12036), and the DOE Program for Scientific Discovery through Advanced Computing (SciDAC; DE-FC02-01ER41176). RDH performed this work under the auspices of the U.S. Department of Energy at the University of California Lawrence Livermore National Laboratory under contract No. W-7405-Eng-48. TR acknowledges support by the Swiss NSF (grant 2000-061031.02, PROFIL professorship 2024-067428.02).

References

[1] T. Abel, G.L. Bryan, M.L. Norman 2002, Sci, 295, 93

[2] V. Bromm, P.S. Coppi, R.B. Larson 1999, ApJ, 527 L5

[3] R.P. Kudritzi 2002, ApJ, 577, 389

[4] I. Baraffe, A. Heger, S.E. Woosley 2001, ApJ, 550, 890

[5] E.E. Salpeter, ApJ, 134, 669 (1961).

[6] T.A. Weaver, G.B. Zimmerman, S.E. Woosley 1978, ApJ, 225, 1021

[7] T. Rauscher, A. Heger, R.D. Hoffman, S.E. Woosley, ApJ, 576, 323 (2002)

[8] A. Heger and S.E. Woosley 2004, in preparation for ApJ

[9] A. Heger and S.E. Woosley, ApJ, 567, 532 (2002)

[10] R. Cayrel, *et al.* 2004, A&A, 416, 1117

[11] E. Depagne, *et al.* 2002, A&A, 390, 187

[12] H. Umeda, K. Nomoto 2003, Natur, 422, 871

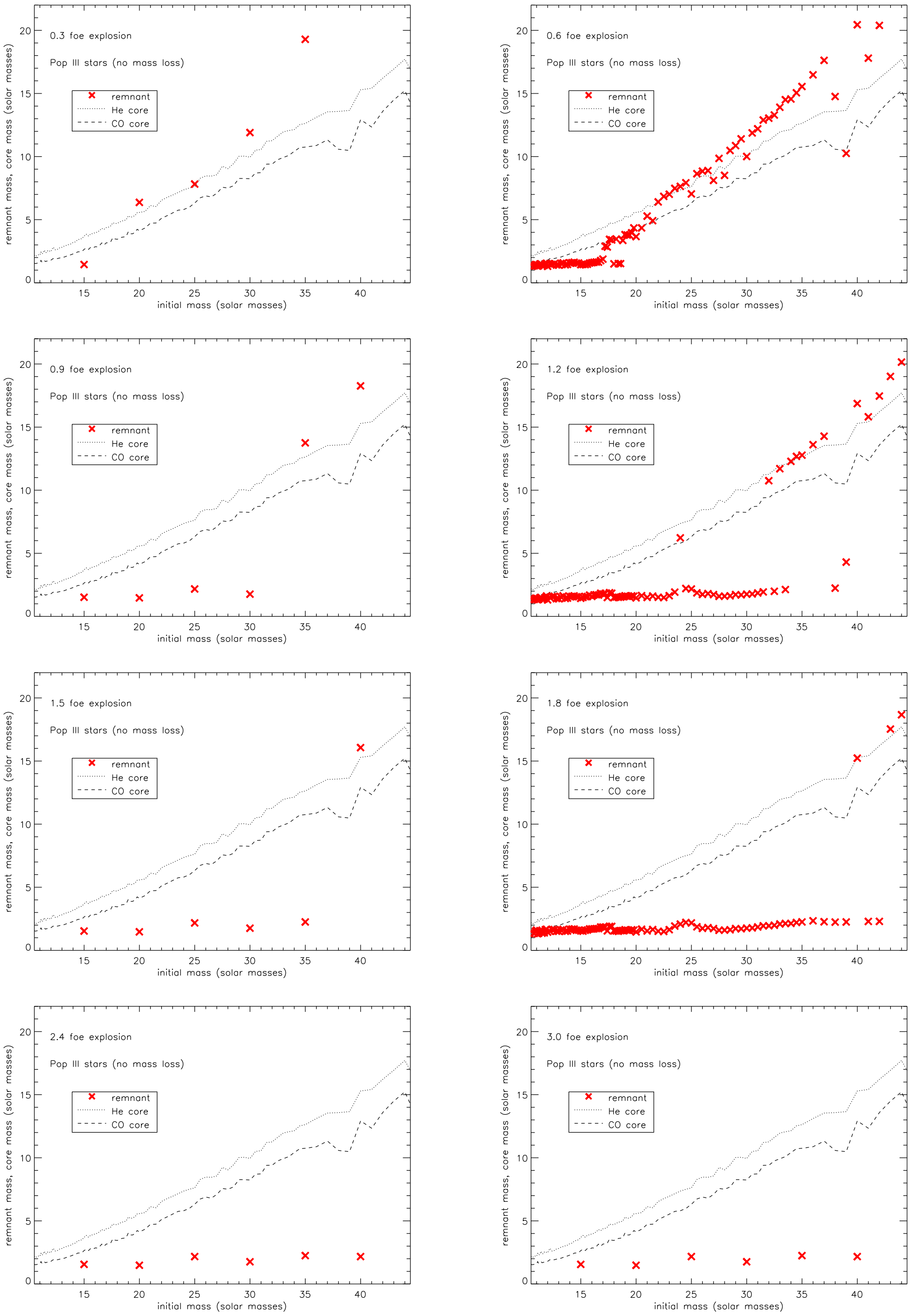

Figure 3: Remnant masses as a function of initial mass for Pop III stars for different assumed explosion energies.

The EK-1-4-1 Story

K.-L. Kratz[1], *W. Böhmer*[1], *C. Freiburghaus*[2], *P. Möller*[3], *B. Pfeiffer*[1], *T. Rauscher*[2], *F.-K. Thielemann*[2]

[1] Institut für Kernchemie, Universität Mainz, Fritz-Strassmann-Weg 2, D-55128 Mainz, Germany
[2] Departement für Physik und Astronomie, Universität Basel, Klingelbergstraße 82, CH-4056, Switzerland
[3] Theoretical Division, Los Alamos National Laboratory, Los Alamos, NM 87545, USA

Abstract

In the framework of our investigation to explain the nucleosynthetic origin of the correlated Ca-Ti-Cr isotopic anomalies in the Ca-Al-rich "FUN" inclusion EK-1-4-1 of the Allende meteorite, the nuclear-physics basis in the neutron-rich $N = 28$ region has been updated by including recent experimental data on β-decay properties and microscopic predictions of neutron-capture cross sections. Charged-particle and subsequent r-process calculations within an entropy-based approach were performed using a complete reaction network. It is shown that there exist two astrophysical scenarios within which the observed isotopic anomalies can be reproduced simultaneously; one at low entropies ($S \simeq 10$) which confirms the earlier suggested SN Ia mechanism, and another at high entropies ($S \simeq 150$) which would be compatible with the neutrino-wind scenario of a SN II.

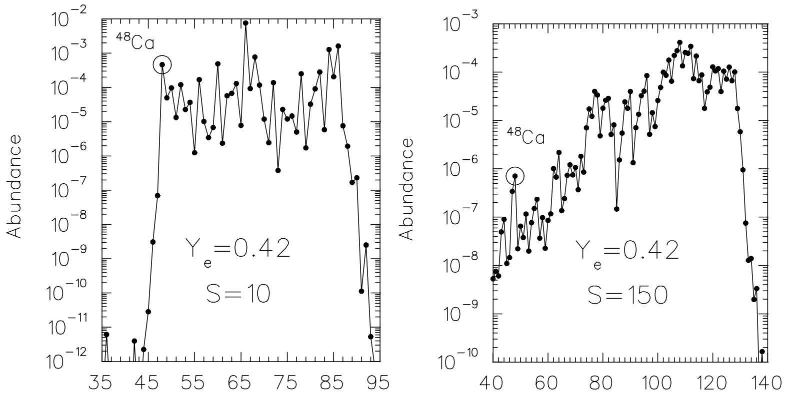

Figure 1: Isotopic abundances calculated for a proton-to-nucleon ratio $Y_e = 0.42$ and entropies of $S = 10\,k_\mathrm{B}$/baryon (left part) and $S = 150\,k_\mathrm{B}$/baryon (right part).

Breaking Gravity Waves: A Mechanism for Nova Enrichment

A.C. Calder[1,2], *A. Alexakis*[1,3], *A. Heger*[4,5], *E.F. Brown*[6], *L.J. Dursi*[1,2], *J.W. Truran*[1,2,6], *R. Rosner*[1,2,3,6], *J. Jose*[7,8]

[1] Center for Astrophysical Thermonuclear Flashes, University of Chicago, Chicago, IL 60637
[2] Department of Astronomy and Astrophysics, University of Chicago, Chicago, IL 60637
[3] Department of Physics, University of Chicago, Chicago, IL 60637
[4] Los Alamos National Laboratory, Los Alamos, NM 87545
[5] Enrico Fermi Institute, University of Chicago, Chicago, IL 60637
[6] Department of Physics and Astronomy, Michigan State University, East Lansing, MI 48824
[7] Institut d'Estudis Espacials de Catalunya (IEEC), 08034 Barcelona, Spain
[8] Dept. Física i Enginyeria Nuclear, Universitat Politècnica de Catalunya, E-08800 Vilanova i la Geltru, Spain

Classical novae occur when an accreted H-rich envelope on the surface of a white dwarf experiences a thermonuclear runaway. Observations indicate the ejecta of some classical novae can be significantly enriched in the intermediate-mass elements C, N, O, and Ne [1]. In addition, CNO elements act as catalysts for the nuclear reactions, and significant enrichment must occur to produce the energetics of fast novae [2, 3, 4]. The requisite enrichment could result from mixing white dwarf material into the accreted H/He envelope [5], and explaining the mechanism for this mixing is an outstanding problem in nova research.

Recently, Rosner et al. [6] suggested that the enrichment might result from a resonant interaction between large-scale shear flows in the accreted envelope and gravity waves on the surface of the white dwarf. Studying the interaction between wind and waves on the ocean, Miles demonstrated that in the presence of a shear flow, gravity waves with a group velocity matching a velocity in the shear flow are resonantly amplified [7]. These waves form cusps and break, which leads to mixing. On an accreting white dwarf, the accumulated H/He overlays the white dwarf substrate, which is composed of C/O (or O/Ne for $M_{WD} \geq 1.1 M_{\odot}$). The difference in the mean molecular weight implies that the interface supports gravity waves, and the breaking of C/O waves here would lead to enrichment of the envelope.

We investigated applying this mechanism to the nova case with two-dimensional simulations performed with the FLASH code [8, 9]. The initial conditions consisted of a "wind" applied to an isentropic envelope in hydrostatic equilibrium and a perturbation applied to the interface consisting of specific modes and a small velocity representing the motion of the gravity waves. The wind profile is described by

$$U(z) \;=\; U_{\max}(1 - e^{-z/\delta}), \tag{3}$$

where z is the vertical direction ($z = 0$ corresponds to the initial interface), $U_{\max}$ is the asymptotic maximum velocity at $z \gg \delta$, and δ is the length scale of the shear boundary layer. The wind profile is an initial condition and is not forced during the simulation.

We performed the study in two parts. The first consisted of simulations of an H/He layer over C/O with a density ratio of 0.6 between the surface white dwarf material (as would be expected in the degenerate conditions prior to ignition). Using dimensional analysis and the numerical results, we found that the total mass per unit area, $dM_{\mathrm{C/O}}/dS$, mixed into the accreted H/He saturates at

$$\frac{dM_{\mathrm{C/O}}}{dS} \;=\; \alpha \frac{U_{\max}^2}{g} \rho_{\mathrm{WD}}\;, \tag{4}$$

where α is a non-dimensional constant. We found $\alpha \simeq 0.6$, but note that in general it depends on ρ_2/ρ_1 and possibly on the Mach number. Our study had Mach numbers ≤ 0.4. From eq.4, we construct an expression for the fraction of the envelope mixed as a function of the Mach number $\mathsf{Ma} = U_{\max}/C_{\mathrm{s}}$. Multiplying $dM_{\mathrm{C/O}}/dS$ by C_{s}^2, we have

$$\frac{dM_{\mathrm{C/O}}/dS}{dM/dS} = \alpha\gamma(\mathsf{Ma})^2 \frac{\rho_2}{\rho_1}\;, \tag{5}$$

where $\gamma = 5/3$ is the adiabatic exponent, dM/dS is the mass per unit area of the accreted envelope, and $\rho_2/\rho_1 \approx 1.7$ is the ratio of the densities of the C/O and H layer at the interface. For $\mathsf{Ma} = 0.4$, we see that the mass of C/O entrained into the atmosphere is $\approx 25\%$ of the mass of the envelope.

We applied the results of these mixing simulations to enrichment in one-dimensional models evolved by a stellar evolution code, KEPLER, with a large nuclear network [10, 11]. We investigated two scenarios, one in which the only shearing considered is that from convective cells driving the wind at the interface and one in which the shearing originates from a wind during the accumulation of the envelope.

Our results indicate that breaking resonant gravity waves lead to significant mixing under nova-like conditions. We found that this process can mix

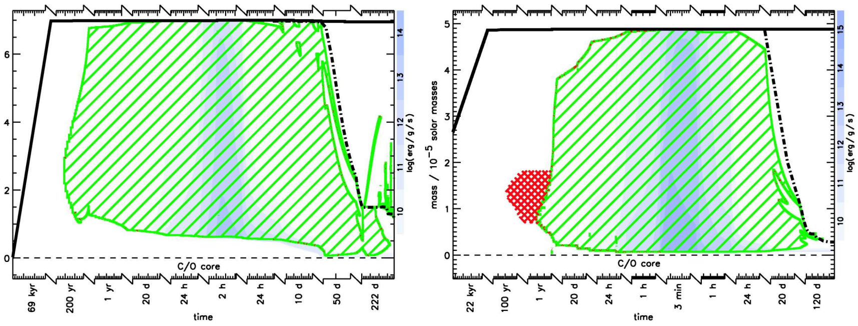

Figure 1: Kippenhahn diagrams illustrating the effect of enrichment on simulations of classical novae (from [12]) Left panel: a nova model without enrichment. Right panel: a nova with added enrichment in the inner 4.6×10^{28} g of the envelope. In both, the x-axis represents evolution time and the y-axis represents the mass above the C/O white dwarf. The hatched region indicates convection, and the shading indicates nuclear energy generation, for which each darker level indicates an increase of an order of magnitude starting from 10^{10} erg g^{-1} s^{-1}. The thick black line shows the total mass of the star (increasing through accretion), and the dotted-dashed line shows mass outside a radius of 10^{12} cm. The thin dashed line marks the white dwarf/envelope boundary. In the right panel, the cross hatched region represents semiconvection. Note that the convection zone does not reach the surface of the white dwarf even in the enriched nova model.

about 10^{-6}–10^{-5} $M_\odot$ of C/O into the accreted envelope for $\mathsf{Ma} = 0.4$ and yielded an expression for the saturated mixture. Applying these results to one-dimensional Lagrangian nova simulations gave two principal results. We found that if no enrichment occurs prior to the onset of convection, then no additional mixing occurs during the evolution because the convective zone does not reach the C/O interface. In contrast to this result, we found that if enrichment occurs in a layer just above the surface of the white dwarf, we can get a vigorous nova and with the ejecta enriched by up to 25% in C/O for $\mathsf{Ma} = 0.4$, an amount consistent with the enrichment observed in some nova ejecta. (See figure 1 for the results of two simulations, one without enrichment and one with enrichment.) Complete details may be found in [12]. Further testing with an independent one-dimensional code with time-dependent convection based on mixing length theory [4] confirmed the result that convection does not reach down to the C/O interface.

The second part of our effort consisted of an extensive parameter study for configurations with a density ratio of 0.1 between the underlying material and the wind and $\mathsf{Ma} = 0.2$. We identified two mixing regimes, an overturning regime and a cusp-breaking regime (see figure 2). The former

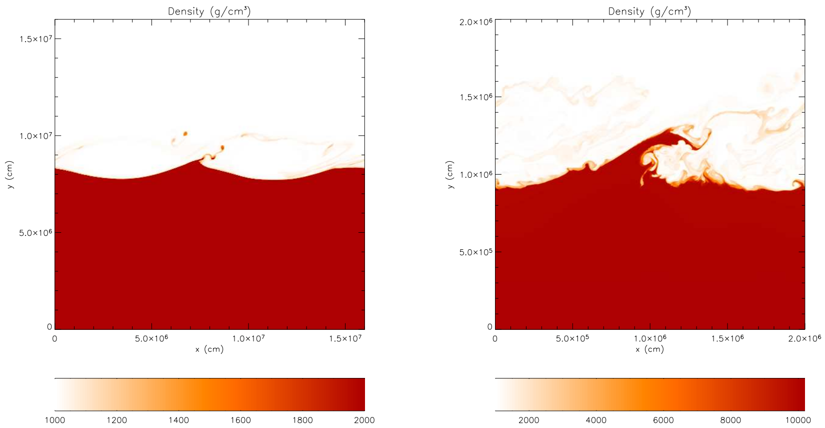

Figure 2: Images of density from simulations illustrating the two types of breaking waves. Left panel: The cusp instability. Right panel: An overturning wave.

occurs when the wind is strong enough to overcome gravity and overturn the wave. The latter occurs when the wind is only strong enough to produce an unstable singular structure at the cusp of the wave that leads to mixing. Complete details about this part of the study may be found in [13].

Our work demonstrates that under some circumstances, mixing by breaking gravity waves can provide sufficient enrichment of the accreted envelope to produce a vigorous nova. A few cautionary remarks are in order, though. First, the simulations of breaking gravity waves in this study were all two-dimensional. The behavior of the energy cascade and the advection of spray and vorticity will be different in three dimensions. Next, although the parameter study covered more than an order of magnitude in δ, the question remains as to whether these results will hold at larger values. Also, if δ becomes a large fraction of the scale height, stratification may affect the results. Finally, the origin and nature of the winds that can drive the gravity waves are currently in the realm of speculation. Detailed simulations of the long-term evolution of nova precursors are needed to better understand this mixing process.

This work is supported in part by the U.S. Department of Energy under Grant No. B341495 to the Center for Astrophysical Thermonuclear Flashes at the University of Chicago. JWT acknowledges support of the NSF Frontier Center for Nuclear Astrophysics under grant PHY 02-16783 and DOE support under grant DE-FG 02-91ER 40606. LJD is supported by the Krell Institute CSGF. AH performed this work under the auspices of the U.S. Department of Energy at the Los Alamos National Laboratory operated by the University of California under contract No. W-7405-ENG-36, in part through support by the Department of Energy under grant B341495 to the Center for Astrophysical Thermonuclear Flashes at the University of Chicago, and by support through a Fermi Fellowship at the University of Chicago. Additional details about the project and information about requesting a copy of FLASH may be found at `http://flash.uchicago.edu`.

References

[1] R.D. Gehrz, J.W. Truran, R.E. Williams, and S. Starrfield, PASP, **110** (1998) 3.

[2] S.G. Starfield, J.W. Truran, W.M. Sparks, and G.S. Kutter, ApJ, **176** (1972) 169.

[3] S.G. Starfield, J.W. Truran, M.C. Wiescher, and W.M. Sparks, MNRAS, **296** (1998) 502.

[4] J. José and M. Hernanz, ApJ, **594** (1998) 680.

[5] M. Livio, (1994) in *Interacting Binaries* eds. S.N. Shore, M. Livio, E.P.J. van den Heuvel (Berlin: Springer-Verlag) 135.

[6] R. Rosner, et al., ApJ, **562** (2001) L177.

[7] J. Miles, J. Fluid Mech., **3** (1957) 185.

[8] B. Fryxell, et al., ApJS, **131** (2001) 273.

[9] A.C. Calder, et al., ApJS, **143** (2002) 201.

[10] T.A. Weaver, B.A. Zimmerman & S.E. Woosley, ApJ, **225** (1978) 1021.

[11] T. Rauscher, A. Heger, R.D. Hoffman, and S.E. Woosley, ApJ, **576** (2002) 323.

[12] A. Alexakis, et al., ApJ, **602** (2004) 931.

[13] A. Alexakis, et al., Phys. Fluids, in press.

Survey for the companions of SN 1572 and SN 1006

P. Ruiz–Lapuente[1,2], *F. Comeron*[3], *J. Méndez*[1,4], *R. Canal*[1], *A.V. Filippenko*[5], *R.L. Kurucz*[6], *S. Smartt*[7], *R. Chornock*[5], *R. Foley*[5], *V. Stanishev*[8], *R. Ibata*[9]

[1] Department of Astronomy, University of Barcelona
[2] Max–Planck Institut für Astrophyik, Garching
[3] European Southern Observatory
[4] Isaaac Newton Group, La Palma
[5] Department of Astronomy, University of California at Berkeley
[6] Harvard–Smithsonian Center for Astrophysics
[7] Institute of Astronomy, Cambridge
[8] Department of Physics, Stockholm University, Stockholm, Sweden
[9] Observatoire de Strasbourg, Strasbourg, France

Type Ia supernovae have long been recognized as close binary systems where one of the stars, a carbon-oxygen WD (C+O WD), undergoes a thermonuclear runaway after reaching the explosive conditions at its center. While the remnants and the ejecta left by the explosion have been studied in great detail, little is known about the companion stars. Several possibilities for the companion have been proposed. It could be a white dwarf, giant, subgiant, or a main sequence star [1] [2] [3] [4], [5], [6]. In all but the first of the above scenarios, a fast-moving companion should be observable close to the center of the remnant [7], [8].

Motivated by the lack of definitive constraints on the progenitors of SNe Ia, a direct observational approach was started to find the moving companion of the exploding WD in SN 1572 and SN 1006 [9]. The method and first results is described in [10], while the concluding results from the survey in Tycho Brahe's supernova are in [9].

Tycho's supernova, the Type Ia SN that exploded in 1572, gives a perfect field for the search for the companion star. The youth of the SNR (just 431 yr) has preserved well the spherical symmetry, which helps in defining the centre of the search, and the field to be explored covers only a small angle on the sky. We have completely surveyed a circle of 0.65 arcmin radius, centred on the *Chandra* X-ray Observatory coordinates for the centre of the SNR, up to an apparent visual magnitude $m_V = 22$. The search covers 15% of the radial extent of the remnant.

Since 1997 we have been gathering high-resolution spectra of the stars in the field using the Utrecht Echelle Spectrograph and the highest-resolution gratings available for the spectrograph ISIS (gratings H2400 and R1200) at the 4.2 m William Herschel Telescope (WHT). Intermediate-resolution spectra using the Echelle Spectrograph and Imager (ESI) at the 10 m Keck II telescope and low-resolution spectra using the Low Resolution Imaging Spectrometer (LRIS) on the Keck I telescope have also been acquired. Imaging has been done both with the Auxiliary Port Camera and the Prime Focus Camera at the WHT and with the Wide Field Camera at the 2.5 m Isaac Newton telescope (INT). The Advanced Camera for Surveys and the Wide Field Planetary Camera 2 on board the *Hubble Space Telescope (HST)* have provided additional imaging in the F555W filter during Cycle 12, allowing us to measure proper motions of the stars with a precision of 2 milliarcsec per yr (mas yr^{-1}).

Synthetic spectra, under the assumption of local thermodynamic equilibrium (LTE), have been fitted to the observed spectra. We have used Kurucz's grids of model atmospheres [11], with an spectral synthesis code based on the Uppsala Synthetic Spectrum Package [12], and the atomic data from the line lists of Kurucz. This determines the atmospheric parameters T_{eff} (effective temperature) and log g (surface gravity), and thus the spectral type and luminosity class. Comparison of spectra covering a wide wavelength range ($\lambda\lambda$3300–10400 Å) with those in the library of Lejeune, Cuisiner & Buser (1997) [13], after dereddening gives as well fits for a effective temperature T_{eff}, surface gravity log g, and metallicity. Intrinsic colors and absolute visual magnitudes are deduced from the relationships between spectral type and color and between spectral type and absolute magnitude for the different luminosity classes. Comparison with our photometric measurements in the BVR bands then yields the reddening, quantified by the colour excess $E(B-V)$, from which the visual extinction A_V and the corrected apparent visual magnitude $m_{V,0}$ are calculated. Comparison with the absolute visual magnitude then gives the distance.

The star most likely to have been the donor of SN 1572 has to show a multiple coincidence: at the distance of SN 1572 (conservatively in the range between 2 and 4 kpc), showing an unusual radial velocity in comparison to the stars at the same location (much above the velocity dispersion for its spectral type), and having stellar parameters consistent with being impacted by the SN explosion. It should also lie near the remnant center (i.e., within the search radius).

Stars at distances $d \approx$ 2–4 kpc, in that direction, are moving at average radial velocity $v_r \approx -20$ to -40 km s^{-1} (in the Local Standard of Rest), with a $\sim$ 20 km s^{-1} velocity dispersion [14], [15], [16]. We found an outlier in the sample that exceeds by a factor of 3 the velocity dispersion of its stellar type and its at the distance of SN 1572 (namely d $= 2.83 \pm 0.79$ kpc [17]). This star is certainly not from the halo as derived from its metallicity. Its stellar parameters, T_{eff}, log g, its mass and metal content as well as the plausible evolutionary path followed are discussed [9].

A similar survey to the one described above has been conducted for SN 1006. Its distance has been recently determined through the expansion of the optical filaments and seems to be at 2.17 $\pm$ 0.08 kpc [18]. Modeling of the spectra obtained through UVES at the UT2 of the VLT and EMMI at NTT has allowed us to measure distances, radial velocities and the stellar parameters. Constraints have been set on the types of stars giving rise to these explosions.

The direct approach to the companion of a supernova explosion has proved extremely fruitful. It requires the precise determination of distances to stars, careful modeling of the spectra to determine the stellar parameters and a good study of the kinematics at the location of the explosion. In SN 1572 we have likely detected the companion of SN 1572. Our search for the binary companion of SNe Ia has shown that the SN explosion would affect the companion mainly through the kinematics. This survey typifies as well the color of th stars found in the SNR of Type Ia class. It excludes giants and supergiants as the donor in SN 1572. The results of this survey set a long list of strong constraints on the post-explosion hydrodynamics of supernovae which should be explored in the future.

Acknowledgements

Wolfgang's vision, generosity and enthusiasm has made a difference to many of us. It is a pleasure to thank you, Wolfgang, and to wish you a happy birthday! PRL is grateful to the hospitality offered by the Max–Planck Institut für Astrophysik in Garching where this survey has been partially conducted.

References

[1] P. Ruiz–Lapuente, R. Canal & A. Burkert: in *Thermonuclear Supernovae*, Ed. P. Ruiz–Lapuente, R. Canal & J. Isern (Kluwer, Dordrecht), 205 (1997) W.D. Arnett: *Supernovae and Nucleosynthesis* (Princeton Univ. Press, Princeton) (1996)

[2] E. Livne, Y. Tuchman & J.C. Wheeler, ApJ 399, 665 (1992)

[3] E. Marietta, A. Burrows & B. Fryxell, ApSS, 128, 615 (2000)

[4] M. Livio & J. W. Truran, ApJ 389, 695 (1992)

[5] D. Branch, M. Livio, L. R. Yungelson, F. Boffi & E. Baron. PASP, 107, 1019 (1995)

[6] . P. Podsiadlowski, astro-ph/0303660 (2003)

[7] P. Ruiz–Lapuente: Science 276, 1813 (1997)

[8] R. Canal, J. Mendez, & P. Ruiz–Lapuente: ApJ 550, L53 (2001)

[9] P. Ruiz–Lapuente, F. Comeron, J. Méndez, R. Canal, A. V. Filippenko, R. L. Kurucz, S. Smarrt, R. Chornock, R. J. Foley, V. Stanishev & R. Ibata, submitted (2004)

[10] P. Ruiz-Lapuente, F. Comeron, S. Smartt, R. Kurucz, J. Méndez, R. Canal, A. Filippenko, R. Chornock *From Twilight to Highlight: the Physics of Supernovae*, 140, ed. W. Hillebrandt & B. Leibundgut (Berlin: Springer-Verlag) (2003)

[11] R.L. Kurucz: *ATLAS9 Stellar Atmospheres Programs, Grids of Model Atmospheres and Line Data* (CD–Rom, Smithsonian Astrophysical Observatory, Cambridge) (1993)

[12] B.A. Gustafsson et al.: A&A 42, 407 (1975)

[13] Th. Lejeune, F. Cuisinier & R. Buser. A standard stellar library for evolutionary synthesis. *Astron. & Astrophys. Supp. Ser.* **125**, 229–246 (1997).

[14] J. Brand & L. Blitz. The velocity field of the outer Galaxy, *Astron. Astrophys.*, **275**, 67–90 (1993).

[15] J. Binney & M. Merrifield *Galactic Astronomy* (Princeton: Princeton University Press) (1998), 639

[16] W. Dehnen & J. Binney. Local stellar kinematics from *Hipparcos* data *MNRAS*,**298**, 387 (1998)

[17] P. Ruiz–Lapuente. ApJ. Sept. (2004)

[18] P.F. Winkler, G. Gupta & K.S. ApJ. 585 (2003)

Stability of SN Ia progenitors against radial oscillations

I. Baraffe[1], *H. Heger*[2], *S. Woosley*[3]

[1] Ecole Normale Supérieure, C.R.A.L, 46 allée d'Italie, Lyon, France
[2] Theoretical Astrophysics Group, T-6, MS B227, Los Alamos National Laboratory, Los Alamos, USA
3 Department of Astronomy and Astrophysics University of California, Santa Cruz, USA

Introduction

We analyze the possible existence of a vibrational instability excited by the ϵ-mechanism during the last few centuries of evolution of a Chandrasekhar white dwarf prior to its explosion as a Type Ia supernova. Our analysis is motivated by the extreme sensitivity of the nuclear energy generation rate on temperature in combination with the relativistic degenerate matter in the center of the white dwarf. Based on a linear stability analysis, we find that the fundamental mode and higher order radial modes are indeed unstable and that the fundamental mode has the shortest growth time scale. Fig. 1 displays the work $\mathrm{d}W/\mathrm{d}M$ done by pressure gradient and gravity forces in each layers during one pulsation cycle, with W the so-called work integral ([1], [2]). Positive work indicates driving regions whereas negative work corresponds to damping zones. The positive value of $\mathrm{d}W/\mathrm{d}M$ in the center is due to the perturbation of the nuclear energy and characterizes the ϵ-mechanism.

Such pulsational instability could in principle result in phases of expansion and contraction with growing amplitude and thus affect the structure of the supernova progenitor. Further study shows however that the growth time scale for such instability never becomes shorter than the evolutionary timescale. Therefore, even though the star *is* pulsationally unstable, we do not expect these radial modes to have time to grow and to affect the structure and thereby the explosion properties of SN Ia progenitor stars.

References

[1] Cox, J.P. 1980, *Theory of Stellar Pulsations*, Princeton University Press.

[2] Unno W., Osaki Y., Ando, H., Saio, H., Shibahashi, H. 1989, *Nonradial oscillations of stars*, Univ. of Tokyo Press.

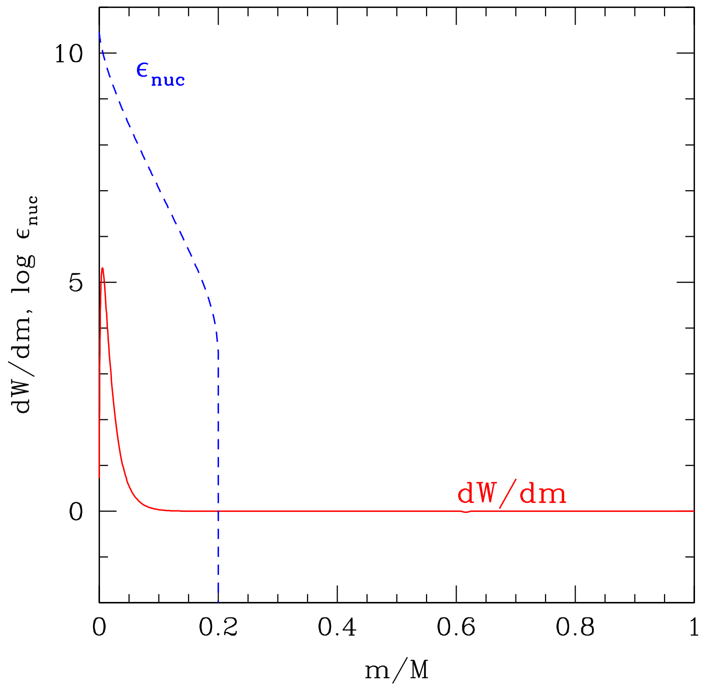

Figure 1: Differential work $\mathrm{d}W/\mathrm{d}M$, in arbitrary units, as a function of mass (in units of the total mass) in the interior structure of a model 6 days before explosion (with central temperature $T_\mathrm{c} = 5\,10^8 K$). The dashed line corresponds to the nuclear energy generation log ϵ_nuc (erg/gr/s).

Adventures of a Supernova Observer

B. Leibundgut[1], *M. Stritzinger*[2]

[1] European Southern Observatory, Karl-Schwarzschild-Strasse 2, D-85748 Garching, Germany
[2] Max Planck Institute for Astrophysics, Karl-Schwarzschild-Strasse 1, D-85748 Garching, Germany

Abstract

If you keep your contribution short (about 3 pages including everything) you will not need an abstract at all—your contribution is meant to be an "extended abstract". If you can't live without an abstract, please put it here.

The bright, the faint and the invisible

Supernova research heavily relies on tight links between observations and theory. Progress in the past decades has been hampered by the lack of densly sampled observational data to be compared to theoretical models. In particular, the very early epochs before maximum and a complete coverage of wavelengths as function of time were missing. While there were the occasional data sets for single supernovae available, a comprehensive study of a significant sample was missing. The European Supernova Collaboration under the leadership of Wolfgang Hillebrandt is trying to remedy this situation for Type Ia supernovae (SNe Ia). The first objects with extensive data sets have been recently published [2, 13]. They show the value of such dense coverage and the information that can be extracted for explosion models and radiation transport physics.

The infrared light curves of SNe Ia proved to contain a puzzling surprise. Their peak luminosity appears to be constant without the additional application of a light curve correction [9]. If confirmed, this would make them simple standard candles, in stark contrast with the situation in the optical (e.g. [11]). Since the near-infrared is much less dependend on absorption corrections, infrared light curve may prove to become the tool of choice for cosmology in the future.

There are many reasons to observe fainter supernovae as well. Since supernovae are extremely rare, it helps to increase the volume in which they can be observed. Increasing the sample to test for various supernova characteristics is essential. Other reasons are of course the possibility to use SNe to measure cosmological parameters (e.g. [10, 12]). Core-collapse supernovae, in particular the hydrogen-rich Type II supernovae, show characteristics that allow to derive distances [6, 7, 4]. The Hubble constant derived from these measurements strongly depends on the assumed calibration – currently mostly done through SN 1987A and the distance to the LMC – and the Cepheid distance scale set by the HST observations [15, 5], but are in the range of 55 to 80 km s^{-1} Mpc^{-1}.

The observation of the most distant supernovae has also been achieved with HST and yields the first estimate of the time dependence of the equation of state parameter [14]. It is very intriguing to see that the most distant supernovae indeed show the signature of the (concordant) cosmological model, which was based on the earlier observations of SNe Ia. Simple evolutionary models or problms with dust extinction appear less likely. This picture strengthens the case for dark energy, the component which is responsible for accelerated cosmic expansion.

Connecting cosmology and SN theory

The amount of nickel synthesised in the thermonuclear explosion of a SN Ia to first order determines the peak luminosity. The bolometric light curves [18, 3, 17] assemble the complete measured flux of a supernova. It can be shown – using Arnett's Rule that the emitted energy at peak equals the instantaneous energy input from the radioactive decays at the center of the ejecta [1] – that SN Ia exlosions produce widely different amounts of nickel (up to a factor of 10) [3].

However, there is a simple argument that connects the Hubble constant with the amount of nickel produced in SNe Ia. The Hubble constant directly depends on the luminosity distance, which in turn is nothing but the inverse square law for the ratio of luminosity (L) and the observed brightness (F) of an object. Because the luminosity of a SNe Ia depends on the nickel mass (M_{Ni}), we can use explosion models – and the measured brightness and redshifts (z)– to derive the Hubble constant.

$$H_0 = \frac{cz}{D_L} = cz\sqrt{\frac{4\pi F}{L}} \propto cz\sqrt{\frac{4\pi F}{M_{Ni}}} \tag{6}$$

Since SNe Ia are not identical we can only derive a lower limit for the Hubble constant from current models. The prediction of the explosion models range somewhere between 0.4 and 1.0 $M_\odot$ (e.g. [8]). Hence we can derive interesting lower limits of H_0 [16]. It appears as if H_0 has to be larger than

50 to be compatible with current supernova models. Another option is to go through the classical Hubble diagram and set the limits on the absolute luminosity through the nickel mass.

References

[1] W.D. Arnett, ApJ **253** (1982) 785.

[2] S. Benetti, et al., MNRAS **348** (2004) 261.

[3] G. Contardo, B. Leibundgut, W.D. Vacca, A&A **359** (2000) 876.

[4] A. Elmhamdi, et al., MNRAS **338** (2003) 939.

[5] W.L. Freedman, et al., ApJ **553** (2001) 47.

[6] M. Hamuy, et al., ApJ **558** (2001) 615.

[7] M. Hamuy, ApJ **582** (2003) 905.

[8] W. Hillebrandt, J.C. Niemeyer, ARA&A **38** (2000) 191.

[9] K. Krisciunas, M.M. Phillips, N.B. Suntzeff, ApJ **602** (2004) L81

[10] B. Leibundgut, ARA&A **39** (2001) 67.

[11] B. Leibundgut, ApSS **290** (2004) 29.

[12] B. Leibundgut, N.B. Suntzeff, in Supernovae and Gamma–Ray Bursts, ed. K. Weiler, Heidelberg: Springer, (2003) 77.

[13] G. Pignata, et al., A&A, (2004), submitted.

[14] A.G. Riess, et al., ApJ (2004), in press (astro-ph/0402512).

[15] A. Saha, et al., ApJ **522** (1999) 802.

[16] M. Stritzinger, B. Leibundgut, A&A (2004), in preparation.

[17] L. Strolger, et al., AJ **124** (2002) 2905.

[18] W.D. Vacca, B. Leibundgut, ApJ **471** (1996) L37.

Type Ia Supernovae: What can we learn from better data?

W. Hillebrandt[1]

[1] Max-Planck-Institut für Astrophysik, Garching

Abstract

Recent 3-dimensional hydrodynamic simulations of type Ia supernovae have considerable predictive power and allow to study observable properties, such as their light curves and spectra, without adjustable non-physical parameters, and they make firm predictions for the nucleosynthesis yields from the explosions. This raises a quest for better data, covering the spectroscopical and photometric evolution in all wave bands from very early epochs all the way into the nebular phase. First such results obtained by the European Supernova Collaboration (ESC) for a sample of nearby SNe Ia and their implications for constraining the models and systematic differences between them are discussed.

Introduction

In order to constrain the models of type Ia supernovae or to search for the cause of the observed correlations, high-quality data of lightcurves and spectra are needed. However, especially very early observations and complete coverage of lightcurves and spectral evolution are available only for a small number of supernovae. Therefore, more data are needed urgently. Following the spectral evolution all the way into the nebular phase allows "abundance tomography" for the exploded star. Accurate bolometric lightcurves constructed from filter lightcurves and spectra constrain the energetics of the explosion and, thus, provide tools to test the "standard candle" hypothesis.

In this contribution we will present first results of a European initiative to study the physics of type Ia supernovae by means of both, systematic and targeted observations and by increasing the quality and the predictive power of theoretical models at the same time.

In order to improve our knowledge of type Ia supernovae through an advance in both observations and modeling, a group of European astronomers has recently organized as a European Research Training Network (RTN), also named the *European Supernova Collaboration* (ESC). The idea is that accurate observations and modeling of relatively nearby SNe is the only way to understand their nature and the causes of their range of properties. Par-

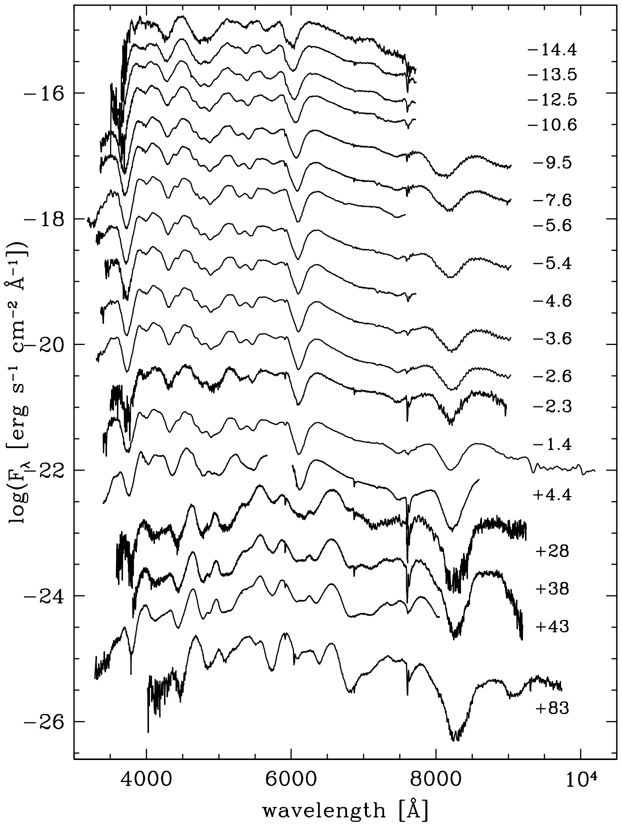

Figure 1: Spectral evolution of SN 2002bo. Wavelength is in the observers frame. The earliest spectrum is on scale. The others are shifted with increments 0.6 ([1]).

ticipants to the RTN include German, British, Italian, French, Spanish and Swedish institutes, and more recently also groups in Australia and China. They have successfully applied for joint observing time on most major European telescopes, thus maximizing and optimizing the amount of telescope time allocated for SNe Ia studies.

In the short time since the beginning of the RTN, the ESC has already collected very accurate data on 8 nearby SNe Ia, including SNe 2002bo and 2002er, the latter appearing to be rather standard. A series of spectra of SN 2002bo are shown in Fig. 1. It is possible to identify many of the lines in the spectra, which near maximum are dominated by elements such as Fe, Si, S, Ca. The photometry of SN 2002er (Fig. 2) is perhaps the most accurate

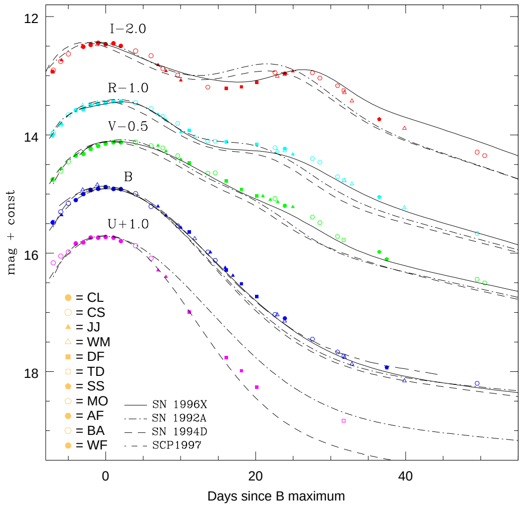

Figure 2: Color light curves of SN 2002er. A total of 11 telescopes was used for the imaging of this supernova, indicated by different symbols (from [2]).

coverage of the evolution of a SN Ia available to date.

These data (and those still to come) allow us to constrain the models and to search for the cause of differences between and the observed correlations of SNe Ia. Until now, especially early observations and complete coverage of light curves and spectral evolution are available only for a small number of supernovae, but this will change in the near future. Following the spectral evolution from very early epochs all the way into the nebular phase allows "mass tomography" and to constrain the models (see Fig. 3). Accurate bolometric light curves constructed from filter light curves and spectra constrain the energetics of the explosion and, thus, provide tools to test the "standard candle" hypothesis.

Acknowledgements

This work was supported by the European Commission under contract HPRN-CT-2002-00303 and the DFG-SFP 375. Support by ECT* in Trento is also acknowledged. The observations of SN 2002bo and SN 2002er presented were carried out at Assiago, Calar Alto, La Palma, ING/UKIRT, ESO/La Silla, and Wendelstein Observatories, mostly as ToO observations.

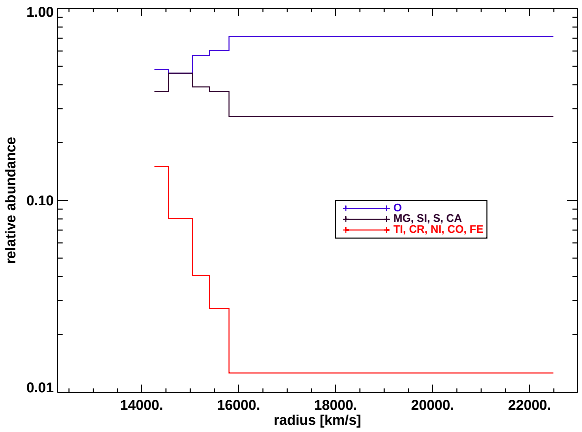

Figure 3: Abundances of the major elements in the outer shells of the ejecta of SN 2002bo, inferred from spectral fits to the data shown in Fig. 1 for the first couple of days past discovery. Therefore the matter shown represents the outermost few percent of the supernova only. It is surprising that these layers do not contain any carbon, indicating some (weak) nuclear processing all the way to the surface of the white dwarf. Also some iron-group elements (in particular Ni) have been mixed well into this matter, explaining the nice lightcurve fits [3].

References

[1] S. Benetti et al. (The European Supernova Collaboration), MNRAS **348** (2004) 261.

[2] G. Pignata et al. (The European Supernova Collaboration), astro-ph/0405560, and submitted to MNRAS (2004) **55** (1983) 727.

[3] M. Stehle et al., in preparation (2004).

Before the flame is born: the ignition process in Type Ia Supernovae

L. Iapichino, W. Hillebrandt

Max-Planck-Institut für Astrophysik, Karl-Schwarzschild-Strasse 1, D-85740 Garching, Germany

The ignition process of thermonuclear flames in Chandrasekhar mass C + O white dwarfs, leading to the explosion of Type Ia Supernovae (SNe Ia), is considered a key detail for the understanding of these events ([1]). In fact, the initial flame location in SNe Ia explosions depends on the progenitor evolution, whose issues are discussed e.g. in [2]. Initial conditions of large eddy simulations are parametrized accordingly, in several ways (see, for example, [3], [4] and [5]).

Previous models ([6], [7], [8]), based on analytical calculations of the white dwarf's evolution prior to runaway, suggest that the ignition occurs off-center, starting in many points ("bubbles"), distributed at a distance between 100 and 250 km from the white dwarf center. The diameter of such bubbles, as deduced in [8] from turbulence arguments, is about 1 km or smaller.

In this talk, a new approach to 2D numerical simulations of buoyant bubbles in the white dwarf's interior is presented. In the simulations, performed using the AMR explicit FLASH code ([9]), a single bubble is set at rest in the computational domain. The bubble is subject to buoyancy and rises along the domain; a small alpha-chain reaction network is used in order to follow the C-burning. The bubble evolution depends on the balance between the nuclear heating and the cooling, caused by bubble dispersion; if the bubble temperature reaches about 10^9 K, a flame is generated. The work is currently under way; an example of these simulations is given by figure 1, where a bubble that disperses before reaching the thermal runaway is shown. This study is intended to probe the bubble features at runaway (diameter, temperature excess with respect to the background and evolutionary time scales) and infer some clues about the SN Ia explosion.

Acknowledgements

The software used in this work was in part developed by the DOE-supported ASCI/Alliance Center for Astrophysical Thermonuclear Flashes at the University of Chicago.

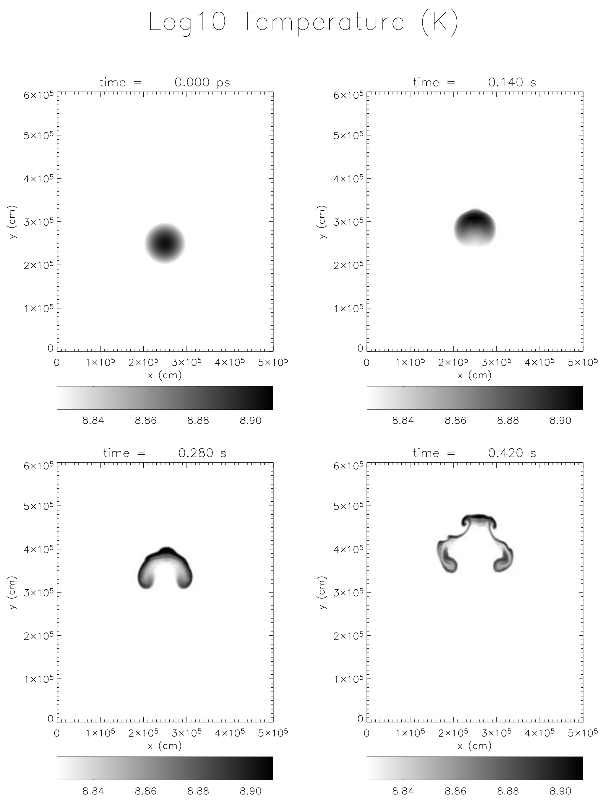

Figure 1: Evolution of a buoyant, reactive bubble, at four different times. A logarithmic temperature scale is shown.

References

[1] W. Hillebrandt and J.C. Niemeyer, ARA&A **38** (2000) 191.

[2] S.E. Woosley and T.A. Weaver, ARA&A **24** (1986) 205.

[3] M. Reinecke, W. Hillebrandt and J.C. Niemeyer, A&A **347** (1999) 739.

[4] M. Reinecke, W. Hillebrandt and J.C. Niemeyer, A&A **386** (2002) 936.

[5] M. Reinecke, W. Hillebrandt and J.C. Niemeyer, A&A **391** (2002) 1167.

[6] D. Garcia-Senz and S.E. Woosley, ApJ **454** (1995) 895.

[7] S.E. Woosley, Nucl. Phys. **A688** (2001) 9c.

[8] S.E. Woosley, S. Wunsch and M. Kuhlen, astro-ph/0307565.

[9] B. Frixell et al., ApJ Suppl. **131** (2000) 273.

Numerical Simulations of Type Ia Supernova Explosions

F.K. Röpke[1], *W. Hillebrandt*[1], *M. Gieseler*[1], *M. Reinecke*[1], *C. Travaglio*[2]

[1] Max-Planck-Institut für Astrophysik, Karl-Schwarzschild-Str. 1, 85741 Garching,
Germany
[2] INAF – Osservatorio Astronomico di Torino, Strada dell'Osservatorio 20, I-10025 Pino Torinese, Torino, Italy

Introduction

Recent numerical simulations of Type Ia Supernova (SN Ia) explosions [1, 2] have successfully modeled the Chandrasekhar-mass deflagration scenario (for a review see [3] or J. Niemeyer's contribution to these proceedings) in three spatial dimensions. In this SN Ia model a carbon/oxygen white dwarf (WD) star accretes matter from a binary companion until it reaches the Chandrasekhar mass. At this point, thermonuclear burning in the center of the WD forms a subsonic deflagration flame which—mediated by thermal conduction of the degenerate electrons—propagates outward. Since the resulting stratification of dense fuel and light ashes in the gravitational field is unstable (Rayleigh-Taylor instability), burning bubbles of hot ashes ascend into cold fuel. At the interfaces a secondary shear instability gives rise to the local development of turbulence which wrinkles the flame front. This effect accelerates the effective burning velocity and thus the energy generation can account for SN Ia explosions. In the explosion process the WD material is converted to iron group elements and a smaller fraction of intermediate-mass elements (like Si, S, and Ca). However, it is only the radioactive decay of ^{56}Ni that powers the observed lightcurve.

Numerical implementations of such models must fulfill a number of requirements. They have to be robust against variations of the initial conditions in an astrophysically reasonable range, but on the other hand they are expected to explain the observed diversity of SNe Ia. The final goal is, of course, to explain the correlation between the peak luminosity and the light curve shape on the basis of theoretical models. This relation is of great importance to calibrate cosmological distance measurements. Three-dimensional SN Ia explosion simulations have reached a quality where these issues can be addressed. Furthermore, nucleosynthetic post-processing of the explosion data has opened the possibility to calculate synthetic light

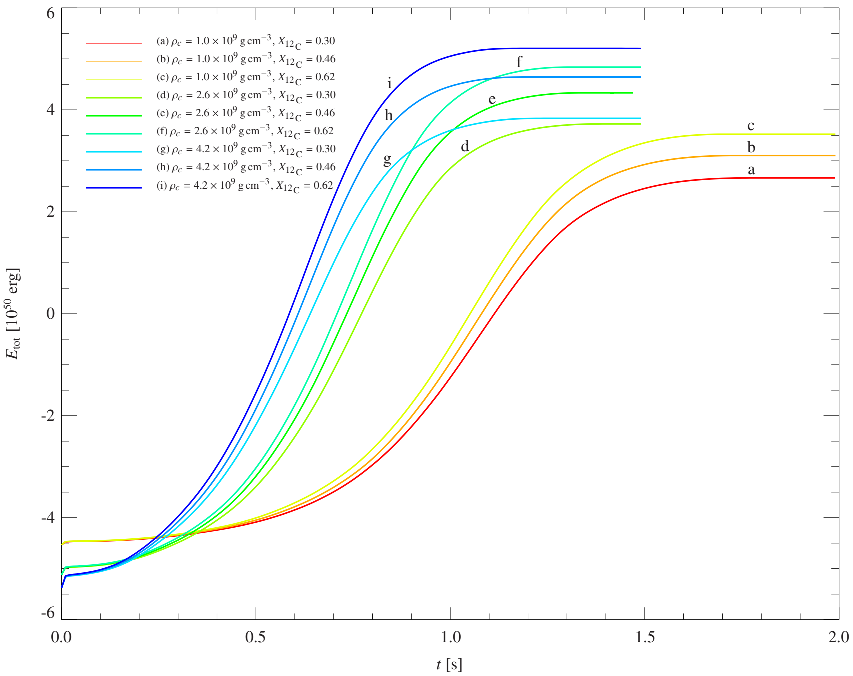

Figure 1: Total energy of the different models as a function of time.

curves and spectra which can be directly compared to observations. This provides a way to discriminate between different astrophysical models (e.g. pure deflagration or delayed detonation).

We present the first systematic study on what answers three-dimensional deflagration models can give. What are the possible parameters that have the potential to explain the SN Ia diversity? Among others the progenitor's carbon-to-oxygen ratio, its metallicity, and the central density at ignition are commonly suggested. In our survey we vary these three parameters independently to explore the effects on the explosion models. However, we are aware of the fact that in principle they are interrelated by stellar evolution of the progenitor WD star. Our study covers the following parameter space: We apply three different carbon mass fractions of the WD material, $X(^{12}\mathrm{C}) = 0.30, 0.46, 0.62$, three different central densities at ignition, $\rho_c = [1.0, 1.6, 4.2] \times 10^9\,\mathrm{g\,cm^{-3}}$, and three different metallicities of the WD (represented by the ^{22}Ne mass fraction), $Z = [0.3, 1.0, 3.0] Z_\odot$. This defines the 27 models of our survey.

Numerical models

Our numerical model is based on the PROMETHEUS implementation [4] and describes the flame as a discontinuity between fuel and ashes applying the level set method [5]. Turbulence on unresolved scales is treated with a subgrid-scale model [6]. Details of the implementation can be found in [7, 8]. The thermonuclear burning is assumed to proceed to nuclear statistical equilibrium (NSE) consisting of iron group elements (represented by “Ni” in our model) and α-particles at high fuel densities. Below $\rho_{\text{fuel}} = 5.25 \times 10^7\,\text{g}\,\text{cm}^{-3}$ burning is assumed to terminate at intermediate mass elements represented by “Mg” and below $\rho_{\text{fuel}} = 1.0 \times 10^7\,\text{g}\,\text{cm}^{-3}$ the reactions are so slow that it is no longer followed. Our numerical setup is analogous to the *c3_3d_256* model of [8]. The carbon/oxygen ratio of the progenitor and the central density at ignition are varied in the explosion models. In these models tracer particles are distributed equally in mass shells. They record the temperature, the density, and the internal energy of the explosion process. With help of this data it is possible to post-process the nucleosynthesis of the explosion models (see C. Travaglio’s contribution to these proceedings). Here the WD’s metallicity is varied by changing the mass fraction of ^{22}Ne.

Results

Figure 1 shows the total energy of our models. Obviously, a lower central density leads to a lower energy release and delays the evolution of the model. The differences in the total energy productions for varying ρ_c and fixed other parameters amount to $\sim$40%. The reason for this effect is the different gravitational acceleration experienced the flame front which leads to a change in the evolution of the nonlinear Rayleigh-Taylor instabilities. For higher ρ_c the evolution is faster and more pronounced, so that the flame is affected by stronger turbulence. This accelerates the flame propagation and leads to an increased energy release.

Contrary to that, a change in the carbon mass fraction does not lead to a significant delay of the evolution. The change of the total energy production of the models amounts to $\sim$12%. This is due to the different binding energies of fuel with varying C/O ratio.

The ^{56}Ni masses produced by the different models are plotted in Fig. 2. With increasing central density of the WD at ignition, the ^{56}Ni production rises to a maximum at $\rho_c \approx 2.5 \times 10^9\,\text{g}\,\text{cm}^{-3}$ and then declines again (cf. Fig. 2b). The variation is of the order of 10%. This behavior can be expected from the fact that two effects are competing here. The effect of the different

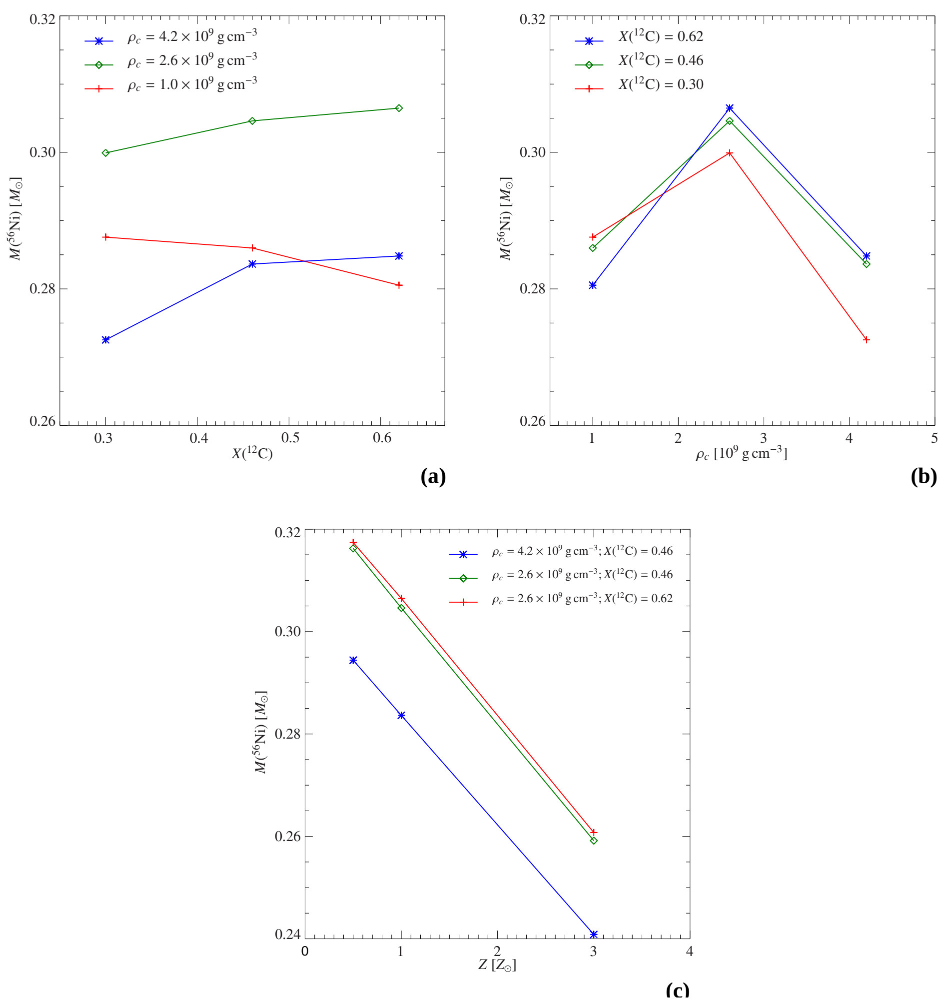

Figure 2: ^{56}Ni masses produced by the models as a function of (a) carbon mass fraction of the progenitor, (b) central density at ignition, and (c) progenitor's metallicity .

gravitational acceleration experienced by the flame leads to a faster flame propagation for higher ρ_c, as discussed above. Consequently, more material is processed at high densities resulting in an increased amount of iron group elements. On the other hand, at higher densities the neutronization of the burnt material becomes important and thus an increasing fraction of the iron group elements is present in form of neutron-rich nuclei (like ^{58}Ni) instead of ^{56}Ni.

With increasing metallicity of the progenitor, i.e. higher mass fraction of ^{22}Ne (a nucleus with neutron excess), neutron-rich iron group nuclei in the ashes are favored and less ^{56}Ni is produced. This is evident in our models (cf. Fig. 2c). The variation amounts to $\sim$20%. Our results are consistent with a linear relation that was proposed by [9] (see also the contribution of E. Brown to these proceedings).

With varying $X(^{12}\mathrm{C})$ the change in the nickel masses is only of the order of a few percent (see Fig. 2a). This result is unexpected in a simple picture. Although the total explosion energy increases with $X(^{12}\mathrm{C})$, the flame evolution in the different models is found to be surprisingly similar. This results in little changes in the ^{56}Ni production. The explanation of this effect is a higher fraction of α-particles in NSE in the ashes at maximum energy generation for increasing $X(^{12}\mathrm{C})$. This acts as an energy buffer due to the reduction of the binding energy and increased particle number in the burnt material. Details can be found in [10].

Conclusions

In the present study it has been shown that our SN Ia models are robust to astrophysically reasonable variations in the initial parameters. To what degree the deflagration scenario is able to explain the full observed SN Ia sample has to be decided by more detailed studies. The current survey indicates that it can account for some of the observed features. A simple deduction of the peak luminosities from the ^{56}Ni masses (Arnett's rule, [11]) produced by our models leads a diversity in the luminosities that can—at least partly—explain the observed scatter.

However, it would predict a significant change with varying metallicity but almost no change with varying C/O ratio of the progenitor WD. On the other hand, the former will not influence the explosion dynamics while the latter leads to a significant change in the total energy release. Thus the light curve shape will probably not change much in the first case but vary significantly in the second. Therefore, it is clear that a single parameter will not explain the peak luminosity–light curve shape relation of SNe Ia. It seems likely that a combination of progenitor parameters (based on stellar evolution models of the WD) will be necessary for this task. Additionally, synthetic light curves from the models are needed to to deduce their characteristics and to take into account multidimensional effects. Arnett's rule may be a too strong simplification here. One of the next steps in improving the explosion models will be a refined description of the thermonuclear reactions. Moreover, it will be necessary to take into account electron captures at high densities to improve the reliability of the results for varying central densities at ignition. A detailed analysis of the parameter study presented here can be found in [12].

Acknowledgements

The junior authors of this text would like to congratulate W. Hillebrandt on his 60th birthday.

References

[1] M. Reinecke, W. Hillebrandt, and J.C. Niemeyer, A&A **391** (2002) 1167.

[2] V.N. Gamezo, A.M. Khokhlov, E.S. Oran, A.Y. Chtchelkanova, and R.O. Rosenberg, Science **299** (2003) 77.

[3] W. Hillebrandt and J.C. Niemeyer, Annu. Rev. Astron. Astrophys. **38** (2000) 191.

[4] B.A. Fryxell and E. Müller, MPA Green Report **449** (Max-Planck-Institut für Astrophysik, Garching, 1989).

[5] S. Osher and J.A. Sethian, J. Comp. Phys. **79** (1988) 12.

[6] J.C. Niemeyer and W. Hillebrandt, ApJ **452** (1995) 769.

[7] M. Reinecke, W. Hillebrandt, J.C. Niemeyer, R. Klein, and A. Gröbl, A&A **347** (1999) 724.

[8] M. Reinecke, W. Hillebrandt, and J.C. Niemeyer, A&A **386** (2002) 936.

[9] F.X. Timmes, E.F. Brown, and J.W. Truran, ApJ **590** (2002) L83.

[10] F.K. Röpke and W. Hillebrandt, A&A Lett. (2004) in press.

[11] W.D. Arnett, ApJ **253** (1982) 785.

[12] F.K. Röpke, M. Gieseler, M. Reinecke, C. Travaglio, and W. Hillebrandt, (2004) in preparation.

Deflagrations Evolved from an Off-Center Ignition

J.W. Truran[1,2,3], *A.C. Calder*[1,2], *T. Plewa*[1,2], *N. Vladimirova*[1,2], *D.Q. Lamb*[1,2,3], *E.F. Brown*[4]

[1] Center for Astrophysical Flashes, University of Chicago, Chicago, IL 60637
[2] Department of Astronomy and Astrophysics, University of Chicago, Chicago, IL 60637
[3] Enrico Fermi Institute, University of Chicago, Chicago, IL 60637
[4] Department of Physics and Astronomy, Michigan State University

Introduction

The standard model for a Type Ia supernova event, first proposed by Hoyle and Fowler [6], involves the incineration of a Chandrasekhar mass carbon-oxygen white dwarf. While there exists no universally accepted progenitor model, it is generally understood that growth to the Chandrasekhar limiting mass is most likely achieved via mass transfer from a binary stellar companion [15, 10]. While observations of the ejecta of SNe Ia confirm that the CO white dwarf is largely incinerated, the precise nature of the ignition process and the subsequent flame evolution remains to be established. In this context, we have studied the hydrodynamics of thermonuclear deflagration of a massive white dwarf. Most previous investigations have focused upon the case of central ignition. In contrast, we have considered a flame initiated slightly off center and followed its evolution through a full three-dimensional simulation of an entire white dwarf, with no imposed symmetry (Calder *et al.* [2]). Simulations were performed specifically for effective resolutions of 6.4, 3.2, and 1.6 kilometers. The results displayed in this paper are those corresponding to the highest resolution simulation.

Theoretical models of thermonuclear flame fronts indicate that, for conditions typical of white dwarf interiors, the flame thickness is between 8 and 12 orders of magnitude smaller than the stellar radius [14]. Because of this difference in length scales, multidimensional Type Ia models must make use of an appropriate subgrid model for the evolution of the thermonuclear burning front.

In our modeling effort, we performed entire-star simulations of the deflagration phase of Type Ia supernovae using the FLASH code, a parallel adaptive mesh multiphysics astrophysical hydrodynamics code [4, 1]. A recent addition to the code is a custom implementation of the “thick flame” flame capturing scheme of Khokhlov [9] in which the flame is advanced by evolving a passive scaler variable with an advection-diffusion-reaction equation. We used a step-like reaction profile and chose reaction and diffusion coefficients to reproduce the results of direct numerical simulations of the laminar and turbulent nuclear flames. Specifically, we take the flame speed to be the maximum of the laminar speed [14] and a turbulent flame speed based upon the assumption that the turbulent burning on macroscopic scales is driven by Rayleigh-Taylor instabilities [9]. The model energetics account for the burning of carbon, magnesium, and silicon.

The evolution of the flame witnessed the formation of a Rayleigh-Taylor-unstable bubble of hot nuclear ash and its rapid rise toward the stellar surface. The rising bubble takes the form of a typical mushroom-shaped plume and is composed of intermediate mass (carbon-to-silicon) and iron-peak elements. As it rises, the bubble is continuously accelerated by buoyancy driven by heating from the energy released by nuclear burning, and supersonic speeds are achieved. Furthermore, the morphology of the surface of the bubble, determined by the Rayleigh-Taylor instability, displays characteristics similar to those obtained in earlier numerical studies of deflagrating white dwarfs [13, 5]: generations of bubbles form on the surface of the initial bubble. Representative images displaying this bubble evolution are shown in Figures 1 and 2.

We find that the evolution of the flame front (the bubble of hot ash) consists of three distinct phases. The first lasts for approximately 0.3-0.4 seconds and is a period of slow, mostly radial growth of the bubble. The position of the bubble changes only slightly. The next phase is characterized by substantial growth of the asymmetry created during the first phase and the development of Rayleigh-Taylor instabilities at the bubble surface. The onset of third phase of the evolution is marked by the time at which the bubble reaches the surface layers of the star where there is a large decreasing density gradient.

While our model does not incinerate the white dwarf, our calculated bubble evolution provides a robust mechanism for the transport of heavy elements (at a level ≈ 0.03 $M_\odot$) to the stellar surface. If combined with a subsequent explosion, then the implied modified surface composition may offer an explanation of the presence of iron-group elements at high velocity, as observed e.g. in SN 1991T like supernovae [3, 8]. Questions concerning possible effects of convective motions remain open, but we believe that since the buoyancy-driven velocities realized soon after ignition rapidly become comparable to expected convective velocities [7], such effects may not significantly influence the evolution of the bubble.

We infer from the fact that our initial condition deviated from perfect

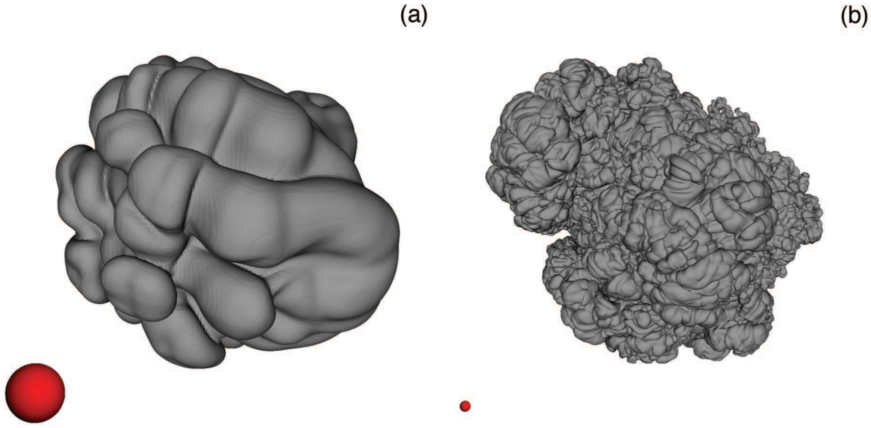

Figure 1: Flame surface evolution. a) The bubble at the moment the Rayleigh-Taylor unstable top surface begins to grow rapidly (i.e, at the end of the first phase of its evolution). b) The bubble as it approaches the stellar surface (i.e., at the end of the second phase of its evolution). The complex structure results from the merging of secondary and later generations of bubbles produced by RTI. Filaments and sheets of largely unburned material are present throughout the bubble. For comparison, the sphere has a radius of 25 km in both images.

symmetry by only a minute amount, yet led to a result drastically different from a central ignition model [13, 5], that central ignition models may generally not be expected to represent "typical" initial conditions for the explosion. Further implications of this evolution for supernova Type Ia are discussed by Plewa, Calder, and Lamb [12]. Their two-dimensional study continued the simulations from a slightly off-center ignition point. The study found that the bubble breaks out of the star at a very high speed and during the break out laterally accelerates fuel-rich material from the outer layers of the star. The material is confined by gravity to the surface of the white dwarf an races around the surface, eventually focusing at a point opposite of the bubble break out. Conditions in the focused region are sufficient for ignition of a detonation that may consume the entire white dwarf and produce an energetic Type Ia supernova. Further, the displacement of mass from the center of the star by the rising bubble leads to some expansion of the star prior to the ignition of a detonation. Observations of significant fractions of intermediate-mass nuclei require such pre-expansion.

In summary, we note that our model shares characteristics with standard DDT models: mild ignition; an increase in velocity to values approaching the sound speed; virtually complete incineration of the white dwarf; the

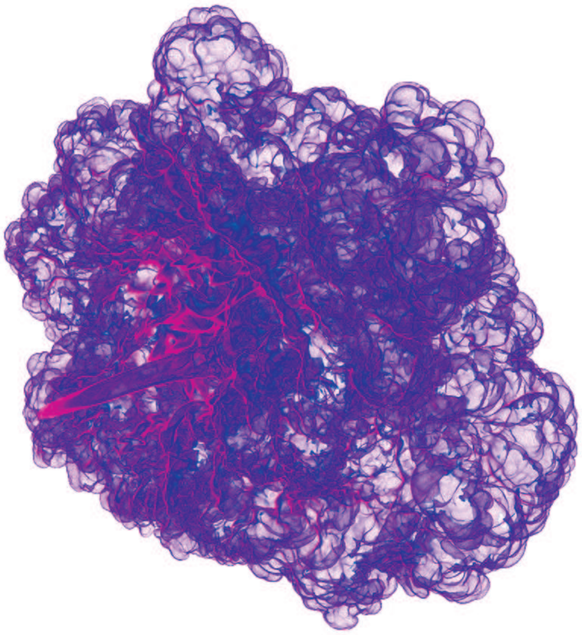

Figure 2: Volume rendering of the bubble of hot ash as it approaches the stellar surface (i.e., at the end of the second phase of its evolution). The complex structure is formed by the merging of secondary and later generations of bubbles produced by RTI. The length scale in the image is identical to that of Fig. 1(b).

requirement of pre-expansion to explain the observed abundance levels of intermediate mass nuclei; layered ejecta; and a modest degree of global asymmetry.

Strengths of our model are associated with a number of unique features: it accommodates possible variations in initial conditions, including specifically off center ignition and associated single bubble deflagration; the pre-expansion required to account for intermediate mass nuclei is powered by gravity; the timescale for pre-expansion depends on the energetics of the deflagration and the time required for the surface wave to travel about the star.

In closing, we note that our results stem principally from our choice of initial conditions, namely one slightly off-center ignition point. We are aware that this is a choice we make without a complete understanding of conditions in the white dwarf just prior to ignition. As things stand, there are disparate results for the effects of convection [16, 7]. It is our belief that our choice of ignition geometry is at least as reasonable as a spherical centered ignition point or set of point given the lack of knowledge concerning conditions in the core.

This work is supported in part by the U.S. Department of Energy under Grant No. B341495 to the Center for Astrophysical Thermonuclear Flashes at the University of Chicago. JWT acknowledges support of the NSF Frontier Center for Nuclear Astrophysics under grant PHY 02-16783 and DOE support under grant DE-FG 02-91ER 40606.

References

[1] A.C. Calder, et al., ApJS, **143** (2002) 201.

[2] A.C. Calder, T. Plewa, N. Vladimirova, D.Q. Lamb, and J.W. Truran, ApJ, submitted.

[3] A.V. Filippenko, ARA&A, **35** (1997) 309.

[4] B. Fryxell, et al., ApJS, **131** (2000) 273.

[5] V. Gamezo, et al., Science, **299** (2003) 77.

[6] F. Hoyle and W.A. Fowler, ApJ, **132** (1960) 565.

[7] P. Höflich and J. Stein, ApJ, **568** (2002) 779.

[8] D.J. Jeffrey et al., ApJ, **397** (1992) 304.

[9] A. Khokhlov, ApJ, **449** (1995) 695.

[10] M. Livio, in Type Ia Supernovae: Theory and Cosmology, ed. J.C. Niemeyer and J.W. Truran (Cambridge: Cambridge University Press) (2000) 33.

[11] J.C. Niemeyer, W. Hillebrandt, and S.E. Woosley, ApJ, **471** (1996) 903.

[12] T. Plewa, A.C. Calder, and D.Q. Lamb, ApJL, in press.

[13] M. Reinecke, W. Hillebrandt, and J.C. Niemeyer, A&A, **391** (2002) 1167.

[14] F.X. Timmes and S.E. Woosley, ApJ, **396** (1992) 649.

[15] J. Whelan and I. Iben, Jr., ApJ, **186** (1973) 1007.

[16] S.E. Woosley, S. Wuhsch, and M. Kuhlen, ApJ, **607** (2004) 921.

Nucleosynthesis in multi-dimensional SNIa explosions

C. Travaglio[1,2], *W. Hillebrandt*[2], *M. Reinecke*[2]

[1] Osservatorio Astronomico di Torino, Italy
[2] Max-Planck Institut für Astrophysik, Garching bei München, Germany

Introduction

The detailed nucleosynthetic yields for 3D hydrodynamical simulations of the thermonuclear burning phase in type Ia supernovae are presented. They are calculated by post-processing the ejecta, using passively advected tracer particles. The nuclear reaction network employed in computing the explosive nucleosynthesis contains 383 nuclear species, ranging from neutrons, protons, and α-particles to ^{98}Mo. Our models follow the common assumption that SNIa are the explosions of white dwarfs that have approached the Chandrasekhar mass ($M_{ch} \sim 1.39$), and are disrupted by thermonuclear fusion of carbon and oxygen. We discuss the nucleosynthetic yields obtained in 3D models with two different choices of ignition conditions (*centrally ignited*, in which the spherical initial flame geometry is perturbated with toroidal rings, and *bubbles*, in which multi-point ignition conditions are simulated), but keeping the initial composition of the white dwarf unchanged. Details of these models are given in a series of papers (Reinecke et al. 1999, 2002a, 2002b). We show that in our simulations unburned C and O varies typically from ~40% to ~50% of the total ejected material. Some of the unburned material remains between the flame plumes and is concentrated in low velocity regions at the end of the simulations. The main differences between all our models and standard 1D computations are, besides the higher mass fraction of unburned C and O, the C/O ratio (in our case is typically a factor of 2.5 higher than in 1D computations), and somewhat lower abundances of certain intermediate mass nuclei such as S, Cl, Ar, K, and Ca, and of ^{56}Ni. We also demonstrate that the amount of ^{56}Ni produced in the explosion is a very sensitive function of density and temperature. Because explosive C and O burning may produce the iron-group elements and their isotopes in rather different proportions one can get different ^{56}Ni-fractions (and thus supernova luminosities) without changing the kinetic energy of the explosion. We also show that we need the high resolution multi-point ignition (bubbles) model to burn most of the material in the center (demonstrating that high resolution coupled with a large number of ignition spots is crucial to get rid of unburned material in a pure deflagration SNIa model). Finally, we investigate the metallicity effect (measured by the original ^{22}Ne content) on the nucleosynthesis and yields.

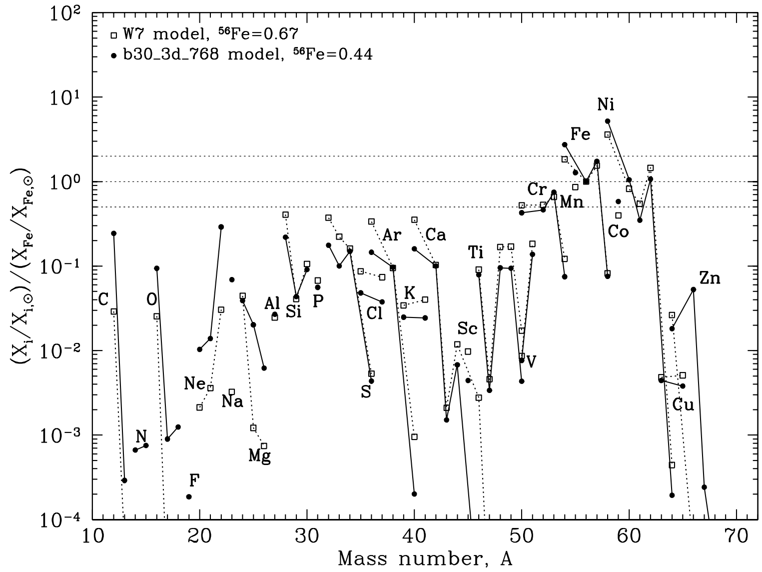

Figure 1: Nucleosynthetic yields (in mass fraction normalized to the solar value and to the corresponding solar ratio) obtained using 19683 tracer particles in the 3D model *b30_3d_768* compared to the W7 yields given by Thielemann et al. (2003).

Discussion and results

Our research focused on the sensitivity of the explosion on the ignition conditions and on the detailed nucleosynthetic yields that they predict. We demonstrated that multi-dimensional explosion models allow us to predict their nucleosynthesis yields with some confidence. We showed that only 3D models are potentially able to produce enough ^{56}Ni to explain the light curves of "normal" type Ia supernovae, and that also the ignition conditions (central ignition vs. several off-center ignition spot) affect the nucleosynthesis yields. Since the number of ignition spots we can put into the numerical models depend on the spatial resolution and since the explosion energy as well as the Ni-mass increase with increasing number of spots, we expect that our best resolved *b30_3d_768* model (a 3D model with ignition in 30 bubbles and grid size of 768^3) is closest to what a "typical" pure-deflagration supernova might eject. The other model presented in this work is the *c3_3d_256* model (a 3D model with central ignition and grid size of 256^3). When the model is centrally ignited, as *c3_3d_256*, the dominant component of unburned material is in the outermost regions. Instead with a floating-bubble model with comparable resolution unprocessed material can also be concentrated in the center. Nevertheless the amount of unprocessed material in the center for a floating-bubble model depends on the amount of ignition-spots together with the resolution used. In fact for the *b30_3d_768* case most of the unburned component in the innermost regions disappeared. We note that the initial conditions (in this case 30 ignition spots) are crucial for a more precise study of the nucleosynthesis, in particular of the innermost regions. Possibly, a model with even higher number of ignition bubbles would give us a still higher ^{56}Fe mass.

The number of tracer particles used for both simulations is 19693. The reason for this number is the following. In the 3D simulations the star is subdivided into 27^3 grid cells equidistant in the integrated mass M(r), azimuthal angle φ and cos θ, so that each grid cell contains the same mass. A tracer particle was placed randomly in each of those grid cells, therefore the total number of tracer particles we used is $27^3 = 19683$.

The initial WD composition we used consists of (mass fraction) 0.475 $M_\odot$ of ^{12}C, 0.5 $M_\odot$ of ^{16}O, and 0.025 $M_\odot$ of ^{22}Ne (in agreement with the W7 initial composition, Iwamoto et al. 1999). With this initial composition we typically simulate a solar metallicity SNIa. When the flame passes through the fuel, ^{12}C, ^{16}O and ^{22}Ne are converted to ashes with different compositions depending on the intial T and ρ. We stop our nucleosynthesis calculations after $\sim$1.5 sec. When the temperature in the markers dropped at $\sim$1.5 10^9 K the explosive nucleosynthesis is almost frozen.

In Fig. 1 we show the yields obtained for our 'standard' model *b30_3d_768* compared with the W7 yields (Brachwitz et al. 2000, Thielemann et al. 2003), scaled to their relative solar abundances and to the ^{56}Fe abundance. As one can see from the figure, a part from the difference in the relative ^{56}Fe mass (0.44 $M_\odot$ for the *b30_3d_768* and 0.669 $M_\odot$ for W7), as well as in the unburned material (i.e. ^{12}C, ^{16}O and ^{22}Ne), the trend for the production of different isotopes is quite similar.

Finally, recent calculations by Timmes et al. (2003) indicate large variations of the ^{56}Ni mass as a function of metrallicity (measured by the original ^{22}Ne content). An investigation of the metallicity effect on the nucleosynthesis and yields is in progress.

More details on all our nucleosynthesis calculations are presented in the recent paper Travaglio et al. (2004).

References

[1] Brachwitz, F., Dean, D.J., Hix, W.R., Iwamoto, K., Langanke, K., Martinez-Pinedo, G., Nomoto, K.I., Strayer, M.R., Thielemann, F.-K., & Umeda, H. ApJ **536** (2000) 934

[2] Iwamoto, K., Brachwitz, F., Nomoto, K.I., Kishimoto, N., Umeda, H., Hix, W.R., & Thielemann, F.K. ApJS **125** (1999) 439

[3] Reinecke, M., Hillebrandt, W., & Niemeyer, J.C. A&A **347** (1999) 739

[4] Reinecke, M., Hillebrandt, W., & Niemeyer, J.C. A&A **386** (2002a) 936

[5] Reinecke, M., Hillebrandt, W., & Niemeyer, J.C. A&A **391** (2002b) 1167

[6] Thielemann, F.-K., Argast, D., Brachwitz, F., Hix, W.R., Höflich, P., Liebendörfer, M., Martinez-Pinedo, G., Mezzacappa, A., Nomoto, K., & Panov, I. (2003), "From Twilight to Highlight: The Physics of Supernovae.", proceedings ESO/MPA/MPE Workshop, Garching, Germany, p. 331.

[7] Timmes, F.X., Brown, E.F., & Truran, J.W. ApJ **590** (2003) L83

[8] Travaglio, C., Hillebrandt, W., Reinecke, M., & Thielemann, F.-K. A&A (2004) submitted

Masses and Radii of Neutron Stars and the Equation of State

J. M. Lattimer

Department of Physics & Astronomy, Stony Brook University, Stony Brook, NY 11794

Introduction

Two of the most important, but unknown, astrophysical quantities are the maximum mass and the typical radius of a neutron star. Determination of these quantities will severely constrain the equation of state (EOS) of dense matter, both near the nuclear saturation density and at much higher densities. New astronomical observations, some of which are summarized here, are highly relevant to these issues.

Masses and Radii – Theoretical Expectations

Rhoades & Ruffini [1] demonstrated that general relativity, coupled with a causal EOS, implies an upper mass limit of $4.2\sqrt{\rho_s/\rho_f}$ $\mathrm{M}_\odot$, where the nuclear equilibrium density is $\rho_s \cong 2.7 \cdot 10^{14}$ g cm^{-3} and ρ_f is a fiducial density. In principal, we understand the EOS up to $\rho_f \approx 1 - -2\rho_s$, so the maximum mass is less than $3 - -4$ $\mathrm{M}_\odot$. On the other hand, the largest accurately measured neutron star mass is that of PSR 1913+16, $1.4408^{+0.0003}_{-0.0003}$ $\mathrm{M}_\odot$ [2]. This wide range does little to constrain the high-density EOS, as shown in Fig. 1.

The causality constraint on masses and radii shown in Fig. 1 is very nearly given by $R = 3GM/c^2$ [5], *i.e.,* 50% larger than the Schwarzschild condition. The radius of the fastest pulsar can also be constrained by the mass-shedding limit, which is

$$R_0 < 15.5 \left(\frac{641\ \mathrm{Hz}}{\nu}\right)^{2/3} \left(\frac{M}{\mathrm{M}_\odot}\right)^{1/3}\ \mathrm{km}\,, \tag{7}$$

where $\nu = 641$ Hz is the spin frequency of PSR B1937+21 and R_0 is the radius of the star of mass M that is not spinning. This relation is approximately independent of the EOS (unpublished). Another limit has been derived from the Vela pulsar glitch observations [6] assuming that the fraction of the moment of inertia involved in glitching ($\Delta I/I > 0.014$) was confined to the star's crust.

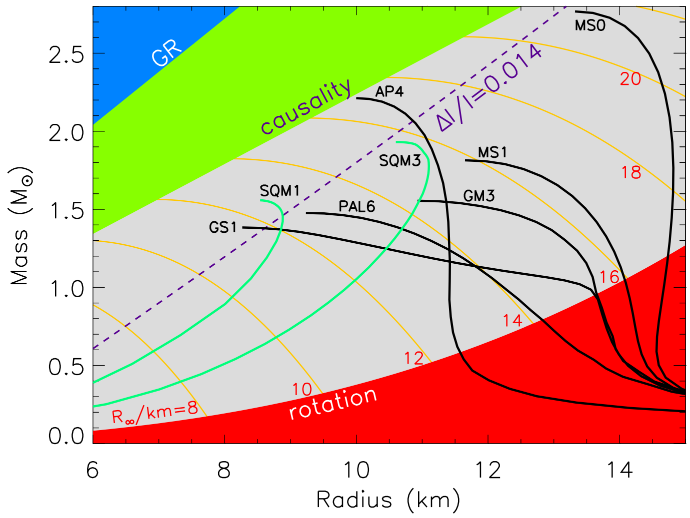

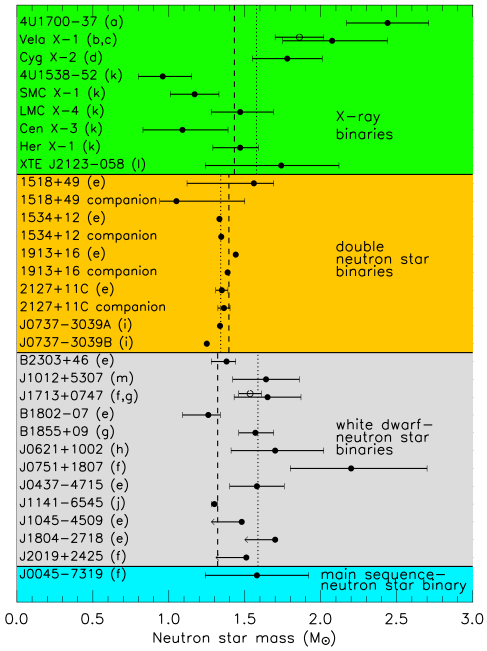

Figure 1: **Top:** Neutron star mass-radius diagram for normal (black) and SQM (green) equations of state identified in [3]. Regions excluded by the GR, causality and rotation constraints are indicated. The $M-R$ limit established from Vela pulsar glitches is indicated by $\Delta I/I = 0.014$. **Bottom:** Neutron star masses determined from binary radio pulsars and selected X-ray binaries (references identified in Ref. [4]). The indicated error bars are 1σ. The dotted (dashed) lines indicate normal (weighted) mean for each group.

Recent Observations Relevant to Masses and Radii

New estimates of neutron star masses have been rapidly accruing, especially from radio binary pulsars. These observations are summarized in Fig. 1 (see Ref. [4] for reference codes, and Ref. [7] for more details and evolutionary implications for these binaries). Among the most interesting of these objects is the pulsar PSR J0751-1807 which has an estimated mass of 2.2 ± 0.2 $M_\odot$ [8]. Some X-ray binaries have estimated masses in excess of 2 $M_\odot$ also (but note that 4U1700-37 might, in fact, be a black hole [9]). Needless to say, a maximum mass in the range of 2 $M_\odot$ would have profound implications; the roles of strange quark matter, hyperons and Bose condesates would be severely limited as is apparent in Fig. 1. Of the curves shown, only PAL6, MSO and AP4 do not have such exotica in their interiors, and PAL6 has an unrealistically small incompressibility of 120 MeV.

It has been hoped that observations of thermal X-ray emission from neutron stars could shed light on neutron star radii. However, this has proven to be an elusive goal. Perhaps the best candidate for a radius measurement is the nearby isolated neutron star RX J1865-3754 discovered by Walter [10] at Stony Brook. Non-magnetic atmospheric fits to combined X-ray and optical emission imply that the atmosphere is dominated by heavy elements and that $R_\infty/d \simeq 0.12 \pm 0.01$ km/pc [11], where d is the distance to the star. With a parallax measurement [12] of 117 ± 12 pc, this implies $R_\infty = 15 \pm 2$ km. In addition, in order to prevent heavy element absorption edges from entering the observed spectra, the redshift z was estimated to be $z \simeq 0.35 \pm 0.05$. These numbers imply a centroid of $M, R = 1.7$ $M_\odot$, 12 km. However, the atmosphere models predict that narrow spectral features should be present, but XMM and Chandra observations have failed to identify them. It might well be that large magnetic fields suppress such features, but in that case, the atmospheric analysis presented by Ref. [11] has to be revised to include the effects of the magnetic fields.

For most other neutron stars with identified thermal emission the problems are compounded by the necessity of extracting the thermal spectrum from (sometimes) dominant non-thermal emission. In at least one of these stars, 1E1207.4-5209, strong spectral features have been observed. Ref. [13] identified these with He-like O ions, indicating $z = 0.06 - 0.21$.

Thermal emission from quiescent neutron stars in binaries is another possibility, since recent accretion may imply that the neutron stars have hydrogenic atmospheres and low magnetic fields, both of which simplify the atmospheric modelling. Finally, X-ray flashes from accreting neutron stars in binaries have yielded, in one case, broad spectral features that Ref. [14]

identified with He-like Fe ions, giving $z \simeq 0.35$. However, the presence of heavy elements in the atmosphere of the star, given the rapid gravitational settling time in the presence of light elements, is problematic [15].

Acknowledgments

I thank M. Prakash for stimulating discussions, and D. Nice for providing neutron star mass data in advance of publication. This research has been supported in part by DOE grant DE-AC02-87ER80317.

References

[1] C.E. Rhoades & R. Ruffini, *Phys. Rev. Lett.* **32** (1974) 324

[2] J.M. Weisberg and J.H. Taylor, in *Radio Pulsars*, ed. M. Bailes, D.J. Nice & S.E. Thorsett (Astron. Soc. Pac. 302, San Francisco, 2003).

[3] J.M. Lattimer & M. Prakash, *Astrophys. J.* **550** 426 (2001).

[4] J.M. Lattimer & M. Prakash, *Science* **304** (2004) 536.

[5] J.M. Lattimer, M. Prakash, D. Masak & A. Yahil, *Astrophys. J.* **355**, 241 (1990).

[6] B. Link, R.I. Epstein & J.M. Lattimer, *Phys. Rev. Lett.* **83** (1999) 3362.

[7] I.H. Stairs, *Science* **304** (2004) 542.

[8] Nice, D. J., Splaver, E. M. & Stairs, I. H., IAU Symp. 218, ASP Conference Proceedings, eds. F. Camillo & B. M. Gaensler (2004) [astro-ph/0311296].

[9] J.S. Clark *et al.*, *A. & A.* **392** (2002) 909.

[10] F.M. Walter, S. Wolk & R. Neuhauser *Nature*, **379** (1996) 233.

[11] J.A. Pons, F.M. Walter, J.M. Lattimer, M. Prakash, R. Neühauser & P. An, *Ap. J.* **564** (2002) 981.

[12] F.M. Walter & J.M. Lattimer, *Ap. J.* **576** (2002) L145.

[13] C. Hailey & K. Mori, *Ap. J.* **578** (2002) L133.

[14] J. Cottam, F. Paerels & M. Mendez, *Nature* **420** (2002) 51.

[15] L. Bildsten, P. Chang & F. Paerels, *Ap. J.* **591** (2003) L29.

Cooling of neutron stars: effects of accreted envelopes, magnetic field and crustal superfluidity

G. Chabrier[1], *A. Y. Potekhin*[2], *D. G. Yakovlev*[2]

[1] Ecole Normale Supérieure de Lyon, CRAL (UMR CNRS 5574), Lyon, France
[2] Ioffe Physico-Technical Institute, St.-Petersburg, Russia

Abstract

We briefly review recent theoretical studies of the effects of accreted envelopes, magnetic fields and crustal superfluidity on the cooling of neutron stars. These effects are especially important for slowly cooling low-mass neutron stars, where direct Urca process of neutrino emission is forbidden. The effects are useful for interpretation of observations of several isolated middle-aged neutron stars.

Introduction

It is conventional to separate a neutron star (NS) into the isothermal interior and the outer heat-blanketing envelope. The envelope can be treated separately in the plane-parallel quasi-Newtonian approximation (Gudmundsson et al. [1]; hereafter GPE). The evolution of NSs is controlled by the relationship between the surface temperature T_s and the temperature T_b at the envelope bottom, at a density $\rho_b \lesssim 10^{10-11}$ g cm^{-3}. The temperature distribution in the blanketing envelope is determined by the equation (see, e.g., GPE)

$$\frac{dT}{dP} = \frac{3}{16} \frac{K}{g} \frac{T_s^4}{T^3}, \tag{8}$$

where g is the surface gravity, P is the pressure, and $K = 1/(K_r^{-1} + K_e^{-1})$ denotes the total mean opacity, including the radiative and electron contributions (K_r and K_e, respectively).

The first accurate model of a non-magnetized, pure iron blanketing envelope was developed by GPE. This model has been improved in recent years in several respects. The thermodynamic and transport properties of the plasma in the envelope have been updated; a possible presence of accreted, light-element surface layers has been taken into account [2, 3, 4, 6]; the effects of magnetic fields in the blanketing envelope have been analyzed

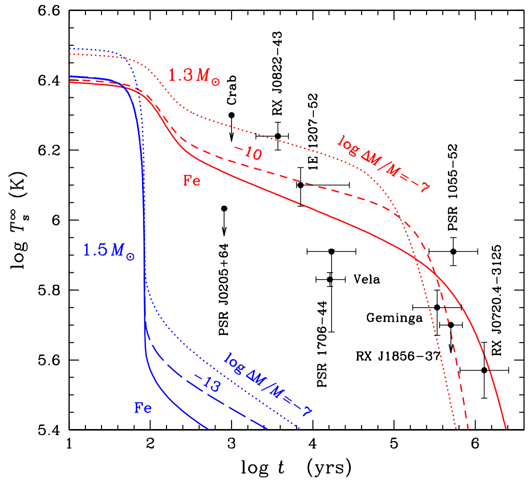

Figure 1: Cooling of nonsuperfluid 1.3 and 1.5 $M_\odot$ NSs with different masses ΔM of accreted layers, as compared with observation. Solid curves refer to nonaccreted (Fe) envelopes.

[5, 6]. In addition, the effect of superfluidity of neutrons in inner NS crusts (at densities from neutron drip, $\sim 4\times10^{11}$ g cm^{-3}, to $\sim 1.5\times10^{14}$ g cm^{-3}) on the cooling has been considered [6, 7]. Other references can be found in [8].

Here we summarize how the physics of NS crusts affects the cooling. The effect is particularly important for low-mass stars, where the powerful direct Urca process of neutrino emission is forbidden by momentum conservation law.

Below we present theoretical cooling curves (effective surface temperatures as detected by a distant observer, T_s^∞ versus stellar age t) calculated with the physics input described in Ref. [8]. We use the same version of a moderately stiff equation of state in NS cores as in [8]. In this model the direct Urca process is open in the inner cores of NSs with gravitational mass $M > 1.358\,\mathrm{M}_\odot$. We compare theoretical results with observations of thermal radiation from isolated middle-aged NSs. The observational basis is the same as in [8].

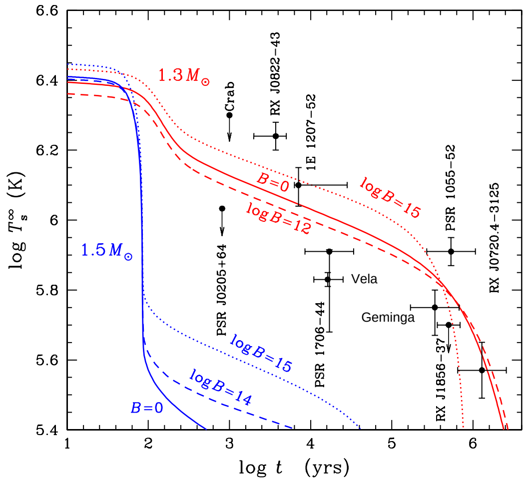

Figure 2: Same as in Figure 1 for nonaccreted envelopes with several dipole magnetic fields.

Effect of accreted envelopes

Figure 1 illustrates the effect of accreted layers on cooling of nonsuperfluid NSs of two masses. A massive star with $M = 1.5\ \mathrm{M}_\odot$ gives an example of rapid cooling dominated by direct Urca process, whereas a low-mass star, $M = 1.3\ \mathrm{M}_\odot$, gives an example of slow neutrino cooling via modified Urca process. Drops of cooling curves at $t \sim 100$ yr manifest the end of thermal relaxation between stellar core and crust. Drops at $t \sim 10^5$–10^6 yr indicate the transition from the neutrino cooling stage to the photon cooling stage. Accreted envelopes have opposite effects at these two stages. At the neutrino cooling stage, the more heat-transparent blanketing envelope, due to accretion of light elements, leads to a larger surface temperature than in the case of iron envelope. In contrast, during the photon cooling stage, the lower thermal insulation of the accreted envelope leads to a faster cooling. Even a very small fraction of accreted matter ($\Delta M/M \sim 10^{-16}$) changes appreciably the cooling [2, 3, 6].

Effect of magnetic field

The thermal structure of NSs is strongly affected by magnetic fields. Landau quantization of electron orbits in a magnetic field affects the thermodynamic

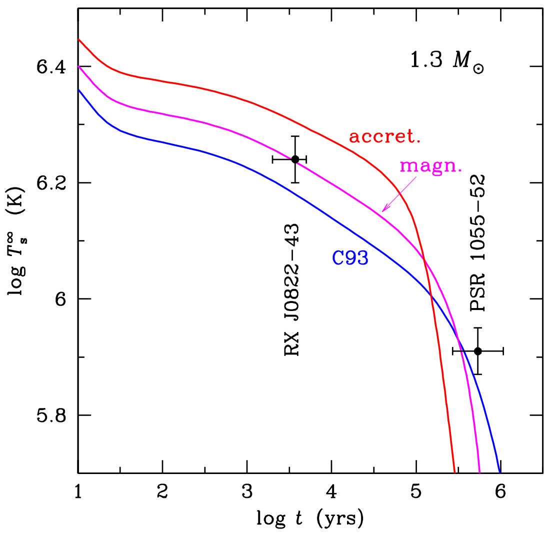

Figure 3: Cooling of superfluid protons in the core and superfluid neutrons in the crust (curve "C93"). Curves "accret" and "magn" include, in addition, the effects of accreted envelope ($\Delta M/M = 10^{-7}$) and surface magnetic field ($B = 10^{15}$ G), respectively.

properties, the heat conduction, and the radiative opacities in the surface layers [10, 11, 12, 13]. In particular, Landau quantization enhances heat transport along the field lines and thus increases T_s (for a given T_b) near magnetic poles. By contrast, classical effect of electron Larmor rotation reduces electron thermal conductivity across the field lines, decreasing T_s near magnetic equator. The case of arbitrary inclination of the magnetic field to the NS surface has been studied in [14, 15, 16, 17]. More recently Potekhin et al. [5, 6] used improved electron conductivities of magnetized envelopes [18], as well as improved radiative opacities and equation of state of partially ionized, strongly magnetized hydrogen in NS atmospheres [12, 13], to calculate the cooling of NSs with strong dipole magnetic fields. Figure 2 displays the effect of dipole magnetic fields on the cooling of nonsuperfluid high-mass and low-mass NSs. The curves are marked by magnetic field strength at the magnetic pole. At $B \gtrsim 10^{12}$ G the temperature distribution over the stellar surface becomes strongly anisotropic, with the magnetic poles much hotter than the equator. Figure 2 shows the effective temperature T_s^∞ averaged over the surface (see, e.g., [5, 6]). As in the case of accreted envelopes, magnetic fields have opposite effects at the neutrino and photon cooling stages. Fields with $B \lesssim 10^{13}$ G make the blanketing envelope overall less heat-transparent, decreasing T_s at the neutrino cooling stage and increasing T_s at the photon cooling stage (especially for low-mass stars). Stronger fields have the opposite effect.

Effect of crustal superfluidity

Observational data can be explained assuming a weak triplet-state pairing of neutrons and a strong singlet-state pairing of protons in stellar cores (see, e.g., Ref. [8] and references therein). Let us focus on cooling of low-mass NSs in the frame of this scenario. The strong proton superfluidity switches off the modified Urca process in the cores. The cooling of these stars becomes exceptionally slow. It turns out to be rather insensitive to the equation of state and models for strong proton superfluidity in stellar cores. However, it becomes sensitive to the models for singlet-state neutron pairing in stellar crusts (whereas cooling of more massive stars does not depend on the crustal superfluidity).

This effect is illustrated in Fig. 3 which shows (curve "C93") cooling of a star ($M = 1.3$ $\mathrm{M}_{\odot}$) with a strong superfluidity of protons (model 1p of Ref. [8]), no triplet-state superfluidity of neutrons in the core, and a model of Chen et al. [9] for singlet-state crustal neutron superfluidity. The crustal superfluidity initiates neutrino emission due to Cooper pairing of neutrons. Because the neutrino emission from the stellar core is weak, the crustal neutrino emission noticeably accelerates the cooling [6]. The acceleration is not too strong and enables to explain the observations of PSR B1055–52, although violates interpretation of the observations of RX J0822–4300. In order to explain the latter source, one can assume that it has either a strong magnetic field or an accreted envelope.

Conclusion

Our calculations show that detailed models of NS cooling, taking into account the effects of accretion, dipole magnetic fields and crustal superfluidity can help to explain observations. These effects are most important for slowly cooling low-mass NSs – isolated middle-aged NSs hottest for their ages. Although several models of crustal superfluidity are currently consistent with observational error bars of effective temperatures T_s^{∞} of these objects, better measurements of T_s^{∞} in the future should lead to a better determination of the surface magnetic fields and the masses of accreted envelopes of these objects and should allow one to discriminate between models of crustal superfluidity.

Acknowledgements

The work of A.P. and D.Y. is supported in part by RFBR (grants 02-02-17668 and 03-07-90200) and by the Russian Leading Scientific Schools Foundation (grant 1115.2003.2).

References

[1] E. H. Gudmundsson, C. J. Pethick, & R. I. Epstein, ApJ **272** (1983) 286 (GPE)

[2] G. Chabrier, A. Y. Potekhin, & D. G. Yakovlev, ApJ **477** (1997) L99

[3] A. Y. Potekhin, G. Chabrier, & D. G. Yakovlev, A&A **323** (1997) 415

[4] E. F. Brown, L. Bildsten, & P. Chang, ApJ **574** (2002) 920

[5] A. Y. Potekhin & D. G. Yakovlev, A&A **374** (2001) 213

[6] A. Y. Potekhin, D. G. Yakovlev, G. Chabrier, & O. Y. Gnedin, ApJ **594** (2003) 404

[7] D. G. Yakovlev, A. D. Kaminker, & O. Y. Gnedin, A&A **379** (2001) L5

[8] D. G. Yakovlev & C. J. Pethick, Ann. Rev. Astron. Astrophys. (2004) in print [astro-ph/0402143]

[9] J. M. C. Chen, J. W. Clark, R. D. Davé, & V. V. Khodel, Nucl. Phys. A **555** (1993) 59

[10] A. Y. Potekhin, G. Chabrier, & Yu. A. Shibanov, Phys. Rev. E **60** (1999) 2193

[11] D. Lai, Rev. Mod. Phys. **73** (2001) 629

[12] A. Y. Potekhin & G. Chabrier, ApJ **585** (2003) 955

[13] A. Y. Potekhin & G. Chabrier, ApJ **600** (2004) 317

[14] L. Hernquist, MNRAS **213** (1985) 313

[15] D. Page, ApJ **442** (1995) 273

[16] Yu. A. Shibanov & D. G. Yakovlev, A&A **309** (1996) 171

[17] D. G. Yakovlev, A. D. Kaminker, P. Haensel, & O. Y. Gnedin, A&A **389** (2002) L24

[18] A. Y. Potekhin, A&A **351** (1999) 787

Equation of state under the conditions of NSE

D.K. Nadyozhin, A.V. Yudin

Institute for Theoretical and Experimental Physics (ITEP), B. Cheremushkinskaya St. 25, 117259, Moscow, Russia

Beginning from the classical papers of Hoyle and Fowler [7, 2, 8] the thermodynamic properties of stellar matter under the conditions of nuclear statistical equilibrium (NSE) repeatedly were discussed in the literature (for instance, see [9, 10, 12, 5] and references therein).

Here we report the first results of our new project aimed at calculating the equation of state (EOS) for NSE which depends on three variables – temperature T, density ρ, and the ratio of total number of neutrons to that of protons θ (free plus bounded in nuclei; cf. [3]). The main objective of the project is to analyze in detail the influence on EOS of such effects as the nuclear excitation, degeneration of free nucleons, Coulomb interaction, and the presence of the neutron-rich nuclei. We concentrate on subnuclear densities $\rho \lesssim 10^{13}\,\mathrm{g\,cm^{-3}}$ when the strong nuclear interaction is not yet important [5].

In total 129 nuclides were taken into account – from Ca through Kr plus a chain of α-nuclei: ^{4}He,^{12}C,^{16}O,... ,^{36}Ar. The binding energies and properties of the experimentally detected excited states were extracted from interactive data-bases NUCLEUS [13] and Isotope Explorer [4]. The nuclides are considered to obey the Boltzmann statistics whereas the Fermi-degeneracy of free nucleons is described by expansion in series of the half-integer Fermi–Dirac functions. The full Fermi–Dirac statistics is assumed for the electron-positron component as described by the code EPEOS [1].

A long-standing problem of accounting for the nuclear partition functions $\omega_{A,Z}(T)$, has not yet a strict solution, especially for a high-temperature regime when the mean excitation energy $\langle E_{\rm ex}\rangle$ becomes comparable to the nuclear binding energy $Q_{A,Z}$ (see the discussion in [6, 11, 14, 15]). To estimate $\omega_{A,Z}$ we have used for each nucleus (A,Z) the number $N_{\rm ex}(A,Z)$ of low, experimentally measured, excited states available from [4] (more than ~ 100 states for some nuclei). Then for the higher excited states at the low-temperature regime ($T_9 < 40$), we have used the noninteracting Fermi-gas model with parameters as provided in [14]. In the high-temperature regime ($T_9 \geq 40$) the following simple analytical approximation was implemented:

$$\ln\omega_{A,Z}(T) \quad = \quad a_{A,Z} - \frac{Q_{A,Z}}{T}\left(0.8 - \frac{b_{A,Z}}{T} - \frac{c_{A,Z}}{T^2}\right), \qquad (9)$$

$$\langle E_{\rm ex}\rangle = T\frac{{\rm d}\ln\omega}{{\rm d}\ln T} \quad = \quad Q_{A,Z}\left(0.8 - 2\frac{b_{A,Z}}{T} - 3\frac{c_{A,Z}}{T^2}\right), \tag{10}$$

where T is in energy units ($k = 1$). The coefficients $a_{A,Z}$, $b_{A,Z}$, and $c_{A,Z}$ are determined by continuity of ω, ω', and ω'' on the interface with the low-temperature regime at $T_9 = 40$. According to Eq. (10), the mean excitation energy never exceeds $0.8\,Q_{A,Z}$. The number "0.8" is actually a free parameter. If it were replaced by "1" all the thermodynamic quantities would change only by $\sim$1% .

Figure 1 shows how the above approach works for ^{56}Fe-nucleus ($N_{\rm ex} = 111$). The thick solid curve for $\ln\omega$ and dashed one for $\langle E_{\rm ex}\rangle$ are provided by our approach – specifically, at $T_9 > 40$ they reproduce Eqs. (9) and (10), respectively. The thin almost straight solid line for $\ln\omega$ and dotted one for $\langle E_{\rm ex}\rangle$ are due to the Fermi-gas model. Already at $T_9 \sim 100$ the excitation energy for the Fermi-gas model turns out to be close to the ^{56}Fe binding energy $Q_{56,26} = 492$MeV.

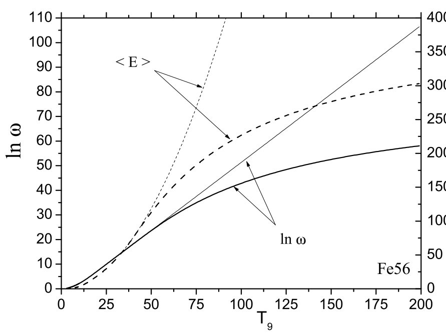

Figure 1: Logarithm of the partition function (left vertical scale) and the mean excitation energy (right vertical scale) for ^{56}Fe as functions of temperature.

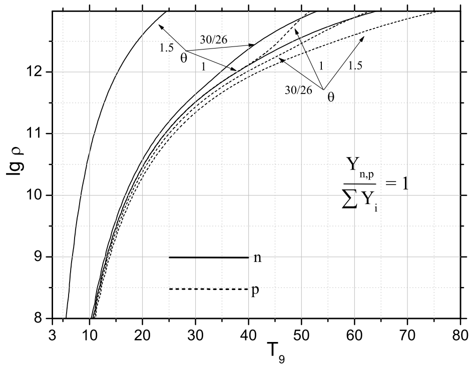

Figure 2: The loci of equal number densities of free nucleons and heavier nuclei for $\theta = 1, 30/26$, and 1.5. Free neutrons are shown by the solid curves while free protons by the short-dashed ones.

Let us proceed to a brief survey of some our results. Figure 2 shows the (T, ρ)-plane with the lines along which the number densities of free neutrons $Y_{\rm n}$ and protons $Y_{\rm p}$ are equal to those of heavier nuclides, including ^{4}He: $Y_{\rm n} = \sum Y_i$ and $Y_{\rm p} = \sum Y_i$. Free nucleons dominate by number right of the corresponding lines. Their density, especially that of free protons, is very important for calculating the kinetics of the non-equilibrium neutronization during the first neutrino-transparent stage of gravitational collapse.

Another important quantity is the adiabatic index $\gamma = \left(\frac{\partial \ln P}{\partial \ln \rho}\right)_{S,\theta}$. The lines of constant γ on the (T, ρ)-plane are shown in Fig. 3. The thick solid and dashed curves correspond to

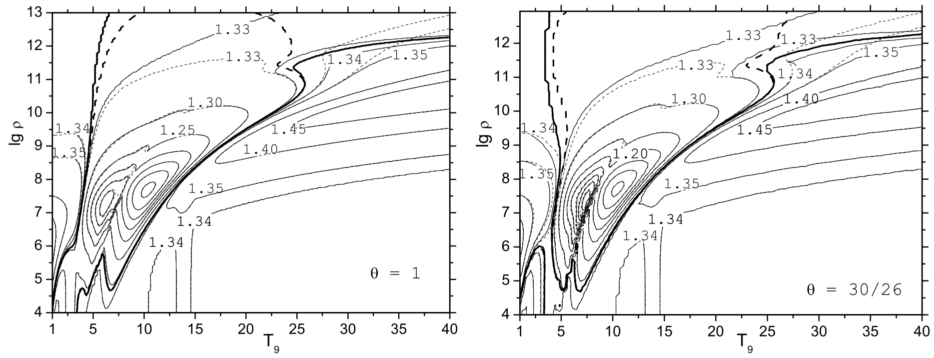

Figure 3: The level lines of γ with (solid lines) and without (dashed lines) taking into account the nuclear excited states. The left panel is for $\theta = 1$ and the right one for $\theta = 30/26$.

the level $\gamma = 4/3$ with and without the nuclear excitation, respectively. (Note that curves labelled as 1.33 relate to exact value $1.33 < 4/3$.) One can observe two deep minima of γ [9]. The first one $\gamma_{\min} \approx 1.07\,(\theta = 1)$, $0.94\,(\theta = 30/26)$ is located at $\rho \approx 2 \times 10^7 \mathrm{g\,cm}^{-3}$ and $T_9 \approx 6.3\,(\theta = 1)$, $7.5\,(\theta = 30/26)$. It appears owing to a simultaneous action of the electron-positron pairs and dissociation of *heavy nuclei* into α-particles and free nucleons. The second minimum $\gamma_{\min} \approx 1.04 \div 1.05$ is connected with the dissociation of *α-particles* into free nucleons in the presence of pairs and occurs at $\rho \approx 5 \div 6 \times 10^7 \mathrm{g\,cm}^{-3}$ and $T_9 \approx 10.5 \div 10.6$.

At low densities ($\lesssim 10^6 \mathrm{g\,cm}^{-3}$), γ becomes less than 4/3 due to pairs while at higher densities due to the dissociation of heavy nuclei into α-particles and free nucleons. For $\theta = 1$, the two effects overlap to produce a simply connected domain of instability $\gamma < 4/3$. However in the case $\theta = 30/26$, there appears a narrow (moreover rather low: $\gamma - 4/3 \approx 0.002$) "bridge" at $3 \lesssim T_9 \lesssim 4$ that divides the instability domain into two parts. This happens because in the case $\theta = 30/26$ the NSE is dominated by the most bounded nuclides (^{56}Fe) and the dissociation begins at slightly higher temperature than for $\theta = 1$ when NSE is dominated by less bounded ^{56}Ni. This weakens the overlap of above effects and the bridge appears. For $\theta = 1.5$, the NSE shifts again to less bounded nuclides thereby recreating the integrity of the domain $\gamma < 4/3$.

One can see that the nuclear excitation notably affects γ only at the densities $\rho \gtrsim 3\times10^9 - 10^{10}\,\mathrm{g\,cm^{-3}}$ widening the domain of instability $\gamma < 4/3$.

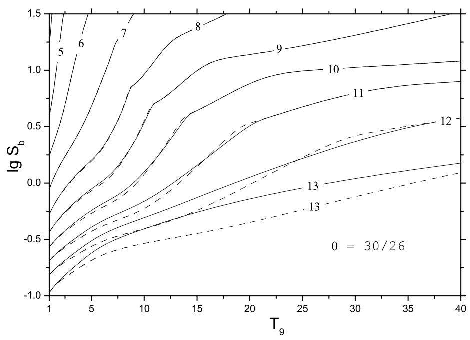

Figure 4: The dimensionless entropy $S_b = \frac{m_\mathrm{u}}{k} S$ versus T_9 for different $\lg\rho$ indicated at the curves. The dashed curves correspond to the case when the nuclear excitation is neglected.

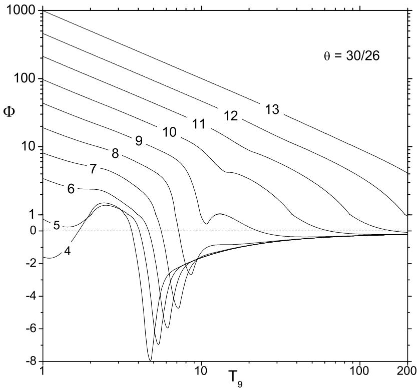

Figure 5: The dimensionless quantity Φ versus T_9 for different $\lg\rho$ indicated at the curves. Note a linear scale for the lower part of the vertical axis ($\Phi \le 1$) and a logarithmic scale for the upper one ($\Phi > 1$).

Figure 4 shows total entropy S_b per nucleon versus temperature at different densities for $\theta = 30/26$. The contribution of every individual nucleus to S_b increases when one takes into account the excited states. However, the nuclear excitation hinders the dissociation of nuclei into free nucleons thereby decreasing their contribution to S_b. Thus at given T and ρ, the nuclear excitation can change S_b in opposite directions (compare solid and dashed curves in Fig. 4).

One of the important questions is the temporal behavior of entropy during the collapse. The first law of thermodynamics in our case reads (see also [10]):

$$\mathrm{d}E + P\,\mathrm{d}V = T\,\mathrm{d}S + \frac{kT}{m_\mathrm{u}}\Phi\,\mathrm{d}Y_l \qquad \left(V \equiv \frac{1}{\rho}\right), \tag{11}$$

where Y_l is the lepton charge per nucleon. In absence of the neutrino component in EOS (our case):

$$Y_l = Y_\mathrm{e} = \frac{1}{1+\theta}, \quad \Phi = -\frac{1}{kT}\left(\mu_\mathrm{n} - \mu_\mathrm{p} - \mu_\mathrm{e}\right), \tag{12}$$

where μ_n, μ_p, and μ_e are chemical potentials of neutrons, protons, and electrons. Figure 5 shows Φ as a function of T for different ρ and $\theta = 30/26$.

For the adiabatic process ($\mathrm{d}E + P\,\mathrm{d}V = 0$), we have $\mathrm{d}S_\mathrm{b} = -\Phi\,\mathrm{d}Y_l$ and S_b would increase during neutronization ($\mathrm{d}Y_l < 0$) if $\Phi > 0$. However since some energy is being taken away by the electron neutrino, the inequality $\Phi > 0$ is only *necessary* but not yet sufficient condition for S_b to increase in collapse.

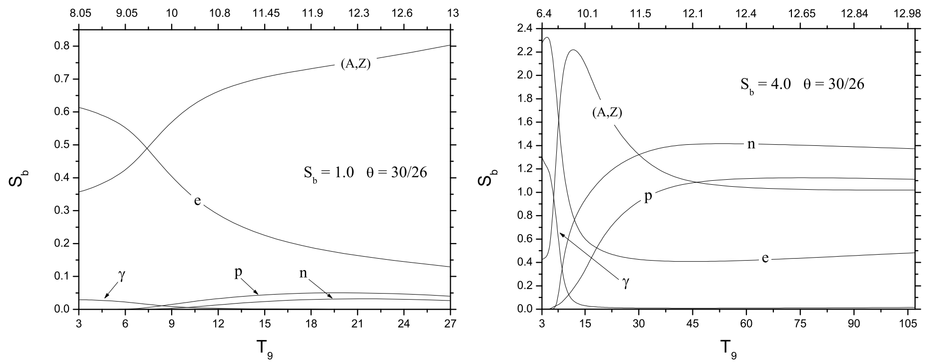

Figure 6: Contribution to total constant entropy $S_\mathrm{b} = 1$ (left panel) and $S_\mathrm{b} = 4$ (right panel) of all the nuclides (A, Z), electron-positron component e, free neutrons n, protons p, and black body radiation γ as a function of the temperature (lower horizontal scale) or the corresponding density ($\lg \rho$ is shown on the upper horizontal scale).

Figure 6 shows the contribution of different components to total entropy $S_\mathrm{b} = \sum S_{A,Z} + S_\mathrm{n} + S_\mathrm{p} + S_\mathrm{e} + S_\gamma$. Detailed analysis suggests that for low entropies ($S_\mathrm{b} \lesssim 2$) the contribution of heavy nuclei dominates up to subnuclear densities. In this case very neutron-rich nuclei prove to be thermodynamically important. On the contrary, for larger entropies ($S_\mathrm{b} > 2$) the abundances of those nuclei are never large enough to be thermodynamically significant.

In conclusion we can summarize our results as follows:

- The partition functions are not very crucial for EOS and can result in moderate changes in entropy and γ only for $\rho \gtrsim 10^{10}\,\mathrm{g\,cm^{-3}}$.
- For low entropies ($S_\mathrm{b} \lesssim 2$) the neutron-rich nuclei can have a strong impact on EOS by contributing to entropy and by lowering Y_n and Y_p.
- The free nucleon degeneracy is of a slight influence since at low T nearly all neutrons and protons are packed in heavy nuclei.

The study of the role of Coulomb interaction and neutron-rich nuclei is under way. Our ultimate goal is to construct a 3-parametric table for free energy and to supply it with a smooth interpolation procedure useful for calculating EOS in hydrodynamic modelling of the gravitational collapse, especially of its first neutrino-transparent stage coupled with non-equilibrium neutronization of infalling matter.

Acknowledgements

One of us (DKN) is grateful to MPI für Astrophysik for financial support and hospitality. The work is supported also by Grant 04-02-16840-a of Russian Foundation for Basic Research.

References

[1] S.I. Blinnikov, N.V. Dunina-Barkovskaya, D.K. Nadyozhin ApJS **106** (1996) 171.

[2] E.M. Burbidge, G.K. Burbidge, W.A. Fowler, F. Hoyle F. Rev. Mod. Phys. **29** (1957) 547.

[3] F.E. Clifford, R.J. Tayler Memoirs Royal Astron. Soc. **69** (1965) 21.

[4] S.Y. Chu S.Y., H. Nordberg, R.B. Firestone, L.P. Ekstrom Isotope Explorer (1999) http://ie.lbl.gov/toi.html

[5] M.F. El Eid, W. Hillebrandt A&A Suppl. **42** (1980) 215.

[6] W.A. Fowler, C.A. Engelbrecht, S.E. Woosley ApJ **226** (1978) 984.

[7] F. Hoyle MNRAS **106** (1946) 343.

[8] F. Hoyle, W.A. Fowler ApJ **132** (1960) 565.

[9] V.S. Imshennik, D.K. Nadyozhin Astron. Zh. **42** (1965) 1154.

[10] V.S. Imshennik, V.M. Chechetkin Astron. Zh. **47** (1970) 929.

[11] T.J. Mazurek, J.M. Lattimer, G.E. Brown ApJ **229** (1979) 713.

[12] M.J. Murphy ApJS **42** (1980) 385.

[13] B. Potet, J. Duflo, G. Audi Proc. of the Int. Conf. on Exotic Nuclei and Atomic Masses ENAM-95 ed. M. de Saint-Simon and O. Sorlin (Editions Frontieres), Arles, France, (June 1995) 151.

[14] T. Rauscher, F.–K. Thielemann, K.–L. Kratz Phys. Rev. **C. 56** (1997) 163.

[15] D.L. Tubbs, S.E. Koonin ApJ **232** (1979) L59.

Collapse and Explosion of 8 - 10 $M_\odot$ Stars

K. Nomoto[1], *S. Wanajo*[2], *N. Iwamoto*[1], *Y. Ishimaru*[3]

[1] Department of Astronomy, University of Tokyo
[2] Department of Physics, Sophia University
[3] Department of Physics, Ochanomizu University

Abstract

The final fate of 8 - 10 $M_\odot$ stars is reviewed. These stars form degenerate O+Ne+Mg cores and eventually undergo collapse, if the mass loss rate is not too high. If the weak explosion results, it can be consistent with the nature of SN 1054. These stars could be important sites of r- and s-process nucleosynthesis as well.

Collapse of O+Ne+Mg Core induced by Electron Capture

For 8 - 10 $M_\odot$ stars, electron degeneracy becomes significant already in a C+O core. In a semi-degenerate C+O core, a temperature inversion appears due to neutrino cooling. This leads to off-center ignition of carbon when the C+O core mass exceeds the critical mass of 1.06 $M_\odot$. (For $M > 10.4 M_\odot$, carbon ignites in the center.) The off-center carbon burning shell moves inward all the way to the center due to heat conduction [5]. After exhaustion of carbon in the central region, an O+Ne+Mg core forms. The core mass does not exceed the critical mass of 1.37 $M_\odot$ for neon ignition and, hence, neon burning is never ignited [5]. Then the O+Ne+Mg core becomes strongly degenerate. The envelope becomes similar to asymptotic giant-branch (AGB) stars with the thin He burning shell that undergoes thermal pulses and thus s-process nucleosynthesis.

The final fate depends on the competition between the mass loss that reduces the envelope mass and the increase in the core mass through the H-He shell burning. If the mass loss is fast, the O+Ne+Mg white dwarf is formed, which could be the case for 8 $M_\odot$ - $M_{\rm up}$ stars, where $M_{\rm up} = 9 \pm 1 M_\odot$. For $M_{\rm up}$ - 10 $M_\odot$ stars, the core mass grows to 1.38 $M_\odot$ and the central density reaches 4×10^9 g cm^{-3}. The electron Fermi energy exceeds the threshold for electron captures ^{24}Mg(e$^-, \nu$) ^{24}Na (e$^-, \nu$) ^{20}Ne and ^{20}Ne (e$^-, \nu$) ^{20}F (e$^-, \nu$) ^{20}O. The resultant decrease in Y_e triggers collapse [7].

The hydrodynamical behavior of collapse could be somewhat different from the iron core collapse of more massive stars [3]. If the explosion energy would be as weak as $E < 10^{50}$ (e.g., Janka, Liebendoerfer, in this volume), the supernova could be similar to SN 1054 because the Crab Nebula does not show significant enhancement of heavy elements and has the small kinetic energy [4, 6]. Recently, we noticed that 8 - 10 $M_\odot$ stars could be important r- and s-process nucleosynthesis.

r-Process in 8 - 10 $M_\odot$ Stars

While the origin of r-process nuclei remains a long-standing mystery, recent spectroscopic studies of extremely metal-poor stars in the Galactic halo strongly suggest that it is associated with core-collapse supernovae. Wanajo et al. [11] has examined r-process nucleosynthesis in a "prompt supernova explosion" from an $8 - 10 M_\odot$ progenitor star, as an alternative scenario to the "neutrino wind" mechanism which has also been considered to be a promising site of the r-process.

Wanajo et al. [11] obtained a very weak prompt explosion, in which no r-processing occurs. Then they further simulated energetic prompt explosions by enhancing the shock-heating energy, in order to investigate conditions necessary for the production of r-process nuclei in such events. The highly neutronized ejecta ($Y_e \approx 0.14 - 0.20$) leads to robust production of r-process nuclei; their relative abundances are in excellent agreement with the solar r-process pattern. Their results suggest that prompt explosions of $8 - 10 M_\odot$ stars with O-Ne-Mg cores can be a promising site of r-process nuclei. The mass of the r-process material per event is about two orders of magnitude larger than that expected from Galactic chemical evolution studies. They propose, therefore, that only a small fraction of r-process material is ejected, owing to the "mixing-fallback" mechanism of the core matter wherein most of the r-process material falls back onto the proto-neutron star [10].

$r + s$-Enhanced Extremely Metal-Poor Stars

Recent spectroscopic studies have revealed the presence of numerous carbon-enhanced, metal-poor (CEMP) stars with [Fe/H] < -2.0 that exhibit strong enhancements of s-process elements. This is believed to be a result of binary mass-transfer from a former AGB companion that underwent s-process nucleosynthesis. However, several such stars exhibit significantly lower Ba/Eu ratios than solar s-process abundances [2, 1]. This might be explained if (1) there were an additional contribution from the r-process, thereby diluting the Ba/Eu ratio by extra production of Eu, or (2) if some fraction of low-metallicity AGB stars undergo s-process nucleosynthesis that produces reduced Ba/Eu ratios. About 50% of the CEMP stars seem to be consistent with the latter case, and also exhibit large enhancements of Pb. There are still, however, a few CEMP stars whose observed elemental abundances do not conflict with the former case. We propose, if there exist such stars, that the double enhancements of r-process and s-process elements originate from a former $8-10M_{\odot}$ companion in a wide binary system, which may undergo s-processing during an AGB phase, and r-processing during its subsequent supernova explosion [12].

Accretion-Induced Collapse of O+Ne+Mg White Dwarfs

If 8 - 10 $M_{\odot}$ stars are in close binary systems, O+Ne+Mg white dwarfs are formed after the envelopes are lost to the companion stars. If the companions of the binary systems are similar to those of Type Ia supernovae, the O+Ne+Mg white dwarfs grow their masses to the Chandrasekhar mass limit and undergo accretion-induced collapse (AIC) [8]. r-process nucleosynthesis could occur (also [9]). During accretion, the helium shell flashes reccur many times to synthesize s-process elements, a part of which is ejected in the helium-rich wind, while the rest is retained in the outer layers of the white dwarfs. Thus the accreting white dwarfs could contaminate the companion stars with s- and r-process elements (also [1]).

Acknowledgements

It is a great pleasure to thank Wolfgang Hillebrandt for a long term support to my visit to MPA since 1981 and international collaborative work there starting from 8 - 10 $M_{\odot}$ stars.

References

[1] Cohen, J. G., Christlieb, N., Qian, Y. -Z. & Wasserburg, G. J. 2003, ApJ, 588, 1082

[2] Hill, V., et al. 2000, A&A, 353, 557

[3] Hillebrandt, W., Nomoto, K., & Wolff, G. 1984, A&A, 133, 175

[4] Nomoto, K., Sparks, W. M., Fesen, R. A., Gull, T. R., Miyaji, S., & Sugimoto, D. 1982, Nature, 299, 803

[5] Nomoto, K. 1984, ApJ, 277, 791

[6] Nomoto, K. 1985, in *The Crab Nebula and Related Supernova Remnants*, ed. M.C. Kafatos & R.B.C. Henry (Cambridge: Cambridge University Press) 97

[7] Nomoto, K. 1987, ApJ, 322, 206

[8] Nomoto, K. & Kondo, Y. 1991, ApJ, 367, L19

[9] Qian, Y. -Z. & Wasserburg, G. J. 2003, ApJ, 588, 1099

[10] Umeda, H. & Nomoto, K. 2002, ApJ, 565, 385

[11] Wanajo, S., Tamamura, M., Itoh, N., Nomoto, K., Ishimaru, Y., Beers, T. C., & Nozawa, S. 2003, ApJ, 593, 968

[12] Wanajo, S., Nomoto, K., Iwamoto, N., Ishimaru, Y., & Beers, T. C. 2004, in preparation

Neutrino-nucleus reactions in supernovae

K. Langanke[1], *A. Juodagalvis*[2], *G. Martínez-Pinedo*[3], *J.M. Sampaio*[1]

[1] *Institute for Physics and Astronomy, University of Aarhus, DK-8000 Aarhus C, Denmark*
[2] *Physics Division, Oak Ridge National Laboratory, Oak Ridge, TN 37831-6373, USA*
[3] *ICREA and Institut d'Estudis Espacials de Catalunya, Edifici Nexus, Gran Capità 2, E-08034 Barcelona, Spain*

Introductory remarks

Neutrino-induced reactions on nuclei play essential roles in various aspects of nucleosynthesis as well as supernova collapse and supernova neutrino detection [1]. Nearly all of them have not been studied experimentally so far and their cross sections, which are needed in these applications, are typically based on nuclear theory. We are interested here in processes mediated by neutrinos with energies of order tens of MeV. It turns out that the theoretical description of such reactions is a challenging proposition, since the processes are quite sensitive to nuclear structure. However, it has recently been shown that important constraints for neutrino-nucleus cross sections can be derived from high-precision electron scattering data and that the nuclear model of choice - the shell model - can be validated by these data.

Demands at the nuclear models

In the derivation of the relevant cross sections one can follow the precription given by Walecka [2] which is based on the standard current-current form for the weak interaction Hamiltonian governing these reactions and adopts a multipole expansion of the weak nuclear current. In this formalism, the nucleus is excited by multipole operators O_λ which scale like $(qR/\hbar c)^\lambda$, where R is the nuclear radius ($R \sim 1.2A^{1/3}$ fm). As the momentum transfer is of the order of the neutrino energy E_i, neutrino-nucleus reactions involve multipole operators with successively higher rank λ with increasing neutrino energy. Since the nuclear Hamiltonian does not commute with O_λ, the response of the operator is fragmented over many nuclear states. However, for each multipole most of the strength resides in a collective excitation, the giant resonance, with a width of a few MeV. The centroids of the giant resonances of the various multipoles grow in energy with increasing rank, roughly like $\lambda\hbar\omega$, where $\hbar\omega \simeq 41/A^{1/3}$ MeV is a typical energy shell splitting in the nucleus. Furthermore, since the phase space is proportional to $p_f E_f$ the higher outgoing neutrino energies E_f are preferred. This suggests that the average nuclear excitation energy $\bar{\omega}$ lags behind the increasing neutrino energy, i.e., for sufficently large neutrino energies the inequality $\bar{\omega} < E_i \simeq E_f$ holds. As a consequence, for neutrino energies significantly larger than the energies of the corresponding giant resonances, the neutrino-induced cross sections will depend on the total strength of the multipole excitation and its centroid energy, but will be less sensitive to its detailed energy distribution. Finally, at very high neutrino energies the neutrino will see the nucleus as an ensemble of independent bound nucleons and will interact with individual nucleons.

From these general considerations we can identify three different energy ranges with quite different demands on the details with which the nuclear structure should be treated:

i) For low neutrino energies, comparable with the nuclear excitation energy, neutrino-nucleus reactions are very sensitive to the appropriate description of the nuclear response, which, in turn, depends strongly on the correlations among nucleons. The model of choice is the nuclear shell model [3].

ii) The Random Phase Approximation (RPA) has been developed to describe the collective excitation of a nucleus by considering the one-particle one-hole excitations of the correlated ground state. The RPA, or its continuum version CRPA, are appropriate methods at intermediate energies (e.g. [4]) where the neutrino reactions are sensitive dominantly to the total strength and the energy centroids of the giant resonances.

iii) At high incoming energies neutrinos, like other electroweak probes, scatter 'quasi-freely' on individual nucleons. The remaining nucleons can be treated as (non-interacting) spectators. This situation is realized in the Fermi gas model [5] where a fully relativistic treatment of the hadronic weak vertex is included. The Fermi motion and the binding energy are characterized by parameters that can be determined from electron scattering experiments.

Neutrinos in and from supernovae

The dynamics of the collapse of a massive star is determined by the competition between gravity and weak-interaction processes involving the many nuclei present in the stellar core. Recently the calculation of the weak-interaction rates has been significantly improved. As discussed in the contribution by Gabriel Martínez-Pinedo, this has important consequences for the collapse and supernova simulations [6, 7]. The main result is that, in contrast to previous belief, electron capture on nuclei dominates over capture on free protons during nearly the entire collapse phase. Importantly, capture on nuclei produces neutrinos with smaller average energy than capture on free protons (mainly due to the less favorable Q values). This difference is quite important as all processes which determine the neutrino transport in the matter scale with E_f^2.

One process, so far neglected in supernova simulations, is inelastic neutral-current neutrino-nucleus scattering. In an exploratory study Sampaio *et al.* have demonstrated that, at low neutrino energies ($E_i \lesssim 10$ MeV), inelastic neutrino-nucleus cross sections can be significantly enhanced due to finite temperature effects [8]. This effect is most relevant for scattering on even-even nuclei. Based on shell-model (for the Gamow-Teller transitions) and RPA calculations (for forbidden transitions) we have thus calculated partial differential cross sections as functions of initial (E_i) and final (E_f) neutrino energies for about 60 nuclei in the iron mass range and for a temperature grid between 0.8 MeV and 2 MeV. A detailed description of the work is given in [9]. The results for the individual nuclei exist as a cross section table for a rather fine neutrino energy and temperature grid. A folding of the individual results with an NSE distribution of the nuclei, as applicable during the collapse phase, is in progress.

Selected results are shown in Figs. 1 and 2. Fig. 1 shows the inelastic neutrino-nucleus cross sections for the iron isotopes $^{52-61}$Fe as a function of initial neutrino energies ('elastic' contributions, i.e. contributions with $E_i = E_f$, are omitted in the cross sections) and for 3 typical supernova temperatures. Obviously, finite temperature effects enhance the cross sections at low neutrino energies significantly. Note that, for even-even isotopes, there would be a sizable neutrino threshold at temperature $T = 0$ as the (dominating) GT transitions can connect the $J = 0^+$ ground state only to $J = 1^+$ states which reside at excitation energies above 2-3 MeV in these nuclei. Thermal populations overcome these thresholds. As a consequence, neutrinos can also be downscattered in energy ($E_f > E_i$) at finite temperature. This can be seen in Fig. 2 which shows the normalized neutrino spectra at selected temperatures and for a few fixed initial energies. It is apparent from the figures that finite temperature effects get less important with increasing neutrino energy and can be neglected once $E_i \gtrsim 15 - 20$ MeV. This is caused by the fact that neutrinos then have sufficient energy to excite the centroid of the GT response in the nuclei which reside in the

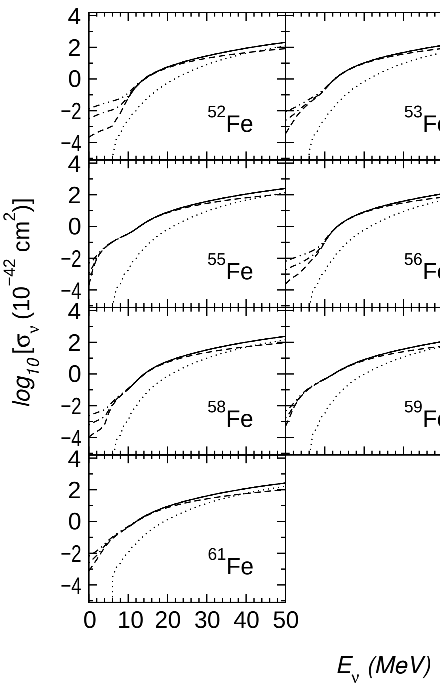

Figure 1: Neutral current neutrino-nucleus inelastic cross-sections for iron isotopes. The dashed lines show shell model contributions at three different temperatures ($T = 0.86$ MeV - dashed line, 1.29 MeV - dash-dotted line, and 1.72 MeV dash double-dotted line); the dotted line is the RPA contribution; the solid line corresponds to the total cross sections. At low neutrino energies the total cross section coincides with SM contributions.

iron isotopes at energies around $E^* \sim 8 - 11$ MeV. As, for excited states, these centroids reside at approximately the same excitation energies relative to the parent state the cross section becomes independent of temperature once the GT centroid dominates the cross sections. The figures also show the contributions of higher multipoles to the cross sections. These are no longer negligible for initial neutrino energies of order 30 MeV and dominate the cross sections for $E_i \gtrsim 40$ MeV.

Constraining neutrino-nucleus cross sections

Currently no data for inelastic neutral-current neutrino-nucleus cross sections are available for supernova-relevant nuclei ($A \sim 60$). However, as has

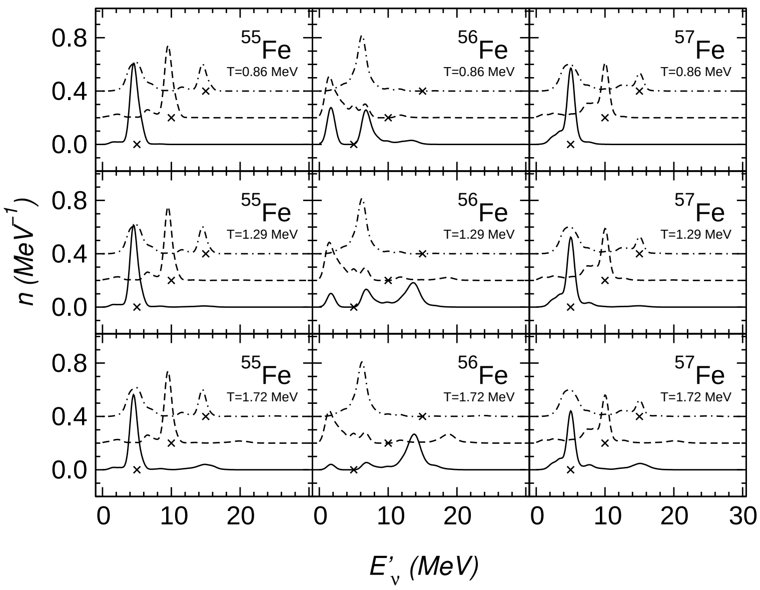

Figure 2: Normalized neutrino spectra for $^{52-57}$Fe for three temperatures ($T = 0.86$, 1.29, and 1.72 MeV) and three energies of the incoming neutrino: $E_i = 5$ MeV (solid line), 10 MeV (dashed line, all values shifted by 0.2), and 15 MeV (dash-dotted line, all values shifted by 0.4). Crosses correspond to the energy of the incoming neutrino.

been demonstrated in [10], precision M1 data, obtained by inelastic electron scattering, supply the required information about the Gamow-Teller GT_0 distribution which determines the inelastic neutrino-nucleus cross sections for supernova neutrino energies. The argumentation is built on the observation that for M1 transitions the isovector part dominates and that the spin part of the isovector M1 operator is proportional to the desired zero-component of the GT operator. Thus, experimental M1 data yield the needed GT_0 information to determine supernova neutrino-nucleus cross sections, to the extent that the isoscalar and orbital pieces present in the M1 operator can be neglected. First, it is wellknown that the major strength of the orbital and spin M1 responses are energetically well separated. Furthermore, the orbital part is strongly related to deformation and is suppressed in spherical nuclei, like ^{50}Ti, ^{52}Cr, ^{54}Fe. These nuclei have the additional advantage that M1 response data exist from high-resolution inelastic electron scattering experiments [11]. We have performed large-scale shell model calculations for the GT_0 and various parts of the M1 response in these nuclei. Satisfyingly, the shell model calculations reproduce the M1 data quite well, even in details [10]. The calculation also confirms that the orbital and isoscalar M1 strengths are much smaller than the isovector spin strength. Thus, the M1 data represent, in a good approximation, the needed GT_0 information (upto a constant factor). Fig. 3 compares the inelastic neutrino-nucleus cross sections for the 3 studied nuclei, calculated from the experimental M1 data and from the shell model GT_0 strength. The agreement is quite satisfactory. It is further improved, if one corrects for possible M1 strength outside of the explored experimental energy window. Also differential neutrino-nucleus cross sections as functions of initial and final neutrino energies, calculated from the M1 data and the shell model, agree quite well [10]. On the basis of this comparison, one can conclude that the shell model is validated for the calculations of inelastic neutral-current supernova neutrino-nucleus cross sections. This model can then also be used to calculate these cross sections at the finite temperature in the supernova environment [10, 8].

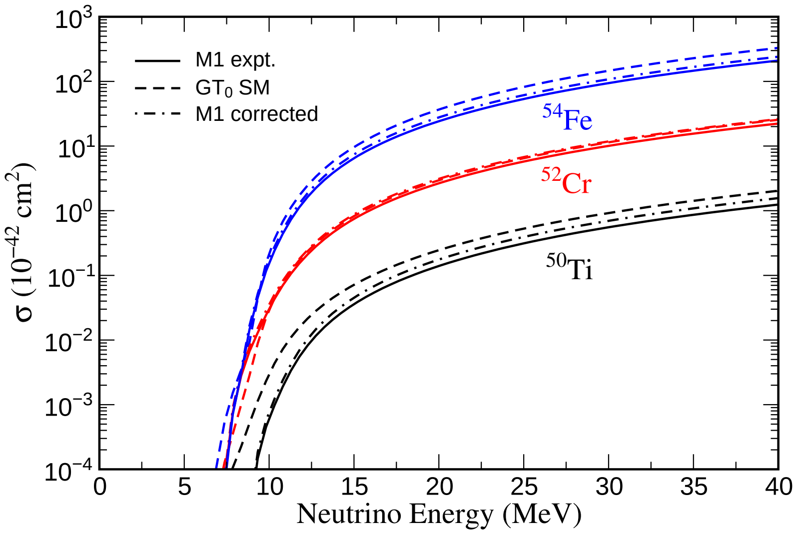

Figure 3: Neutrino-nucleus cross sections calculated from the M1 data (solid lines) and the shell-model GT_0 distributions (dotted) for ^{50}Ti (multiplied by 0.1), ^{52}Cr, and ^{54}Fe (times 10). The long-dashed lines show the cross sections from the M1 data, corrected for possible strength outside the experimental energy window.

Several astrophysical applications are not included in this manuscript, e.g. solar neutrinos and r-process nucleosynthesis. Discussion of these applications and references can be found in [12].

It is a pleasure to thank our collaborators D.J. Dean, R.W. Hix, H-.Th. Janka, M. Liebendörfer, O.B. Messer, A. Mezzacappa, P. von Neumann-Cosel and A. Richter.

References

[1] F.T. Avignone *et al.*, J. Phys. G29 (2003) 2497

[2] J.D. Walecka in *Muon Physics* eds. V.W. Hughes and C.S. Wu (Academic, New York, 1972)

[3] E. Caurier *et al.*, Rev. Mod. Phys., in print

[4] E. Kolbe *et al.*, J. Phys. **G29** (2003) 2569

[5] R.A. Smith and E. Moniz, Nucl. Phys. **B43** (1972) 605

[6] K. Langanke *et al.*, Phys. Rev. Lett. **90** (2003) 241102

[7] W.R. Hix *et al.*, Phys. Rev. Lett. **91** (2003) 201102

[8] J.M. Sampaio *et al.*, Phys. Lett. **B529** (2002) 19

[9] A. Juodagalvis *et al.*, submitted to Nucl. Phys. A

[10] K. Langanke, G. Martinez-Pinedo, P. v. Neumann-Cosel and A. Richter, submitted to Phys. Rev. Lett.

[11] P. v. Neumann-Cosel *et al.*, Phys. Lett. **B443** (1998) 1

[12] K. Langanke and G. Martinez-Pinedo, Rev. Mod. Phys. **75** (2003) 819

The role of electron captures in core-collapse supernovae

G. Martínez-Pinedo

ICREA and Institut d'Estudis Espacials de Catalunya, Edifici Nexus, Gran Capità 2, E-08034 Barcelona, Spain

Stars with masses exceeding roughly 10 $M_\odot$ reach a moment in their evolution when their iron core provides no further source of nuclear energy generation. At this time, the evolution in the core is determined by the competition of gravity, that produces the collapse of the core, and the weak interaction, that determines the rate at which electrons are captured and the rate at which neutrinos are trapped during the collapse. As the density of the star's center increases electrons become more degenerate and their chemical potential grows. For sufficiently high values of the chemical potential electrons are captured by nuclei producing neutrinos, which for densities $\lesssim 10^{11}$ g cm^{-3}, freely escape from the star, removing energy and entropy from the core. Thus entropy stays low during the collapse ensuring that nuclei dominate in the composition over free nucleons.

In current collapse simulations a very simple description of electron capture on nuclei is used. The rates are estimated using an independent particle model (IPM) that assumes pure Gamow-Teller (GT) transitions [1]. In this model GT transitions are Pauli-blocked for nuclei with $N \geq 40$ and $Z \leq 40$ [3]. These nuclei dominate the composition for densities larger than a few 10^{10} g cm^{-3}. As a result, electron capture on nuclei ceases at these densities and the capture is entirely due to free protons.

Recently, we have shown that the model currently employed for electron capture on nuclei is incorrect and that electron capture on nuclei dominates over capture on free protons [6]. The left panel of figure 1 shows that the reaction rate for electron capture on heavy nuclei ($R_h = \sum_i Y_i \lambda_i$, where the sum runs over all the nuclei present and Y_i denotes the number abundance of species i determined assuming Nuclear Statistical Equilibrium) dominates over the one of protons ($R_p = Y_p \lambda_p$) by roughly an order of magnitude throughout the collapse.

Electron capture on nuclei and on free protons differ quite noticeably in the neutrino spectra they generate. The right panel of figure 1 shows that neutrinos produced by captures on nuclei have a mean energy 40–60% smaller than those produced by captures on protons (mainly due to the larger Q-value for capture on nuclei). Despite that, the total neutrino energy loss rate is larger when electron capture on nuclei is considered, caused by the

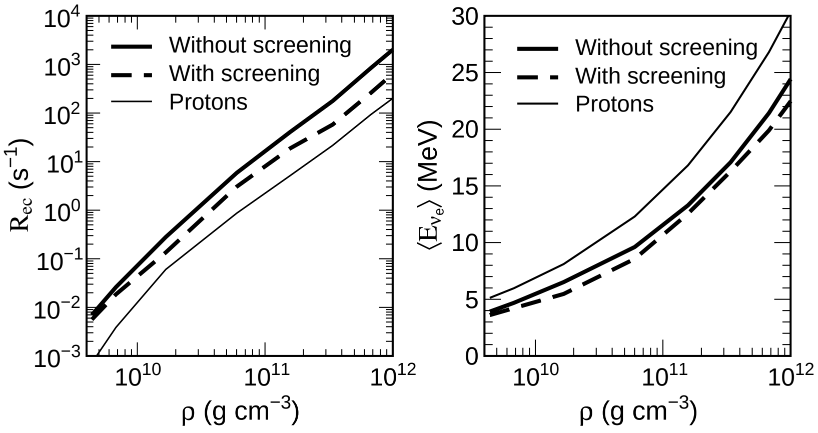

Figure 1: (left panel) The reaction rates for electron capture on protons (thin line) and nuclei (thick lines) are compared as a function of density along a stellar collapse trajectory. The solid (dashed) thick line shows the contribution of nuclei without (with) screening corrections. (right panel) The average energy of the neutrinos emitted by capture on nuclei and protons. A stellar trajectory taken from [7] is used.

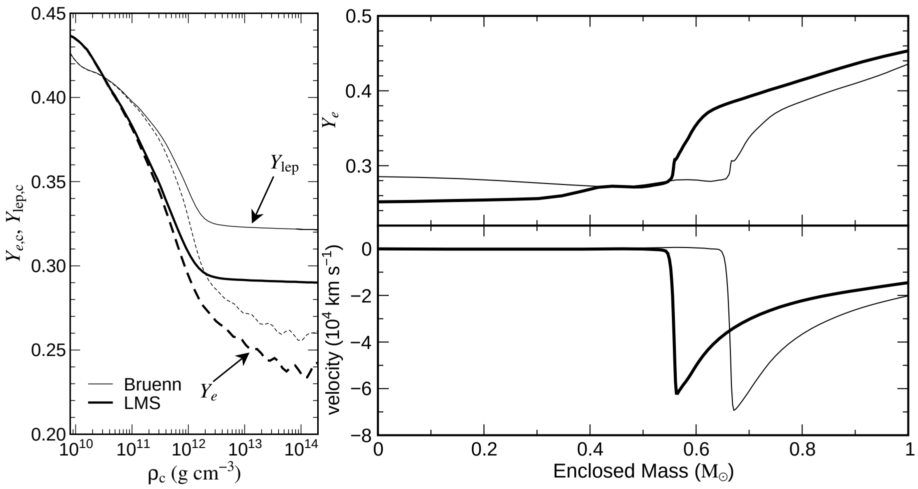

Figure 2: (left panel) Comparison of the evolution of Ye and $Y_{\rm lep}$ in the center of a 15 $M_\odot$ star. The initial presupernova model was taken from [4]. The simulations were done using an approximate General Relativistic treatment of gravity by the Garching collaboration [8] . (right panel) The electron fraction and velocity as functions of the enclosed mass at bounce for a 15 $M_\odot$ star. The simulations were done using Newtonian gravity by the Oak Ridge collaboration. In both panels, the thin line is a simulation using the Bruenn parametrization [1] while the thick line is for a simulation using the new LMSH rate set

increase in the total (nuclei plus protons) electron capture rate.

Figure 1 also shows the effect of including screening corrections in the calculation of the electron capture rates on nuclei. The rates are reduced by a factor 2–3 and the average neutrino energy by $\approx$ 1–2 MeV.

The combination of NSE abundances with electron capture rates for around 200 nuclei with A = 45–112 has been used to compute the rate of electron capture on nuclei and the emitted neutrino spectra as a function of temperature, density, and electron fraction, adequately covering the range until weak equilibrium during the collapse is achieved. This rate set will be denoted LMSH (Langanke, Martínez-Pinedo, Sampaio, and Hix) in the following. The consequences of this more realistic implementation of electron capture rates on heavy nuclei have been evaluated in independent self-consistent neutrino radiation hydrodinamics symulations by the Oak Ridge and Garching Collaborations. The left panel of figure 2 compares the evolution of Y_e and $Y_{\rm lep}$ at the center of a 15 $M_\odot$ star using the standard treatment of Bruenn [1] and the new LMSH rate set. With the improved treatment of electron capture rate on heavy nuclei, the total electron capture rate (heavy nuclei plus protons) is bigger than in the Bruen treatment resulting in smaller Y_e and $Y_{\rm lepton}$ values. The right panel shows the star profiles of several quantities obtained in collapse simulations carried out by the Oak Ridge collaboration [5] at the time of bounce. In the inner regions of the star, the additional electron capture on heavy nuclei results in more electron capture in the LMSH models that produce a reduction in Y_e and a smaller central temperature. In outer regions, where $A < 65$ nuclei dominate, the LMSH models predict less electron capture. This is so, because for these mass ranges the electron capture rates of ref. [2] are smaller than the ones used in the Bruenn parametrization [1]. Due to the smaller electron capture rates, these regions collapse more slowly so that the density and temperature are smaller in the new models. The velocity distribution shows a displacement in the minimum, which marks the eventual location of shock formation, by 0.1 $M_\odot$.

We have also study the effect of screening corrections and found that the reduction of a factor 2–3 in the electron capture rates quoted above has no appreciable effect in consistent simulations.

The results presented in this talk have been obtained in collaboration with D. J. Dean, W. R. Hix, H.-Th. Janka, K. Langanke, M. Liebendörfer, O. E. B. Messer, A. Mezzacappa, M. Rampp, J. Sampaio.

References

[1] Bruenn, S. W., 1985, ApJS, 58, 771

[2] Caurier, E., Langanke, K., Martínez-Pinedo, G., & Nowacki, F., 1999, Nucl. Phys. A, 653, 439

[3] Fuller, G. M., 1982, ApJ, 252, 741

[4] Heger, A., Langanke, K., Martínez-Pinedo, G., & Woosley, S. E., 2001, Phys. Rev. Lett., 86, 1678

[5] Hix, W. R., Messer, O. E. B., Mezzacappa, A., Liebendörfer, M., Sampaio, J., Langanke, K., Dean, D. J., & Martínez-Pinedo, G., 2003, Phys. Rev. Lett., 91, 201102

[6] Langanke, K., Martínez-Pinedo, G., Messer, O. E. B., Sampaio, J. M., Dean, D. J., Hix, W. R., Mezzacappa, A., Liebendörfer, M., Janka, H.-T., & Rampp, M., 2003, Phys. Rev. Lett., 90, 241102

[7] Mezzacappa, A., Liebendörfer, M., Bronson Messer, O. E., Raphael Hix, W., Thielemann, F.-K., & Bruenn, S. W., 2001, Phys. Rev. Lett., 86, 1935

[8] Rampp, M., & Janka, H.-T., 2002, A&A, 396, 361

Understanding Core-Collapse Supernovae

A. Burrows

Steward Observatory and the Department of Astronomy, University of Arizona, Tucson, AZ USA 85721

At the University of Arizona, we have a major effort to study core-collapse supernovae, neutrino opacities and transfer, multi-dimensional radiation hydrodynamics, pulsar kicks, and gravitational radiation from supernovae. We have developed a precision 1D (spherical) multi-group implicit Boltzmann solver, SESAME [1] [1, 2], using the Feautrier technique, with the tangent-ray method to achieve excellent angular resolution. This code provides the spherical benchmark and testbed for our multi-D efforts (e.g., VULCAN/2D, see below).

In an effort to explore non-standard effects quickly and heuristically, Thompson, Quataert, and Burrows[3] (TQB) have modified SESAME to incorporate the centrifugal effects of differential rotation in an approximate way, as well as the heating and angular momentum redistribution effects of viscosity (perhaps due to the magneto-rotational instability, MRI). The neutrino-driven mechanism is already close to explosion and requires an increase in the energy deposition rate in the "gain region" of only about 25% to 40%. TQB have shown that rapid rotation of the initial Chandrasekhar core can provide such a boost through the agencies of centrifugal support and viscous heating alone. As the explosion commences, residual neutrino cooling subsides and neutrino heating takes over, but the initial boost due to viscous heating in these calculations helped trigger explosion. They have also shown that a delayed explosion more naturally ejects high Y_e material ($\sim$ 0.5) than a prompt (never achieved in realistic simulations) or early delayed explosion. Furthermore, the larger residual core mass from which the neutron star is formed is more in keeping with larger measured pulsar masses. However, a core that explodes using a viscous boost is also rotating more rapidly than the inferred birth spin rates of known pulsars. Hence, a mechanism that sheds angular momentum during and after explosion is required. TQB show that here too the viscosity that heats the core can also lead to the diffusion of angular momentum out of the core (by a factor of $\sim$5 by the end of their calculations) on a timescale of seconds. These calculations, being spherical, are by no means definitive, and true multi-D

[1]**S**pherical, **E**xplicit/Implicit, **S**upernova, **A**lgorithm for, **M**ulti-Group/Multi-Angle, **E**xplosion Simulations

simulations, including magnetic fields, are required to answer the questions the work of TQB pose. However, these results are intriguing.

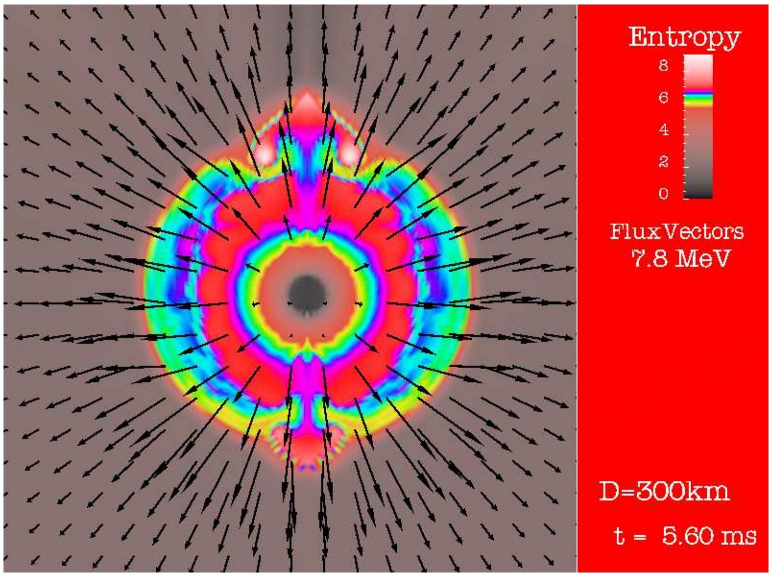

Figure 1: A snapshot 5.6 milliseconds after bounce. The 2D MGFLD variant of VULCAN/2D was used. The color map is of the entropy and the vectors are the electron-neutrino differential fluxes at 7.8 MeV. The core is not rotating, but in the beginning of the calculation it was given a modest anisotropic perturbation in the density at the north pole. The approximate scale is 300 kilometers. (Obtained in collaboration with R. Walder.)

As a biproduct, TQB have also estimated the evolution of a core's rotational profile during collapse and after bounce, i.e. the mapping between the initial and the "final" angular velocities. This study with neutrino transport complements that of Ott et al.[4] without neutrino transport (which nevertheless explored a wide range of initial conditions).

As TQB show, a useful criterion for explosion is that the timescale (τ_{adv}) for matter to flow from the stalled shock into the cooling region near the neutrinosphere is larger than the characteristic heating timescale (τ_H). This criterion is loosely equivalent to the L_ν vs. $\dot{M}$ criterion of Burrows & Goshy[5]. For a given $\dot{M}$, there is a threshold L_ν, above which explosion ensues. That threshold is lower in 2D/3D than in 1D. In 1D, τ_{adv} is too small and matter settles onto the core before sufficient heat is deposited by the neutrinos. However, as shown by Burrows, Hayes, & Fryxell[6] (BHF), Herant et al.[7], and Janka and Müller[8], in 2D with the neutrino-driven overturning insta-

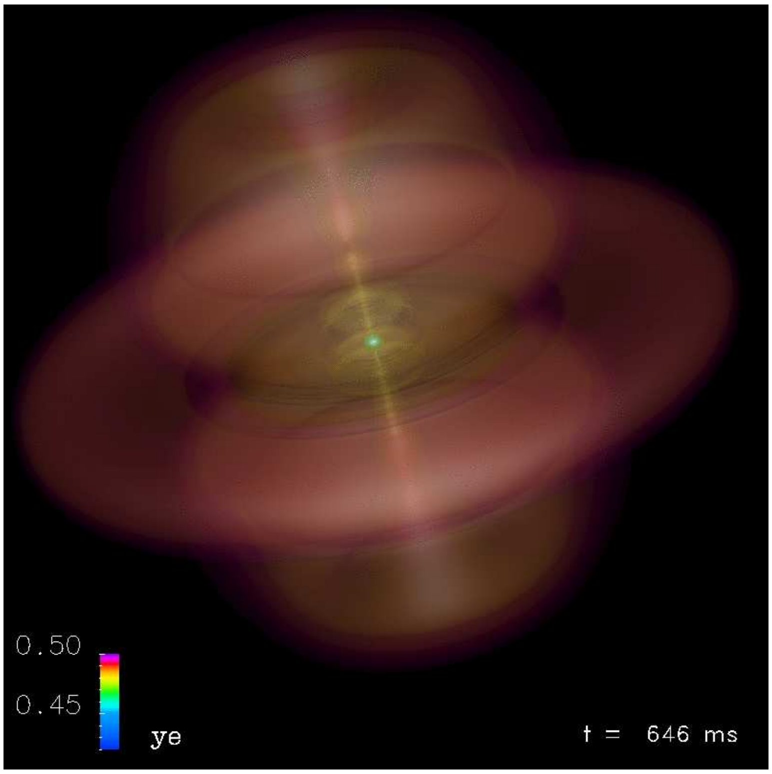

Figure 2: A snapshot after bounce of a calculation of a 20 $M_\odot$ model with rotation. The surfaces are nested isodensity shells and the approximate scale is 600 kilometers. Funnels due to an emerging centrifugal barrier are clearly seen along the poles, as is an equatorial bulge. (Obtained in collaboration with C. Ott and R. Walder.)

bility and convective motions behind the stalled shock enabled, τ_{adv} can be larger than τ_H. The swirling motions keep the matter in the gain region longer, increasing τ_{adv}. As a result, the 2D calculations of BHF and Herant et al., without rotation, led to explosions. Note that if matter did not settle onto the core at all, or if the cooling rates near the neutrinospheres interior to the gain region were low, explosion by neutrino heating would naturally, and trivially, result. We know how to obtain explosions. The question is whether Nature agrees.

Importantly, the results of BHF and Herant et al. were obtained using simple neutrino transfer and transport algorithms. Though they may have been substantially correct, it is thought that better calculations of the neutrino-matter coupling, particularly in the semi-transparent gain region, are required to falsify and/or check the convective neutrino-driven mechanism of explosion that I, for one, think obtains. Hence, a number of groups (for instance, at Arizona, MPA, and ORNL) are developing more sophisticated multi-dimensional, multi-group neutrino transfer schemes and in the next few years we should be able to make a much more detailed assessment of this mechanism.

In this spirit, we [9] have developed the code "VULCAN/2D" and are testing it in full Boltzmann and MGFLD modes. Figure 1 provides a snapshot in a 2D MGFLD run of the electron neutrino flux vector field at 7.8 MeV, superposed on an entropy color map. VULCAN/2D is an ALE code with remapping that implicitly solves the 6-dimensional problem (1(time) + 2(space) + 2(angles) + 1(energy-group)) using the S_n method to tile angular space. It is parallelized using MPI, is flux-conserving, and smoothly matches to the diffusion regime, but does not include the Doppler and aberration velocity terms. The former is important, particularly around bounce and will be included explicitly in operator-split fashion in a later version. However, the achievement of the current VULCAN/2D is a milestone, being the first such time-dependent code available in core-collapse studies with truly "2D", as opposed to ray-by-ray or only spherical, capability. Ray-by-ray codes, such as used by BHF, Rampp & Janka[10], and Buras et al.[11], can exaggerate the variation in the neutrino energy density and flux with angle by as much as 20%-50%, with the concommitent artificial variation in the heating rates with angle. However, it is not yet known how, in the integral sense of global heat deposition, this difference might effect the mechanism itself.

Whether rotation is central to the mechanism of core-collapse supernovae is not known. As the work of BHF, Herant et al.[7], and Janka and Müller[8] suggest, it may not be. However, as TQB, Ott et al.[4], and Fryer & Heger[12] demonstrate, rotation (naturally amplified during collapse and compaction) introduces interesting new phenomena. In addition to decreasing the effective gravity against which the explosion must emerge, enlarging the gain region, and generating funnels along the poles through which an explosion can more easily pierce[13], stars do in fact rotate. Unfortunately, how much the Chandrasekhar core rotates just before collapse is currently a mystery. An example of such post-bounce funnel structures is given in Fig. 2. (I refer the reader to the bi-polar structure that HST has revealed in SN1987A.) Therefore, the consequences of the fact of rotation, and the possible synergistic effects with magnetic fields[3, 14], deserve further scrutiny in the context of the neutrino-driven paradigm of core-collapse supernova explosions.

Acknowledgements

I am happy to acknowledge collaboration with Rolf Walder, Christian Ott, Eli Livne, Todd Thompson, Itamar Lichtenstadt, and Jeremiah Murphy on various of the topics mentioned in this abstract. Support for this work is provided in part by the SciDAC program of the US DOE, grant number DE-FC02-01ER41184.

References

[1] A. Burrows, T. Young, P. Pinto, R. Eastman, & T.A. Thompson, *Ap. J.* **539** (2000) 865.

[2] T.A. Thompson, A. Burrows, & P.A. Pinto, *Ap. J.* **592** (2003) 434.

[3] T.A. Thompson, E. Quataert, & A. Burrows, submitted to *Ap. J.* (2004) (astro-ph/0403224).

[4] C. Ott, A. Burrows, E. Livne, & R. Walder, *Ap. J.* **600** (2004) 834.

[5] A. Burrows & J. Goshy, *Ap. J.* **416** (1993) L75.

[6] A. Burrows, J. Hayes, & B.A. Fryxell, *Ap. J.* **450** (1995) 830.

[7] M. Herant, W. Benz, W.R. Hix, C.L. Fryer, & S.A. Colgate, *Ap. J.* **435** (1994) 339.

[8] H.-Th. Janka & E. Müller, *Astr. Ap.* **306** (1996) 167.

[9] E. Livne, A. Burrows, R. Walder, I. Lichtenstadt, & T.A. Thompson *Ap. J.* , July 1 (2004), in press.

[10] M. Rampp, & H.-Th. Janka, *Astr. Ap.* **396** (2002) 331.

[11] R. Buras, M. Rampp, H.-Th. Janka, & K. Kifonidis, Phys. Rev. Letters **90** (2003) 1101.

[12] C.L. Fryer & A. Heger, *Ap. J.* **541** (2000) 1033.

[13] A. Burrows, C.D. Ott, & C. Meakin, to be published in the proceedings of "3-D Signatures in Stellar Explosions: A Workshop honoring J. Craig Wheeler's 60th birthday," held June 10-13, 2003, Austin, Texas, USA.

[14] S. Akiyama, J.C. Wheeler, D.L. Meier, & I. Lichtenstadt, *Ap. J.* **584** (2003) 954.

Fifty-Nine Reasons for a Supernova to not Explode

M. Liebendörfer

CITA, University of Toronto, Toronto, Ontario M5S 3H8

"We compute the gravitational collapse of cores of massive stars through core-bounce at neutron star densities. In particular we analyze the sensitivity of the results (i.e. the question of whether or not the core bounce gives rise to a supernova explosion of the stellar envelope) with respect to details of the equation of state, neutrino emissivities in the shock region and to properties of the hydrocode. We find that in none of the cases considered is the core-bounce followed by an explosion of the stellar mantle beyond escape velocity. Although a shock always forms, it is never strong enough to accelerate matter to escape velocity. This result is independent of both the details of the equation of state and the assumptions of neutrino losses from the shocked matter". A first glance at this quote does not immediately reveal that it has been written 23 years ago (Hillebrandt & Müller 1981 [1]). One can, however, make out some very clear views. Firstly, the event is appositely called gravitational collapse of massive stars, not supernova explosion. Secondly, only neutrino emissivities in the shock region are mentioned—an adequate focus on the dominant reaction. Thirdly, with visionary marksmanship, shocks are found to *always* form, but *never* lead to explosions. And finally, neutrino *losses* (not absorptions) are scrutinized in the assumptions. But of course, this abstract was written before the suggestion has been made that neutrino heating behind the shock on a time scale of several hundred milliseconds might save the supernova with a delayed explosion mechanism [2]. However, even after the upgrade with the corresponding sophisticated neutrino transport and several input physics improvements, the past five years have still seen an impressive line of supernova models that did not reproduce explosions [3, 4, 5, 6, 7, 8]. Much time has been spent to explain why core collapse supernovae do explode as observed. Here, I review some reasons why they don't.

Reasons 1 & 2

The *electron captures* in the collapse phase stand at the beginning of the causal chain to failed prompt explosions. The condensing material pushes degenerate electrons into increasingly high energy levels from where they are likely to be absorbed on nuclei or free protons. The corresponding neutrino emission leads to deleptonization and the electron fraction decreases, limited only by the neutrino opacity. The latter is dominated by coherent scattering of neutrinos on heavy elements. The thermalization of the trapped neutrinos is important to determine at which neutrino energy the strongly energy-dependent opacities are tapped. The opacities are also affected by ion-ion correlations ([9] and references therein). Fig. 1 compares the entropy and electron fraction evolution in a preliminary simulation with this new liquid structure function to a calculation without ion-ion correlations. The differences are similar to the ones found in previous investigations [10].

After bounce at nuclear density, a pressure wave runs outward through the inner core and turns into a shock at its edge. Because the electron fraction is now low, the causally connected inner core is also small and the shock has to dissociate all material external to its edge. Within 5 ms after bounce, all kinetic energy of the shock is consumed in *nuclear dissociation* and the shock turns into a pure accretion front. Supernova modellers desperately reduced the mass of the progenitor stars (25 $M_\odot$ [1], 15 $M_\odot$ [4], 13 $M_\odot$ [6], 11 $M_\odot$ [7]), but the survival of the prompt hydrodynamic bounce-shock can even be excluded in the collapse simulation of a 9 $M_\odot$ ONeMg core (Fig. 2a). Moreover, each recent improvement in collapse physics made the situation worse: An upper limit to the enclosed mass is given by a self-regulation mechanism in the electron capture on free protons [11]. The consideration of general relativistic dynamics shifts the enclosed mass further inward by 0.1 $M_\odot$ [6], and improved electron capture rates on heavy nuclei subtract another 0.1 $M_\odot$ [12, 13].

Reasons 3 & 4

Whenever kinetic energy is left in the shock at 5 ms after bounce, an energetic neutrino burst will definitely zap it away at that time. Namely, as soon as the shock heats material at neutrino-transparent densities, *neutrino cooling* by electron and positron capture on free nucleons starts to determine the action. The accretion front is still expanding its radius because of the accumulation of shock-heated material on the protoneutron star. But before ~ 50 ms after bounce no neutrino heating is possible, because the dissipated kinetic energy at the accretion front propels the matter already to higher entropies than equilibrium in the neutrino background field. Only later, when the accretion front bounds the accumulated hot matter at a larger radius (not as deep in the gravitational potential) and when the neutrino spectra at the receding neutrinospheres have become harder (deeper in the gravitational potential), the entropy after shock passage is lower than equilibrium. At this time, infalling matter is neutrino-heated until it joins the

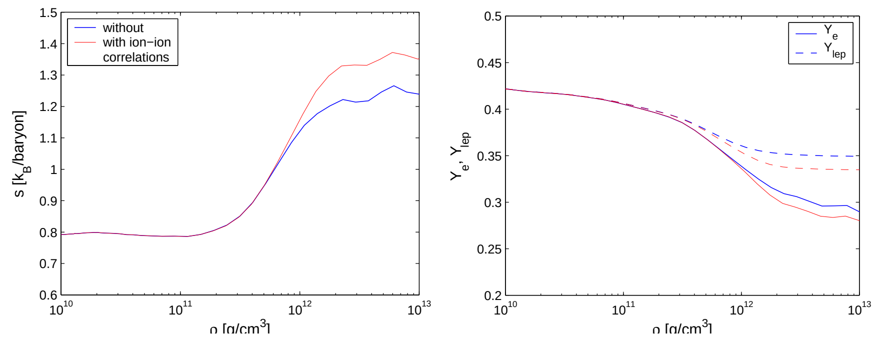

Figure 1: Above simulations with Agile-Boltztran [14] compare the entropy and electron/lepton fraction in a simulation with ion-ion correlations [9] to a simulation without ion-ion correlations. As expected, the former lead to higher entropies and lower electron/lepton fractions. More detailed comparisons between different implementations of liquid structure functions remain to be made.

equilibrium entropy at the gain radius [14]. The delicate balance between cooling and contraction at the surface of the protoneutron star and heating behind the accretion front has been analyzed in stationary [15] and dynamic [16] analytical investigations. In (Janka 2001 [16]) we read "It must be suspected that excessive neutrino emission in the cooling layer, causing mass and energy loss from the gain layer, may have been the main reason why spherically symmetric simulations ultimately failed to produce explosions."

This is clearly illustrated in a time-dependent analysis of the massflux through the heating and cooling region in the supernova simulations of Ref. [6], Fig. 7e-h. Deleptonization at the base of the cooling layers draws matter at a very *high accretion velocity* (twice as high in general relativistic simulations [5]) through the heating region such that the effective heating is small. This pessimistic view neglects that the competition between heating and cooling is positively influenced by convection in the heating region. In a convective environment, part of the energy loss by neutrino emission can be avoided by the more adiabatic expansion of local outflows [17].

Reasons 5 & 5.9

"It is important to note that one is not obliged to unbind the inner core ... as well; the explosion is a phenomenon of the outer mantle at ten times the radius ($50-200$ kilometers)" (Burrows & Thompson 2002 [18]). Indeed, e.g.

at 200 ms after bounce, more than 1.25 $M_\odot$ have been accreted, and for not too massive progenitors, the accretion rate has decreased to a fraction of a solar mass per second [14]. The nature of a supernova explosion might more suitably be characterized as a surface effect on a nascent compact object than as a dynamical consequence of core collapse. The latter is separated from the explosion by an unspectacular accretion phase. The different relevance of input physics divides these two events as well. Collapse relies on neutron-rich heavy nuclei under electron-degenerate conditions, the supernova rather involves the dynamics of dissociated nucleons in the hot mantle. At that time, many details of the collapse history are buried within the innermost solar mass and, together with some uncertainties in the high density input physics, hidden behind the neutrinospheres (the opacities at $\sim 10^{12}$ g/cm^3 are thought to be well-understood). One has to be careful, though, because this view crucially depends on the *convective stability of the protoneutron star* made out in the most sophisticated non-exploding supernova models [8]. Many explosive models relied on [19] or showed [17] vigorous protoneutron star convection. A careful investigation of this issue is very important [20].

Reason 5.9, finally, is not a real reason and therefore gets a lesser weight: *Technical difficulties* in the supernova models could also be responsible for some of the problems. The outcome of supernova simulations depends quite sensitively on details of the input physics and its numerical treatment. But from the computational point of view, it is extremely expensive to guarantee the accuracy of the neutrino transport. On the other hand, confronted with three-dimensional cosmological MHD simulations that resolve 1400 zones cubed [21], one cannot avoid thinking that it would be exciting to have a similar 3D look at a convective heating region, notabene with a resolution of a fluid element per pixel on the laptop screen. In current supernova simulations that solve the Boltzmann equation for the neutrino transport, negligible time is spent on hydrodynamics. Most additional information per invested computation time can be gained if the dimensionality of the hydrodynamics is increased until it consumes about half of the computational load. A code under development at CITA aims to enhance multidimensional hydrodynamics with a neutrino leakage scheme to locally update a spherically averaged neutrino background field in a perturbative approach. The goal is a hydrodynamically well-resolved (but neutrino-approximative) alternative for the study of the heating region, which, by choice of numerical methods, is as orthogonal as possible to the existing three-dimensional simulations in Ref. [22]. Fig. 2b shows the velocity profile in an exploratory three-dimensional test-simulation of core collapse with an equidistant resolution of 0.5 km. It uses the Lattimer-Swesty equation of state and a phenomenologically parameterized deleptonization in place of the not yet implemented neutrino physics. A decomposition of the velocity field according to [23] has been extended such that the entropy equation is solved for the smooth bulk velocity component and the total energy equation is solved for the peculiar velocity component. The purpous is to keep the condition of the fast infalling cool matter stable on the Eulerian grid while still correctly dissipating local turbulence and discontinuities into thermal energy.

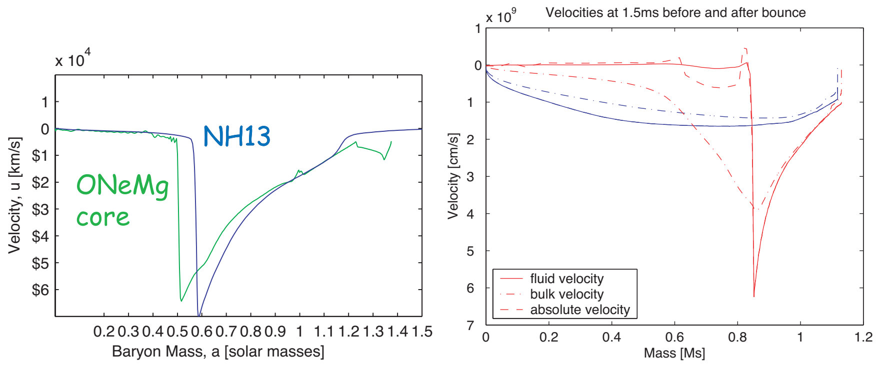

Figure 2: Both graphs show velocity profiles as a function of enclosed mass. The simulation on the left hand side with Agile-Boltztran [14] has been launched from a 13 $M_\odot$ star (NH13) and from a 9 $M_\odot$ ONeMg core [24]. In the ONeMg core, the shock forms even deeper than in the NH13 core, a prompt explosion is therefore not possible. The simulation on the right hand side shows the spherically averaged velocity profile of a 3D test-simulation based on an extended code version of [21] in two time slices around bounce. The smooth bulk velocity (dash-dotted line) and total velocity (solid line) are distinguishable. Convection becomes visible in the large absolute velocities (dashed line) behind the shock. Adequate neutrino physics remains to be implemented.

Acknowledgements

I am greatly indebted to K. Nomoto and S. Wanajo for their collaboration in the calculation of the ONeMg core; to A. Marek, M. Rampp, H.-Th. Janka, and N. Itoh for the collaboration on the ion-ion correlations; to U. Pen and C. Thompson for collaboration and discussions on multidimensional simulations; and to O. E. Messer and A. Mezzacappa for their long-lived contributions to Agile-Boltztran. The calculations have been carried out on the CITA Itanium I and McKenzie Beowulf cluster.

References

[1] W. Hillebrandt, E. Müller, A&A, **103** (1981) 358.

[2] H. A. Bethe, J. R. Wilson, ApJ, **295** (1985) 14.

[3] A. Mezzacappa, A. C. Calder, S. W. Bruenn, J. M. Blondin, M. W. Guidry, M. R. Strayer, A. S. Umar, ApJ, **495** (1998) 911.

[4] M. Rampp, H.-T. Janka, ApJ, **539L** (2000) 33.

[5] S. W. Bruenn, K. R. DeNisco, A. Mezzacappa, ApJ, **560** (2001) 326.

[6] M. Liebendörfer, A. Mezzacappa, F.-K. Thielemann, O. E. B. Messer, W. R. Hix, S. W. Bruenn, Phys. Rev. D, **63** (2001) 103004.

[7] T. A. Thompson, A. Burrows, P. A. Pinto, ApJ, **592** (2003) 434.

[8] R. Buras, M. Rampp, H.-T. Janka, K. Kifonidis, Phys. Rev. Lett., **90** (2003) 241101.

[9] N. Itoh, R. Asahara, N. Tomizawa, S. Wanajo, S. Nozawa, astro-ph/0401488.

[10] S. W. Bruenn, A. Mezzacappa, Phys. Rev. D, **56** (1997) 7529.

[11] O. E. B. Messer, M. Liebendörfer, W. R. Hix, A. Mezzacappa, S. W. Bruenn, in Proc. ESO/MPA/MPE Workshop, ed. W. Hillebrandt, B. Leibundgut (Springer 2003) 70.

[12] K. Langanke, G. Martinez-Pinedo, J. Sampaio, D. Dean, W. Hix, O. Messer, A. Mezzacappa, M. Liebendörfer, H.-T. Janka, M. Rampp, Phys. Rev. Lett, **90** (2003) 241102.

[13] W. R. Hix, O. E. Messer, A. Mezzacappa, M. Liebendörfer, J. Sampaio, K. Langanke, D. J. Dean, G. Martinez-Pinedo, Phys. Rev. Lett., **91** (2003) 201102.

[14] M. Liebendörfer, O. E. B. Messer, A. Mezzacappa, S. W. Bruenn, C. Y. Cardall, F.-K. Thielemann, ApJS, **150** (2004) 263.

[15] A. Burrows, J. Goshy, ApJ, **416L** (1993) 75.

[16] H.-T. Janka, A&A, **368** (2001) 527.

[17] M. Herant, W. Benz, W. R. Hix, C. L. Fryer, S. A. Colgate, ApJ, **435** (1994) 339.

[18] A. Burrows, T. A. Thompson, in Proc. ESO/MPA/MPE Workshop, ed. W. Hillebrandt, B. Leibundgut (Heidelberg, Springer 2003).

[19] J. R. Wilson, R. W. Mayle, Phys. Rep., **227** (1993) 97.

[20] S. W. Bruenn, E. A. Raley, A. Mezzacappa, astro-ph/0404099.

[21] U. Pen, P. Arras, S. Wong, ApJS, **149** (2003) 447.

[22] C. L. Fryer, M. S. Warren, ApJ, **574L** (2002) 65.

[23] H. Trac, U. Pen, New Astron., **9** (2004) 443-465.

[24] K. Nomoto, M. Hashimoto, Phys. Rep., **163** (1988) 13.

Core-Collapse Supernovae: Modeling between Pragmatism and Perfectionism

H.-Th. Janka, R. Buras, F.S. Kitaura Joyanes, A. Marek, M. Rampp

Max-Planck-Institut für Astrophysik, Karl-Schwarzschild-Str. 1, D-85741 Garching, Germany

Abstract

We briefly summarize recent efforts in Garching for modeling stellar core collapse and post-bounce evolution in one and two dimensions. The transport of neutrinos of all flavors is treated by iteratively solving the coupled system of frequency-dependent moment equations together with a model Boltzmann equation which provides the closure. A variety of progenitor stars, different nuclear equations of state, stellar rotation, and global asymmetries due to large-mode hydrodynamic instabilities have been investigated to ascertain the road to finally successful, convectively supported neutrino-driven explosions.

Methods

Our neutrino-hydrodynamic simulations were performed with a conservative, high-resolution shock-capturing scheme that employs an exact Riemann solver and integrates the hydrodynamics equations with third order accuracy in space and second order accuracy in time. This code is coupled to a neutrino transport scheme that solves the energy-dependent moment equations of neutrino number, energy, and momentum of order (v/c) by making use of a variable Eddington factor closure which is calculated from a model Boltzmann equation [1]. In addition to radial derivatives, the moment equations are supplemented by (v_θ-dependent) terms that correspond to the advection of neutrinos with fluid motions in lateral direction (with v_θ being the lateral component of the velocity vector in spherical coordinates), and the equation of motion of the stellar plasma contains also lateral gradients of the neutrino pressure [2]. General relativistic effects are taken into account approximately by (i) a generalized gravitational potential (the spherical part of which is constructed by a comparison with the Tolman-Oppenheimer-Volkoff equation, including terms due to fluid motion and neutrino effects) and (ii) relativistic redshift terms in the transport equations [1]. A comparison with a fully relativistic treatment in spherical symmetry yields very satisfactory results [3]. We have continuously modernized our treatment of neutrino interactions in the supernova medium, now including a variety of reactions and improvements (e.g., nucleon-nucleon bremsstrahlung; interactions between neutrinos of different flavors; correlations, weak magnetism and recoil in neutrino-nucleon interactions; electron captures on heavy nuclei according to recent calculations by Langanke and coworkers) in extension to the standard treatment of neutrino-matter interactions in supernova simulations (see Refs. [1, 2, 4] and the references to a long list of original papers therein).

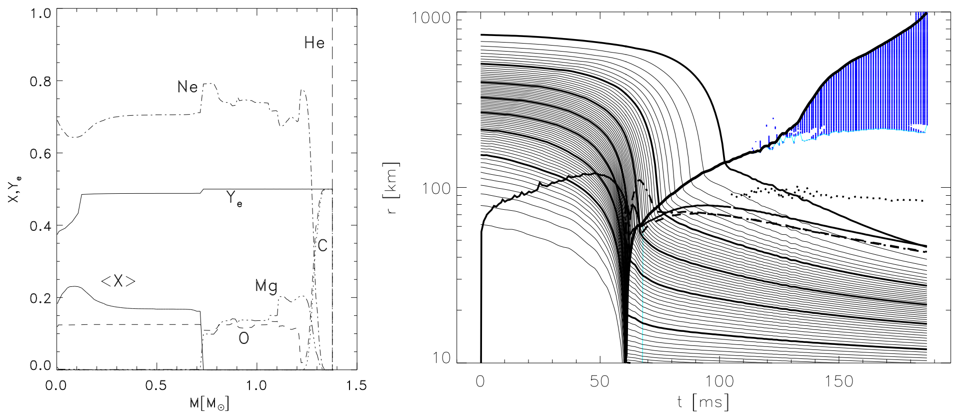

Figure 1: *Left:* Composition in the highly degenerate $1.38\,M_\odot$ core of an 8–10 $M_\odot$ progenitor [6] with O, Ne and Mg in the central region enclosed by an C-O shell. $\langle X\rangle$ denotes the mass fraction of a representative neutron-rich heavy nucleus that appears in nuclear statistical equilibrium, and Y_e is the electron fraction. *Right:* Mass trajectories, shock position (thick solid line that rises to the upper right corner of the plot, where it reaches the surface of the C-O shell), and neutrinospheres (ν_e: solid; $\bar{\nu}_e$: dash-dotted; ν_μ, $\bar{\nu}_\mu$, ν_τ, $\bar{\nu}_\tau$: dashed), and gain radius (dotted) for the collapsing O-Ne-Mg core. The mass trajectories are equidistantly spaced with intervals of $0.01\,M_\odot$. The (blue) hatched region is characterized by a dominant mass fraction of He. (The plots were taken from Ref. [7].)

Results

In the past two years we have applied our new neutrino-hydrodynamics code to core-collapse simulations in one and two dimensions for a broad variety of progenitors, spanning the range from O-Ne-Mg cores on the low-mass end ($\sim$8–10 $M_\odot$) to 25 $M_\odot$ on the high-mass side. We have investigated different input for neutrino-matter interactions and have recently also tested

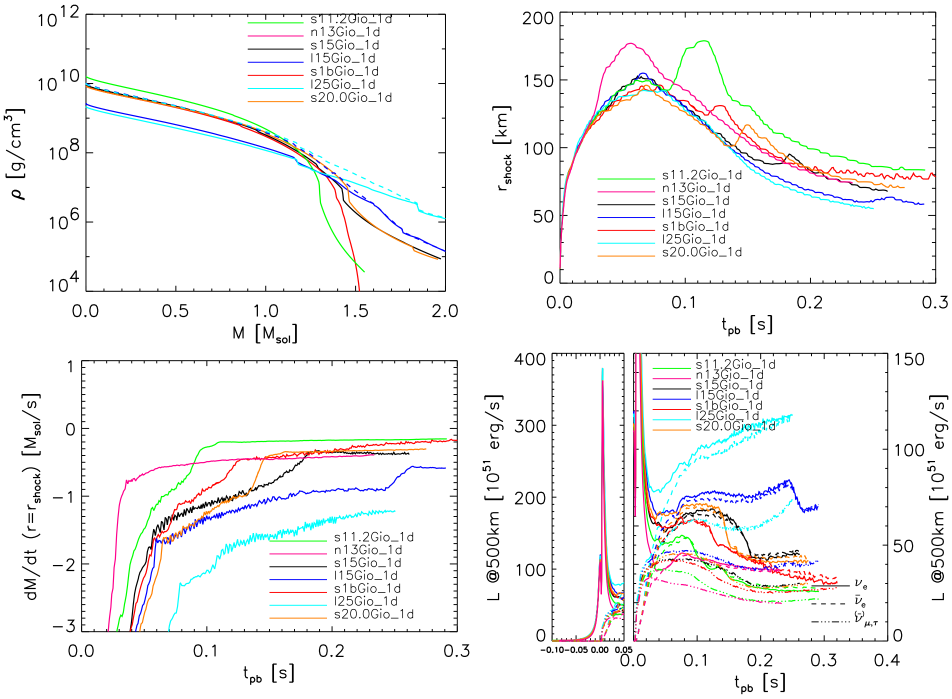

Figure 2: *Top left:* Density profiles of a sample of progenitor cores for stars with main sequence masses between 11.2 $M_\odot$ and 25 $M_\odot$ according to Ref. [13] (13 $M_\odot$, n13Gio_1d), Ref. [14] (11.2, 15, 20 $M_\odot$, s11.2Gio_1d, s15Gio_1d, s20.0Gio_1d, respectively), Ref. [15] (a Type Ib progenitor, s1bGio_1d), and Ref. [16] (15 and 25 $M_\odot$, l15Gio_1d and l25Gio_1d, respectively). The dashed lines show profiles of the latter models after we have evolved them to a central density similar to that of the other progenitors. *Top right:* Shock positions vs. time for the set of progenitors. No explosions were obtained in spherical symmetry. *Bottom left:* Mass accretion rates by the shock as functions of time. The steep density gradients at composition interfaces cause sudden drops of $|\dot{M}|$. *Bottom right:* Luminosities of ν_e (solid lines), $\bar{\nu}_e$ (dashed) and heavy-lepton ν's and $\bar{\nu}$'s (dash-dotted), measured by a comoving observer at 500 km, around the prompt ν_e burst (left panel) and during the post-bounce evolution (right panel).

the effects of different nuclear equations of state. This work was mostly done in course of the PhD Thesis of R. Buras and the Diploma Theses of F.S. Kitaura Joyanes and A. Marek. Below some main results are briefly summarized.

Explosion of an O-Ne-Mg core

The main improvement of our new simulations of O-Ne-Mg core collapse — which we did so far only in spherical symmetry — compared to previous approaches is the more accurate treatment of neutrino transport and neutrino-matter interactions. Using the nuclear equation of state (EoS) of Ref. [5], we could not confirm [7] that a prompt explosion occurs as found in calculations with simpler neutrino treatment but also with a different EoS [8]. The shock is created at a mass coordinate of $\sim 0.45\,M_\odot$ (defined by the moment when the postshock entropy first exceeds $3\,k_\mathrm{B}$ per nucleon) and stalls (defined by the time when the postshock velocity becomes negative) only 1.2 ms later at $\sim 0.8\,M_\odot$, still well inside the neutrinosphere and *before* energy losses by the prompt ν_e burst could have contributed to its damping. We also do not find the powerful shock revival by neutrino heating as seen in Ref. [9] (cf. also Ref. [10]). Instead, the shock continuously expands due to the monotonically decreasing preshock density associated with the steeply dropping density at the interface between C-O shell and He shell (Fig. 1). Towards the end of our simulation the mass accretion rate by the shock has correspondingly dropped to less than $0.03\,M_\odot\,\mathrm{s}^{-1}$. Although our simulation is not yet finally conclusive in this point, we see indications that a neutrino-driven wind begins to fill the volume between neutron star surface and shock and will lead to mass ejection with a rather low "explosion" energy and little Ni production, very similar to the outcome of simulations of accretion induced white dwarf collapse to neutron stars [11]. But the results of O-Ne-Mg core collapse can be sensitive to the properties of the nuclear EoS [12]. We plan to investigate this in future simulations.

One-dimensional core collapse for progenitors between 11 $M_\odot$ and 25 $M_\odot$

In spherical symmetry none of the investigated core collapse models, all evolved with the EoS of Lattimer and Swesty [5], developed an explosion until we stopped the simulations at typically 300 ms after bounce. This confirms the results of fully relativistic simulations by Liebendörfer et al. [17]. In spite of a rapidly dropping rate of mass accretion through the shock (Fig. 2) neutrino heating is not strong enough to reverse the postshock infall of the accreted matter, and the shock retreats in all cases, following the contraction of the neutrinosphere, after it had temporarily expanded to a maximum radius between 140 km and 180 km (Fig. 2). The latter expansion was driven by the accumulation of accreted matter between shock and neu-

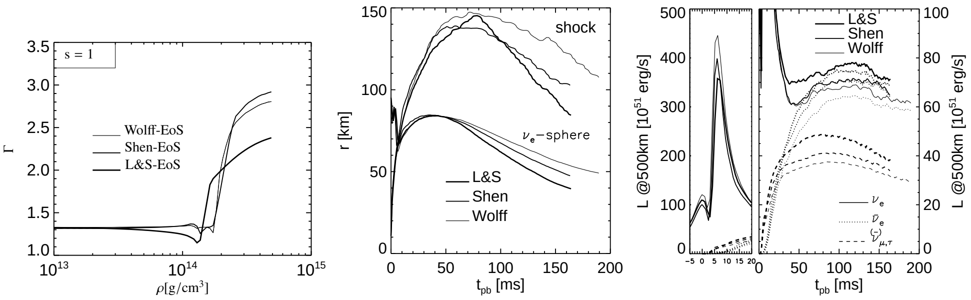

Figure 3: *Left:* Adiabatic index $\Gamma \equiv (\mathrm{d}\ln P/\mathrm{d}\ln\rho)_s$ for an entropy $s = 1\,k_{\mathrm{B}}$ per nucleon (and an electron fraction $Y_e = 0.4$) for the equations of state of Ref. [8] ("Wolff", thin lines), Ref. [23] ("Shen", medium) and Ref. [5] ("L&S", thick). *Middle:* Shock positions and neutrinospheric radii of ν_e as functions of time for collapse simulations of a $15\,M_\odot$ progenitor (Model s15a28 [20]) with the three nuclear equations of state. *Right:* Prompt ν_e burst (left panel) and post-bounce luminosities of ν_e (solid lines), $\bar{\nu}_e$ (dotted) and heavy-lepton ν's and $\bar{\nu}$'s (dashed) for the core collapse simulations of the $15\,M_\odot$ star with the three different equations of state. (The plots were taken from Ref. [24].)

trinosphere during the early post-bounce phase when the accretion rate is very high. The bumps visible in the shock trajectories (Fig. 2) correspond to the density and entropy discontinuities at the interfaces between shells of different composition, where the shock experiences a sudden drop of the mass accretion rate. Note the astonishing similarity of the prompt ν_e burst, which is a consequence of the very similar structure of the inner $\sim\!1\,M_\odot$ of the Fe core for different progenitors before collapse (Fig. 2) and the fact that the structural similarity is still present at bounce. The large luminosity differences during the post-bounce evolution are caused by model-to-model variations of the structure near and beyond the outer edge of the iron core (cf. also [18]). First core-collapse simulations of $15\,M_\odot$ and $25\,M_\odot$ progenitors with electron captures on heavy nuclei being treated according to Ref. [19] suggest that these findings also apply when electron captures on nuclei instead of free protons dominate during the infall phase.

Variations of the nuclear equation of state

For a $15\,M_\odot$ progenitor (Model s15a28 [20]) we have investigated the influence of the nuclear EoS on core collapse, shock formation, and post-bounce evolution in three different cases. We ran simulations with
(i) our standard EoS (Lattimer and Swesty, "L&S") [5], which is based on a compressible liquid drop model and employs a Skyrme force for the nu-

cleon interaction (our choice of the compressibility modulus of bulk nuclear matter is 180 MeV, and the symmetry energy parameter 29.3 MeV, but the differences in the supernova evolution caused by other values of the compressibility were shown to be minor [21, 22]);
(ii) a new relativistic mean field EoS (Shen et al., "Shen") [23] with a compressibility of nuclear matter of 281 MeV and a symmetry energy of 36.9 MeV;
(iii) an EoS that was constructed by Hartree-Fock calculations with a Skyrme force for the nucleon-nucleon interaction (Wolff and Hillebrandt, "Wolff") [8] and has a compressibility of 263 MeV and a symmetry energy of 32.9 MeV. The three equations of state show, for example, clear differences in the adiabatic index $\Gamma \equiv (\mathrm{d}\ln P/\mathrm{d}\ln\rho)_s$ around and above the phase transition to homogeneous nuclear matter (Fig. 3).

Significant differences were also found during the core-collapse calculations:
(a) in the nuclear composition of the progenitor core and during infall;
(b) in the maximum density reached at bounce, and the density in hydrostatic equilibrium afterwards;
(c) in the shock formation point, which is shifted outward by $\sim$0.05 $M_\odot$ in case of the stiffer Wolff and Shen EoSs [23, 8];
(d) in the shock stagnation point (defined by the time when the postshock velocities start to become negative), which moves out by up to $\sim$0.1 $M_\odot$ (or $\sim$10 km) for the stiffer EoSs;
(e) concerning the existence and duration of a post-bounce phase where a shell with a sizable mass fraction of heavy nuclei occurs transiently outside of the nuclear core;
(f) in the radius of maximum shock expansion and subsequent shock contraction, which closely follows the contraction behavior of the nascent neutron star (Fig. 3);
(g) in the peak luminosity during the prompt ν_e burst and the evolution of the post-bounce neutrino luminosities (Fig. 3);
(h) despite of differences in details, an application of the Ledoux criterion suggests a qualitatively similar behavior of convectively unstable regions in the neutron star and in the neutrino-heating layer.
The publication of a detailed discussion of these results is in preparation (Marek et al. 2004).

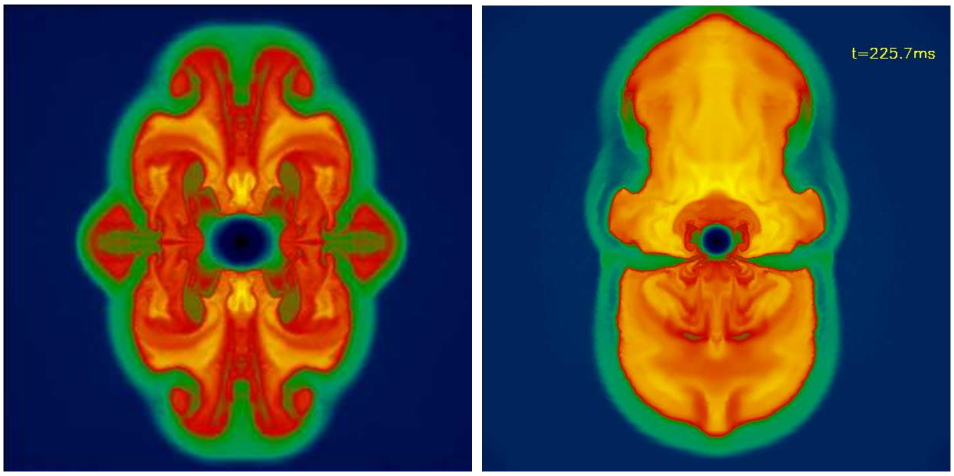

Figure 4: Snapshots of the entropy distribution at $t > 200\,\mathrm{ms}$ post bounce for two two-dimensional simulations with "Boltzmann neutrino transport" as decribed in Sect. . Yellow denotes highest entropies (around 15–25 k_{B} per nucleon), red, green, and blue ($\lesssim 8\ k_{\mathrm{B}}$ per nucleon) successively lower values. *Left:* Result at 245 ms p.b. for a $15\,M_\odot$ progenitor whose Fe core was assumed to rotate rigidly with $\Omega = 0.5\,\mathrm{rad\,s}^{-1}$ [28, 30], which is in the ballpark of predictions from stellar evolution models [31]. Equatorial symmetry was assumed. At the displayed time the shock reaches its largest expansion of nearly 300 km in the axial (in the plot vertical) direction, but lateron contracts again. *Right:* Situation in an $11.2\,M_\odot$ star at 226 ms post bounce (when the simulation had to be stopped because of shortage of computer time) [36]. The shock has reached a maximum radius of 600 km with no sign of return. Global, violent low-mode bipolar oscillations of the postshock layer, which were possible in this simulation due to a 180° grid, support a weak explosion in this *nonrotating* model. Note the significant polar to equatorial deformation.

Two-dimensional models

Convective overturn in the neutrino-heated postshock layer plays an important role during the supernova evolution and can provide the crucial push for delayed shock revival by an enhancement of the efficiency of neutrino energy transfer [25, 26, 27]. This is also seen in our recent simulations which employ a much improved treatment of neutrino transport compared to previous models. Although we found convective enhancement of shock expansion [28], we were, however, not able to confirm the successful explosions obtained in simulations with considerable approximations of the neutrino physics [29].

Rotation of the Fe core of the progenitor star, even at a moderate rate, supports strong postshock convection and brings the star much closer to an explosion by the neutrino-heating mechanism. In a simulation of a $15\,M_\odot$ progenitor we assumed the Fe core to rotate rigidly with a rate of $\Omega = 0.5\,\mathrm{rad\,s^{-1}}$ [28, 30], which is in the ballpark of results from stellar evolution calculations [31] and significantly slower than adopted in other recent works (e.g., by Burrows and collaborators [32] and Kotake et al. [33], see also their contributions to this meeting). Our rotating model showed shock expansion to a maximum radius of nearly 300 km along the rotation axis (Fig. 4, left), whereas postshock convection in the same stellar model, but without rotation, was not strong enough to drive the shock much farther out than in spherical symmetry [28].

All 2D simulations in Ref. [28], however, were computed with a lateral wedge of about 90°. In case of the rotating model, for example, equatorial symmetry was assumed. This restriction, however, constrains the possible modes of the flow pattern in the convective layer. The calculations in fact show growing power in large structures at later times after bounce, and models with a full 180° grid tend to develop a dominance of the $l = 1, 2$ modes in connection with global dipolar oscillations of the postshock layer, a phenomenon which is also seen in the three-dimensional case (cf. Refs. [34, 35] and the contribution by Scheck at this meeting). A first 2D simulation with a 180° grid and accurate neutrino transport for a (nonrotating) $11.2\,M_\odot$ star reveals a dramatic difference compared to the 90° run of this progenitor in Ref. [28]: The shock expands continuously with no sign of return until the simulation was stopped at 226 ms post bounce. At that time the expanding shock is highly deformed and has reached a polar radius of more than 600 km (Fig. 4, right). In the 90° simulation the shock was contracting again at that time [28].

Conclusions

The results reviewed above demonstrate the limits of current state-of-the-art supernova simulations but also indicate the frontiers where ultimate success might be achieved in modeling convectively supported supernova explosions. Rotation of the stellar core, even at a moderate rate, has a strong supporting influence on shock expansion. The same is true for low-mode convection and global nonradial shock instabilities, which are captured by 2D simulations only in case of a full 180° grid and sufficient resolution to follow the amplification of perturbations between shock and neutron star by the "advective-acoustic cycle" [37]. The incompletely known nuclear equation of state adds a component of uncertainty to the problem. Our 1D simulations with different EoSs show interesting and significant differences, but corresponding multi-dimensional simulations with accurate neutrino transport have yet to be done.

Acknowledgements

We are grateful to K. Nomoto, A. Heger, S. Woosley, and M. Limongi for providing us with their progenitor data. Supercomputer time at the John von Neumann Institute for Computing in Jülich and the Rechenzentrum Garching is acknowledged. This work was supported by the Sonderforschungsbereich 375 "Astroparticle Physics" and the Sonderforschungsbereich/Transregio 7 "Gravitational Wave Astronomy" of the Deutsche Forschungsgemeinschaft.

References

[1] M. Rampp and H.-Th. Janka, A&A **396** (2002) 361.

[2] R. Buras et al. (2004), in preparation; R. Buras, PhD Thesis, TU München (2004).

[3] M. Liebendörfer, M. Rampp, H.-Th. Janka, and A. Mezzacappa, ApJ, submitted (`astro-ph/0310662`).

[4] R. Buras, H.-Th. Janka, M.Th. Keil, G. Raffelt, and M. Rampp, ApJ **587** (2003) 320.

[5] J.M. Lattimer and F.D. Swesty, Nucl. Phys. **A535** (1991) 331; J.M. Lattimer, C.J. Pethick, D.G. Ravenhall, and D.Q. Lamb, Nucl. Phys. **A432** (1985) 646.

[6] K. Nomoto, ApJ **277** (1984) 791; ApJ **322** (1987) 206.

[7] F.S. Kitaura Joyanes, Diploma Thesis, TU München (2003).

[8] W. Hillebrandt, R.G. Wolff, and K. Nomoto, A&A **133** (1984) 175; W. Hillebrandt and R.G. Wolff, in *Nucleosynthesis: Challenges and New Developments*, W.D. Arnett and J.W. Truran (Eds.), Univ. Chicago Press (1985), p. 131.

[9] R. Mayle and J.R. Wilson, ApJ **334** (1988) 909.

[10] E. Baron, J. Cooperstein, and S. Kahana, ApJ **320** (1987) 300.

[11] S.E. Woosley and E. Baron, ApJ **391** (1992) 228.

[12] C. Fryer, W. Benz, M. Herant, and S.A. Colgate, ApJ **516** (1999) 892.

[13] K. Nomoto and M. Hashimoto, Phys. Rep. **163** (1988) 13.

[14] S.E. Woosley, A. Heger and T.A. Weaver, Rev. Mod. Phys. **74** (2002) 1015.

[15] S.E. Woosley and T.A. Weaver, ApJS **101** (1995) 181.

[16] M. Limongi, O. Straniero, and A. Chieffi, ApJS **129** (2000) 625.

[17] M. Liebendörfer, *et al.*, ApJS **150** (2004) 263.

[18] M. Liebendörfer, *et al.*, Nucl. Phys. **719** (2003) 144c.

[19] K. Langanke, *et al.*, PRL **90** (2003) 241102.

[20] A. Heger and S.E. Woosley, `http://www.stellarevolution.org`.

[21] T.A. Thompson, A. Burrows, and P.A. Pinto, ApJ **592** (2003) 434.

[22] F.D. Swesty, J.M. Lattimer, and E.S. Myra, ApJ **425** (1994) 195.

[23] H. Shen, H. Toki, K. Oyamatsu, and K. Sumiyoshi, Nucl. Phys. **A637** (1998) 435; Prog. Theor. Phys. **100** (1998) 1013.

[24] A. Marek, Diploma Thesis, TU München (2003).

[25] M. Herant, W. Benz, W.R. Hix, C.L. Fryer, and S.A. Colgate, ApJ **435** (1994) 339.

[26] A. Burrows, J. Hayes, and B.A. Fryxell, ApJ **450** (1995) 830.

[27] H.-Th. Janka and E. Müller, A&A **306** (1996) 167.

[28] R. Buras, M. Rampp, H.-Th. Janka, and K. Kifonidis, PRL **90** (2003) 241101.

[29] C.L. Fryer, ApJ **522** (1999) 413; C.L. Fryer and A. Heger, ApJ **541** (2000) 1033; C.L. Fryer and M.S. Warren, ApJ **574** (2002) L65; ApJ **601** (2004) 391.

[30] E. Müller, M. Rampp, R. Buras, and H.-Th. Janka, ApJ **603** (2004) 221.

[31] A. Heger, S.E. Woosley, N. Langer, and H.C. Spruit, in *Stellar Rotation*, Proc. IAU 215 (`astro-ph/0301374`).

[32] C.D. Ott, A. Burrows, E. Livne, and R. Walder, ApJ **600** (2004) 834.

[33] K. Kotake, S. Yamada, and K. Sato, ApJ **595** (2003) 304.

[34] J.M. Blondin, A. Mezzacappa, and C. DeMarino, ApJ **584** (2003) 971.

[35] L. Scheck, T. Plewa, H.-Th. Janka, K. Kifonidis, and E. Müller, PRL **92** (2004) 011103.

[36] H.-Th. Janka, R. Buras, K. Kifonidis, A. Marek, and M. Rampp, in *Supernovae (10 Years of SN1993J)*, Proc. IAU Coll. 192 (`astro-ph/0401461`).

[37] T. Foglizzo, A&A **392** (2002) 353; T. Foglizzo and P. Galletti, in *3D Signatures in Stellar Explosions*, Proc. Workshop, Austin, Texas, June 10–13, 2003 (`astro-ph/0308534`).

Global Anisotropies in Supernova Explosions and Pulsar Recoil

L. Scheck[1], *T. Plewa*[2,3], *K. Kifonidis*[1], *H.-Th. Janka*[1], *E. Müller*[1]

[1] Max-Planck-Institut für Astrophysik, Garching, Germany
[2] Center for Astrophysical Thermonuclear Flashes, Chicago, USA
[3] Nicolaus Copernicus Astronomical Center, Warsaw, Poland

Observations show that neutron stars can have space velocities much higher than those of their progenitors. On average pulsar birth velocities are in the range of 200-500 km/s and significant fraction might move with more than 1000 km/s (see [1] and references therein). The powerful and highly variable acceleration mechanism that leads to the measured velocities is still unclear. It is possible that a recoil velocity is imparted to the neutron star by explosion asymmetries at the moment of its birth. Herant [3] suggested that an $l = 1$ mode might cause an asymmetry that is sufficiently large to explain pulsar velocities even in excess of 1000 km/s.

However, in previous simulations only anisotropies on relatively small angular scales have been found. Consequently, the neutron star kicks did not exceed 100-200 km/s (see e.g. [5]). Motivated by the hypothesis that the rapid onset of the explosion in these models did not allow the merging of small-scale anisotropies to global modes, we started to conduct a new study of about 50 two-dimensional simulations, where the explosion, based on the neutrino-heating mechanism, was triggered such that the initial expansion set in more slowly [6].

The neutron star core in these simulations was replaced by a boundary condition. In contrast to earlier simulations, we prescribed more *slowly* decaying and initially lower neutrino luminosities at this boundary. This leads to longer explosion time scales and thus gives convective structures between neutron star and shock more time to merge. Shortly after the onset of the explosion most of our models are dominated by an $l = 1$ mode of the mass distribution: Infalling stellar material is concentrated in one downflow and neutrino-heated matter rises in one bubble on the opposite side. We found highly anisotropic explosions for three different 15 solar mass progenitors. A rotating progenitor (from [2]) also developed low-mode structures.

Figure 1 displays neutron star velocities and accelerations one second after core bounce. We found neutron star velocities as high as 520 km/s with

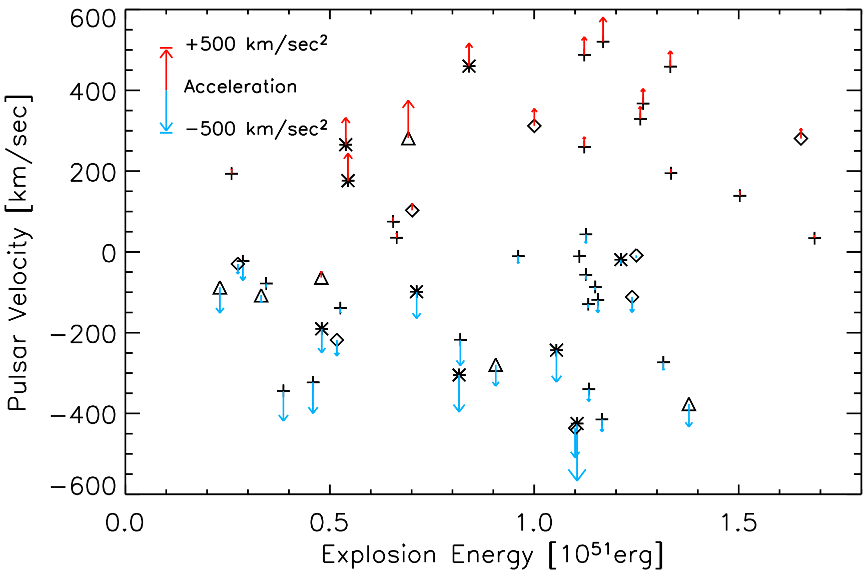

Figure 1: Neutron star velocities and accelerations at one second after core bounce for a sample of simulations [4]. Different symbols denote different progenitor stars.

still large acceleration after the first second. The final neutron star velocities can therefore be significantly higher. The dominant force that mediates the acceleration is the gravitational attraction by the anisotropic ejecta. Therefore the neutron star moves towards the most slowly expanding ejecta, opposite to the main direction of the explosion. Most of the acceleration takes place after the onset of the explosion, substantial acceleration may continue for several seconds.

It has to be shown that the merging of modes in three dimensions is as efficient as in two. A first 3D simulation with still relatively low resolution also developed an $l = 1$ mode and is therefore promising (see figure 2). Simulations with higher resolution are in progress [7].

Acknowledgements

We are grateful to K. Nomoto, A. Heger, S. Woosley, and M. Limongi for providing us with their progenitor data. Supercomputer time at the John von Neumann Institute for Computing in Jülich and the Rechenzentrum Garching is acknowledged. This work was supported by the Sonderforschungsbereich 375 "Astroparticle Physics" of the Deutsche Forschungsgemeinschaft.

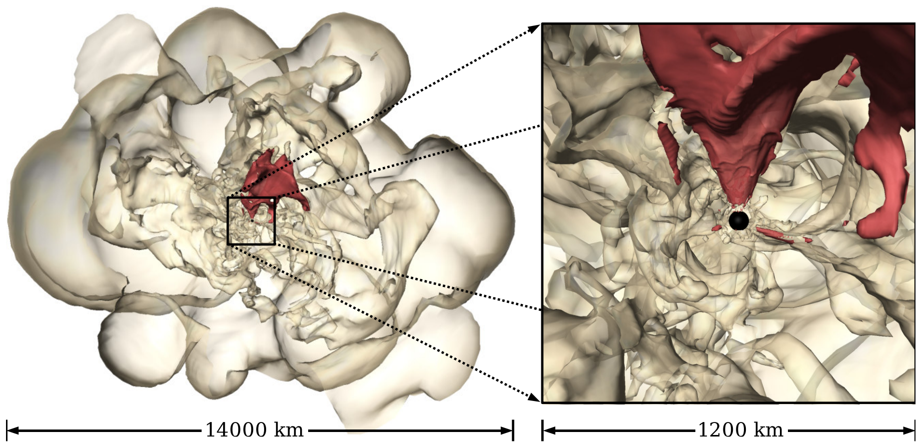

Figure 2: Three-dimensional simulation [7] one second after core bounce. The bright structure is a surface of constant proton-to-neutron ratio which roughly marks the outer boundaries of the neutrino-heated high-entropy bubbles. The dark surface, blown up in the right figure, is defined by a constant value for the mass flux per unit area and defines a downflow of matter towards the neutron star, the surface of which is indicated by the black sphere (corresponding to a density of 10^{11}g/cm^3).

References

[1] Arzoumanian, Z. and Chernoff, D. F. and Cordes, J. M. 2002, A&A, 568, 289

[2] Buras, R., Rampp, M., Janka, H.-T., & Kifonidis, K. 2003, Physical Review Letters, 90, 241101

[3] Herant, M. 1995, Phys. Rep., 256, 117

[4] Janka, H.-T. 2004, IAU Symposium 218 (astro-ph/0402200)

[5] Janka, H.-T. & Müller, E. 1996, A&A, 306, 167

[6] Scheck, L., Plewa, T., Janka, H.-T., Kifonidis, K., & Müller, E. 2004, Physical Review Letters, 92, 011103

[7] Scheck, L. 2004, PhD thesis, in preparation

Rotation and Magnetic Field in Core-Collapse Supernovae

Kei Kotake[1], *Shoichi Yamada*[2], *Katsuhiko Sato*[1,3]

[1] Department of Physics, School of Science, the University of Tokyo, 7-3-1 Hongo, Bunkyo-ku, Tokyo 113-0033, Japan
[2] Science & Engineering, Waseda University, 3-4-1 Okubo, Shinjuku, Tokyo, 169-8555, Japan
[3] Research Center for the Early Universe, School of Science, the University of Tokyo, 7-3-1 Hongo, Bunkyo-ku, Tokyo 113-0033, Japan

Anisotropic Neutrino Radiation in Rotational Core Collapse

So far there have been accumulating observations, which require the revision of the spherically symmetric stellar collapse. Spectropolarimetric observations have commonly shown a percent level of linear polarization, which may be interpreted as the asymmetry of core collapse supernovae It is also well known that SN 1987 A is globally asymmetric, which is directly observed by the *Hubble Space Telescope* [1]. Provided the facts that the progenitors of collapse-driven supernovae are a rapid rotator on the main sequence and that the recent theoretical studies suggest a fast rotating core prior to the collapse [2] (see, however, the second one of [2]), it is important to incorporate rotation in simulations of core collapse. So far there have been some works devoted to the understanding of the effect of rotation upon the supernova explosion mechanism (see [3] for the reference, see also [4] for the recent studies). It seems clear that the rotation does not good to the prompt shock propagation. This is simply because the centrifugal force tends to halt the core collapse, which then reduces the conversion of the gravitational energy to the kinetic energy. Here we pay attention to the effect of rotation on the neutrino heating mechanism. It is demonstrated that anisotropic neutrino radiations induced by rotation may be able to enhance local heating rates near the rotational axis and trigger globally asymmetric explosions [5]. The required anisotropy of the neutrino luminosity appears to be not very large ($\sim 3\%$). In their study, the anisotropy of neutrino heating was given by hand and rotation was not taken into account either. In this study, we investigate how large the anisotropy of neutrino radiation could be, based on the two dimensional rotational core collapse simulations from the onset of gravitational collapse of the core through the core bounce to the shock-stall [3]. We not only estimate the anisotropy of neutrino luminosity but also calculate local heating rates based on that. See Ref. [3] for the method of our calculations.

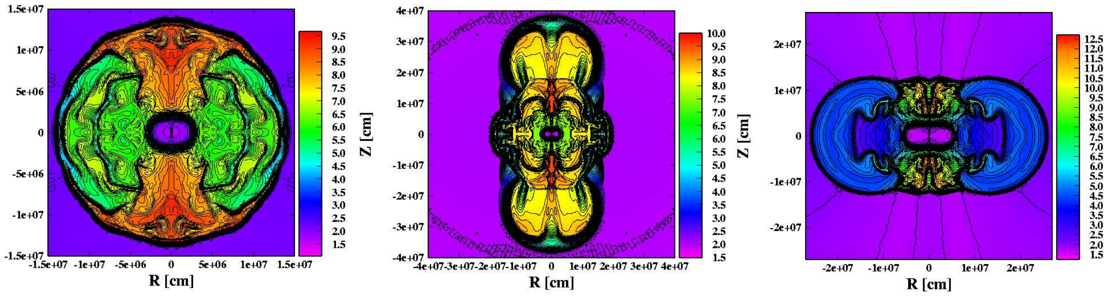

Figure 1: Final profiles of the representative models [3]. They show color-coded contour plots of entropy ($k_{\rm B}$) per nucleon. The initial value of $T/|W|$ is 0.5% for the models of the left (model A) and central panels (model B), 1.5% for the model of the right panel (model C). Here $T/|W|$ is the ratio of rotational to gravitational energy. The model of the central panel is with more differential rotation than that of the left panel.

In Figure 1, the entropy distributions at the final states for some representative models are presented. A variety of the final shapes is immediately seen in the figure. In all the models, the shock wave produced by core bounce stalls in the core and no prompt explosion occurs. As the initial rotation rate becomes larger, the shape of the stalled shock wave becomes more oblate due to the stronger centrifugal force (compare the left with right panel in Figure 1). If the initial rotation rate is the same, the shape of the stalled shock is found to be elongated in the direction of the rotational axis as the differential rotation becomes stronger (compare the left with the central panel of Figure 1). This is related with the production of high entropy blobs by core bounce. For weak differential rotations, the entropy blob formed near the rotational axis floats up parallel to the axis and then stalls. This makes the shock prolate at first. Then the matter distribution returns to be spherical or oblate due to the centrifugal forces. On the other hand, in the case of strong differential rotations, the shock wave first formed near the rotational axis hardly propagates and stalls very quickly. The high entropy blob begins to grow near the equatorial plane in this case. This then induces the flows towards the rotational axis. As a result, the final configuration becomes prolate. Based on the anisotropic matter distributions after the shock stagnation obtained by the hydrodynamic simulations, we analyze the neutrino spheres and calculate the degree of anisotropic neutrino radiation.

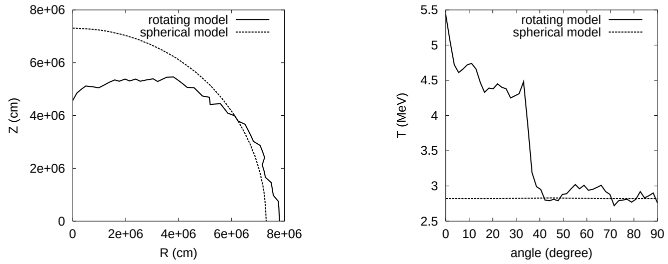

Figure 2: Shapes of neutrino sphere (left panel), neutrino temperature vs. polar angle on the neutrino sphere (right panel) for the rotating model (model A) and the spherical model.

In the left panel of Figure 2, the neutrino spheres for the spherical and the rotating model are presented. Note that the rotating model in the figure is based on the recent stellar evolution calculation [2]. For the rotating model, it is found that the neutrino sphere forms deeper inside at the pole than in the spherical model. This is a result of the fact that the density is lower on the rotational axis in the rotation models than in the spherical model because the matter tends to move away from the axis due to the centrifugal force. We note that the above features are also true for the slow and rapid rotation models. Furthermore, the configurations are more deformed from slow to rapid rotation models due to stronger centrifugal forces. The neutrino temperature profile on the neutrino sphere for the pair is presented in the right panel of Figure 2. It is seen from the figure that the temperature varies with the polar angle for the rotating model. The neutrino temperature is higher at the pole for the rotating model than for the spherical model. This can be understood from the fact that the neutrino sphere is formed deeper inside for the rotational model than that for the spherical model, as mentioned above.

Based on the neutrino sphere, we estimate the heating rates outside the neutrino sphere. We estimate the heating rate by electron neutrinos, which proceeds via the charged-current interaction: $\nu_e + n \rightarrow p + e^-$. The neutrino emission from each point on the neutrino sphere is assumed to be isotropic and take a Fermi distribution with a vanishing chemical potential. For the details about the estimation, see Ref. [3]. In Figure 3, we show

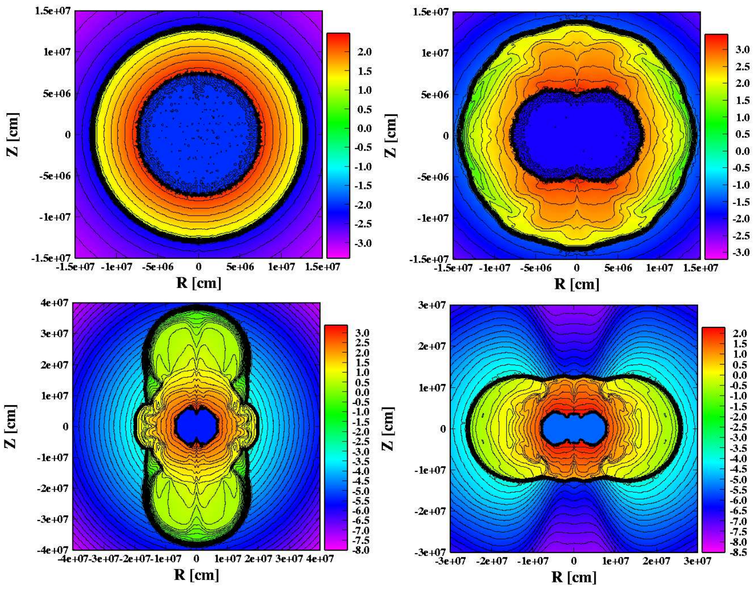

Figure 3: Heating rates outside the neutrino sphere for the spherical model (top left), the models A (top right), B (bottom left), and C (bottom right). All the figures show color-coded contour plots for the logarithm of the heating rate (MeV nucleon^{-1} s^{-1}). The neutrino sphere and the stalled shock are seen as the thick lines separating the bright color from the dark color region. Note that the value within the neutrino sphere is artificially modified to dark colors and has no physical meanings.

the contour plots of the heating rate for the spherical (top left panel) and the some representative rotation models. It is clearly seen from the figure that the neutrino heating occurs anisotropically and is strong along the rotational axis for the rotation models. This is mainly because the neutrino temperatures at the rotational axis are higher than on the equatorial plane. In addition, the radius of the neutrino sphere tends to be smaller in the vicinity of the rotational axis. As a result, the solid angle of the neutrino sphere is larger seen from the rotational axis. These two effects make the neutrino heating near the rotational axis more efficient. By performing the linear analysis for the convective stability in our models, we showed that the convective regions appear near the rotational axis (see Ref. [3]). This is because the gradient of the angular momentum is rather small near the axis and the stabilizing effect of rotation is reduced there. Together with the neutrino heating enhanced near the rotational axis, it might lead to even strong convection there later on. Then, the outcome will be a jetlike explosion considered in Ref. [5]. It should be noted that our results showed that the neutrino heating in the lateral direction is important. In order to clarify the outcome of the neutrino radiation enhanced near the pole, we are currently preparing for two dimensional radiation hydrodynamics with the elaborate neutrino transfer scheme (Kotake et al. 2004 in preparation).

Effects of the Magnetic Fields

Next we discuss the effects of the magnetic fields on the rotational collapse described above. While most of the magnetohydrodynamic (MHD) simulations in the context of core-collapse supernovae choose the poloidal magnetic fields as the initial conditions [6], recent stellar evolution calculations imply that the toroidal magnetic fields may be much stronger than the poloidal ones prior to the collapse [2]. This situation leads us to investigate the effects of the toroidal magnetic fields on the anisotropic neutrino radiation and the convection. We performed a series of the MHD core collapse simulation changing the strength of rotation and the toroidal magnetic fields systematically [7].

The angular velocity profile for the model with the strongest toroidal magnetic fields in our simulations is given in the top left panel of Figure 4. For the model, the values of initial $T/|W|$ and $E_{\rm m}/|W|$ is $0.5, 0.1\%$, respectively, where $E_{\rm m}/|W|$ represents the magnetic to gravitational energy. In addition, the initial profile of rotation and the magnetic field are taken to be cylindrical with strong differential rotation for the model. From the panel,

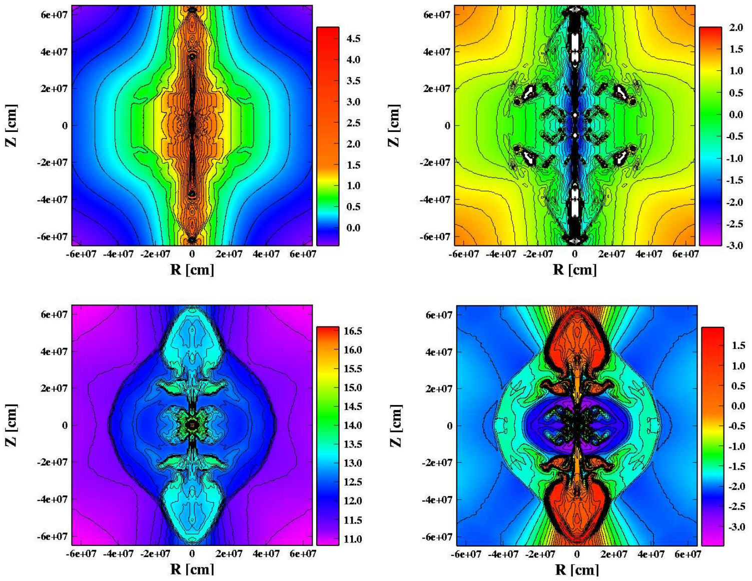

Figure 4: Contour plots of the various quantities for a model with the strongest magnetic field in our computations [7]. Top left panel shows the plot of the logarithm of the angular velocity (s^{-1}). Top right panel represents the magnetorotational unstable regions by the nonaxisymmentric perturbations, in which the contour plot show the growth time scale (s) of the MRI. Note in this panel that the region with white represents the stable regions against the MRI. Bottom left panel shows the contour plot of the logarithm of the magnetic field strength (G). Bottom right panel shows the contour of the logarithm of the ratio of the magnetic to the matter pressure in percentage.

the negative gradient of the angular velocity $d\Omega/dX < 0$ can be seen, where Ω is the angular velocity and X is the distance from the rotational axis. Such regions are known to be unstable to the nonaxisymmetric perturbation and the characteristic timescale for the growth rate of the instability is given as $\tau_{\rm MRI} = 4\pi|d\Omega/d\log X|^{-1}$ [8]. From the top right panel of Figure 4, the contour plot of the $\tau_{\rm MRI}$ for the model is given. From the panel, the timescales are found to be $\sim O(10)$ ms near the vicinity of the rotational axis. It suggests that the MRI induced by the nonaxisymmetric perturbation can grow for the prompt shock timescale. In such a model, the field strength in the protoneutron star becomes as high as $\sim 10^{16}$ G (see the bottom left panel of Figure 4), and the ratio of the magnetic to the matter pressure becomes as high as 90% behind the shock wave (see the bottom right panel of Figure 4). As for the anisotropic neutrino radiation, we find that the qualitative features obtained without the magnetic fields mentioned earlier, are not significantly changed even by the incursion of the very strong toroidal magnetic fields ($\sim 10^{16}$ G in the protoneutron star). Combining with the anisotropic neutrino radiation, which heats the matter near the rotational axis more efficiently, the growth of the instability is expected to enhance the heating rate near the axis. In addition, the magnetic pressure behind the collimated shock wave acts as strong as the matter pressure near the rotational axis. From these results, we expect that the so-called magnetar formation is accompanied by the jetlike explosion.

References

[1] L. Wang et al, Astrophys. J. **579**, 671, (2002).

[2] A. Heger, N. Langer and S.E. Woosley, Astrophys. J. **528**, 368, (2000), A. Heger, S.E. Woosley, N. Langer and H.C. Spruit, to appear in Proc. IAU 215 "Stellar Rotation" (2003).

[3] K. Kotake, S. Yamada, and K. Sato, Astrophys. J. **595**, 304, (2003).

[4] R. Buras, M. Rampp, H.-T. Janka, and K. Kifonidis, Phys. Rev. Lett. **90**, 241101,(2003), A. Burrows in this volume.

[5] T. Shimizu, T. Ebisuzaki, K. Sato, and S. Yamada, Astrophys.J. **552**, 756, (2001).

[6] J.M. LeBlanc and J.R. Wilson, Astrophys. J. **161**, 541 ,(1970), E. Müller and W. Hillebrandt, Astron. Astrophys. **80**, 147, (1979), E. Symbalisty, Astrophys.J. **285**, 729, (1984).

[7] K. Kotake, H. Sawai, S. Yamada and K. Sato, 2004 Astrophys. J. in press.

[8] S. A. Balbus and J. F. Hawley, Astrophys. J. **400**, 610, (1992), S. Akiyama, J.C. Wheeler, D.L. Meier and I. Lichtenstadt Astrophys. J. **584**, 954, (2003).

Supernova Neutrino Oscillation

Georg G. Raffelt

Max-Planck-Institut für Physik (Werner-Heisenberg-Institut)
Föhringer Ring 6, 80805 München, Germany

Neutrino oscillations are now firmly established from solar and atmospheric neutrino observations and from purely terrestrial long-baseline experiments [1]. The mass differences between the three neutrino mass eigenstates are established and the 12 and 23 mixing angles are measured to be large while only an upper limit exists for the 13 mixing angle which is thus known to be small. The absolute neutrino mass scale remains unknown; the best upper limit of about $\sum m_\nu < 1.0$ eV comes from cosmological arguments [2, 3, 4]. In future, the tritium beta decay experiment KATRIN will reach a comparable sensitivity [5], while neutrinoless double-beta decay experiments may well reveal the magnitude of the neutrino masses and their Majorana nature [6]. The magnitude of the 13 mixing angle as well as a possible CP-violating phase are to be searched at future long-baseline experiments [7]. As for the mass ordering, from matter effects in solar neutrino oscillations it is known that $m_1 < m_2$, but it is not known if $m_1 < m_2 < m_3$ (normal hierarchy) or if $m_3 < m_1 < m_2$ (inverted hierarchy). Determining this mass ordering depends on matter effects in 13 oscillations and thus requires a long baseline experiment, probably involving a future neutrino factory.

Alternatively, the mass ordering can be determined from the observation of the neutrino signal of a future galactic supernova because of resonant matter-oscillation effects in the supernova (SN) mantle and envelope [8]. One requirement to observe any oscillation effects in SN neutrinos, of course, is that the fluxes and/or spectra are different for different flavors. Our detailed studies of SN neutrino spectra formation implies that the flavor-dependent spectral differences are much less pronounced than had sometimes been claimed, but on the other hand that such differences do generically exist [9, 10, 11]. However, it will be difficult to establish the occurrence of SN neutrino oscillation simply by comparing a measured signal with theoretical predictions.

A model-independent approach is to take advantage of the Earth matter effect on the SN neutrino signal which leads to partial "regeneration," i.e. the SN oscillation effect is partly undone if the SN is shadowed by the Earth relative to the neutrino detector. If Earth effects were to be observed in the

$\bar{\nu}_e$ channel, the dominant channel in detectors such as Super-Kamiokande or IceCube, and if the 13 mixing angle has been established to be sufficiently large by other experiments ($\sin^2\theta_{13} > 10^{-3}$), then the mass hierarchy would be established to be normal. On the other hand, failing to observe Earth effects in the $\bar{\nu}_e$ channel would be ambiguous as it could be caused by the inverted hierarchy or by a smaller-than-expected flavor dependence of the SN fluxes and spectra.

The Earth effects would manifest themselves in an energy-dependent modulation of the SN neutrino signal [12, 13] or by a difference between the measured signals in a detector that measures the SN signal directly and one that measures it shadowed by the Earth [14]. In this sense Super-Kamiokande or the future Hyper-Kamiokande and IceCube are geographically complementary. In order to establish if the SN was shadowed by the Earth or not requires knowledge of its position in the sky. If the SN were obscured in all electromagnetic bands, the neutrino signal alone can reveal its position with sufficient accuracy, at least in a detector like Super-Kamiokande [15, 16].

In summary, the high-statistics neutrino observation of a future galactic SN would offer a huge scientific harvest regarding our understanding of SN physics. In addition, such a measurement could well reveal the nature of the neutrino mass hierarchy that is extremely difficult to determine in long-baseline experiments.

Acknowledgements

This work was supported, in part, by the Deutsche Forschungsgemeinschaft under grant No. SFB-375 and by the European Science Foundation (ESF) under the Network Grant No. 86 Neutrino Astrophysics.

References

[1] M. C. Gonzalez-Garcia and Y. Nir, "Neutrino masses and mixing: Evidence and implications," Rev. Mod. Phys. **75** (2003) 345 [hep-ph/0202058].

[2] S. Hannestad, "Neutrino masses and the number of neutrino species from WMAP and 2dFGRS," JCAP **0305**, 004 (2003) [astro-ph/0303076].

[3] Ø. Elgarøy and O. Lahav, "The role of priors in deriving upper limits on neutrino masses from the 2dFGRS and WMAP," JCAP **0304** (2003) 004 [astro-ph/0303089].

[4] S. Hannestad and G. Raffelt, "Cosmological mass limits on neutrinos, axions, and other light particles," hep-ph/0312154.

[5] L. Bornschein [KATRIN Collaboration], "KATRIN: Direct measurement of neutrino masses in the sub-eV region," eConf **C030626** (2003) FRAP14 [hep-ex/0309007].

[6] H. V. Klapdor-Kleingrothaus, I. V. Krivosheina, A. Dietz and O. Chkvorets, "Search for neutrinoless double beta decay with enriched Ge-76 in Gran Sasso 1990–2003," Phys. Lett. B **586** (2004) 198 [hep-ph/0404088].

[7] P. Huber, M. Lindner, M. Rolinec, T. Schwetz and W. Winter, "Prospects of accelerator and reactor neutrino oscillation experiments for the coming ten years," hep-ph/0403068.

[8] A. S. Dighe and A. Y. Smirnov, "Identifying the neutrino mass spectrum from the neutrino burst from a supernova," Phys. Rev. D **62** (2000) 033007 [hep-ph/9907423].

[9] G. G. Raffelt, "Mu- and tau-neutrino spectra formation in supernovae," Astrophys. J. **561** (2001) 890 [astro-ph/0105250].

[10] R. Buras, H. T. Janka, M. T. Keil, G. G. Raffelt and M. Rampp, "Electron-neutrino pair annihilation: A new source for muon and tau neutrinos in supernovae," Astrophys. J. **587** (2003) 320 [astro-ph/0205006].

[11] M. T. Keil, G. G. Raffelt and H. T. Janka, "Monte Carlo study of supernova neutrino spectra formation," Astrophys. J. **590** (2003) 971 [astro-ph/0208035].

[12] A. S. Dighe, M. T. Keil and G. G. Raffelt, "Identifying earth matter effects on supernova neutrinos at a single detector," JCAP **0306** (2003) 006 [hep-ph/0304150].

[13] A. S. Dighe, M. Kachelriess, G. G. Raffelt and R. Tomàs, "Signatures of supernova neutrino oscillations in the earth mantle and core," JCAP **0401** (2004) 004 [hep-ph/0311172].

[14] A. S. Dighe, M. T. Keil and G. G. Raffelt, "Detecting the neutrino mass hierarchy with a supernova at IceCube," JCAP **0306** (2003) 005 [hep-ph/0303210].

[15] J. F. Beacom and P. Vogel, "Can a supernova be located by its neutrinos?," Phys. Rev. D **60** (1999) 033007 [astro-ph/9811350].

[16] R. Tomàs, D. Semikoz, G. G. Raffelt, M. Kachelriess and A. S. Dighe, "Supernova pointing with low- and high-energy neutrino detectors," Phys. Rev. D **68** (2003) 093013 [hep-ph/0307050].

Explosive Nucleosynthesis Associated with Formation of Jet-induced Gamma-Ray Bursts in Massive Stars

A. Mizuta[1], *S. Nagataki*[2], *S. Yamada*[3], *H. Takabe*[1], *K. Sato*[4]

[1] Institute of Laser Engineering, Osaka University, JAPAN
[2] Yukawa Institute for Theoretical Physics, Kyoto University, JAPAN
[3] Science and Engineering, Waseda University, Okubo 3-4-1, Shinjyuku, Tokyo 169-8555, Japan
[4] Research Center for the Early Universe, University of Tokyo, Tokyo 113-0033, JAPAN

Abstract

We investigate explosive nucleosynthesis of collapsar model using two-dimensional relativistic hydrodynamic simulations assuming that nucleosynthesis mainly occurs in the ejecta. We concentrate the density structure of a progenitor and energy deposition rate which should be influenced by the mechanism of the explosion and formation of the outflow. Our calculations suggest the origin of GRB980425 associated with very bright supernova SN1998bw is occurred in a very short time scale. A moderate explosion model can explain line emissions of light elements from afterglows observed in GRB011211 because of less synthesized heavy elements.

Introduction

The Gamma-ray bursts (GRBs) are well explained by the fireball model [1] although the origin of GRBs is not perfectly clear. But recent observations of GRBs and connected afterglow give us a number of information of properties of the phenomena. Especially the observations of some GRBs associated with supernovae support the model of the jets from core-collapse supenovae as the origin of GRBs. The core collapse model introduced by Woosley [2] and MacFadyen & Woosley [3] is a death of massive star. As a result, a black hole or neutron star is formed. If a progenitor is very asymmetric due to a very strong rotational effect, the explosion is also asymmetric. As a result, the outflow becomes jet-like.

GRB980425 was observed within the error box of SN1998bw (Supernova type Ic). The explosion energy is a few 10^{52} erg [4] which is a little higher than that of the normal explosion and categorized in hypernovae. The another important property of this object is that the amount of synthesized ^{56}Ni is $\sim 0.5 M_{\odot}$ which is one order greater than that of normal supernovae.

Another observational support for the core-collaps model is line emissions in some X-ray afterglows. For example, line emissions of Mg, Si, S, Ar, and Ca are observed in X-ray afterglow of GRB011211 [5] although there is some incertitudes of this observation [6].

The GRBs and afterglows show a wide variety of their properties. It may be caused by the difference of explosive properties of supernovae. We investigate explosive nucleosynthesis in the context of core-collapse SNe to derive some constrains to the explosive properties of supernovae.

Our model

We performed 2D relativistic hydrodynamic simulations of the explosion with spherical coordinate $(r - \theta)$ using our relativistic hydrodynamic code [7]. It is assumed that the progenitor has about $40 M_{\odot}$ in main sequence which is as same as that of SN1998bw [4, 8] and $\sim 16 M_{\odot}$ helium core. We evolve the $16 M_{\odot}$ helium core to have the presupernova model for the calculation of explosive nucleosynthesis. Two different progenitors which are asymmetric and spherical models are prepared as an initial condition. Keeping the radially free fall of the gas during the times that depend on the zenith angle (faster near the polar axis and slower near the equatorial axis), the asymmetric model is given. Then we have a very similar one with the model used by MacFadyen and Woosley [3]. The another model is spherical one which does not have the zenith angle dependence on the free fall time. The free fall is kept until the mass of the central black hole becomes $3 M_{\odot}$ in both models. Figure 1 shows rest mass density contours of initial conditions of both models.

When a black hole or proto-neutron star is formed in the center, an accretion disk which surrounds the compact object appears. From this a bipolar outflow emerges at the polar region due to neutrino and antineutrino annihilation. This flow should be radiation dominated and baryon less to produce a GRB. We begin our calculation at this time with thermal energy deposition in the inner most grid points. This treatment corresponds to the method taken by MacFadyen, & S. E. Woosley [3], Aloy et al. [9], and Maeda et al. [10]. The different ways for the duration to deposit the energy are investigated. One is the energy 10^{52} erg is deposited at once initially. We label the models as Ab (asymmetric) and Sb (spherical). And the other is constant energy deposition 10^{51} erg s^{-1} for 10 secs, then total amount of energy is 10^{52} erg (models Aa (asymmetric) and Sa (spherical)).

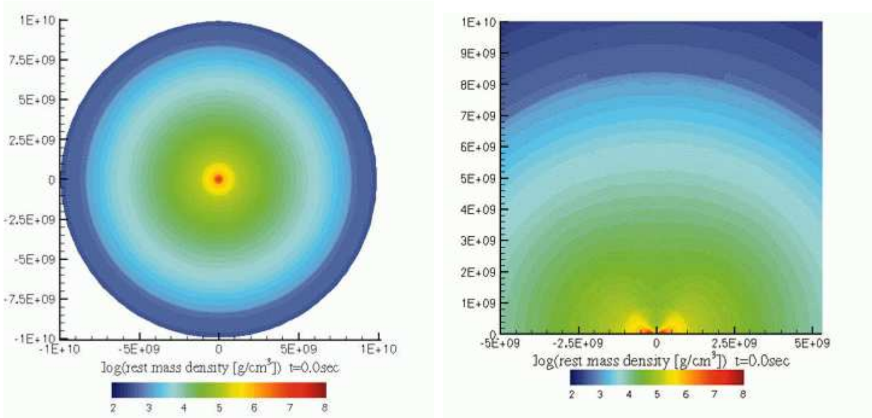

Figure 1: Mass density contours at $t = 0$. *Left*: spherical model. *Right*: asymmetric model; only the northern hemisphere is shown. The unit of a space scale is cm.

It is assumed that high Z matters are synthesized in the ejecta in this study although the nucleosynthesis may mainly occur in the accretion disk which surrounds black hole or proto-neutron star [8, 3, 11]. Nucleosynthesis is also calculated as a post processing method. We put $1 \sim 3.2 \times 10^4$ test particles around the center initially [12, 13] and record the density and temperature for the calculation of nucleosynthesis. Nuclear reaction table which is consist of 250 species by Hashimoto et al.[14] adding some species around ^{44}Ti is adopted in this study. The specific heat ratio γ is 4/3 (constant). In this study, we ignore the effects of the gravitation and rotation.

Results and Discussion

Figure 2 shows temperature profiles of the spherical models at $t = 5.0$ sec; Sa (left) and Sb (right). The speed of the shock wave is faster in the model Sb because large explosion energy is deposited at once. As the deposited internal energy is converted to kinetic one effectively in model Sb, a strong shock propagates in the progenitor. As a result, in model Sb, the large area in which the temperature exceeds 5×10^9 K is kept for longer period than that of case Sa.

Same properties are observed in asymmetric models. Figure 3 shows as same as Fig.2 but in the cases of model Aa (left) and Ab (right). The outflow exhibits jet-like structure because there is a kind of wall to the equatorial

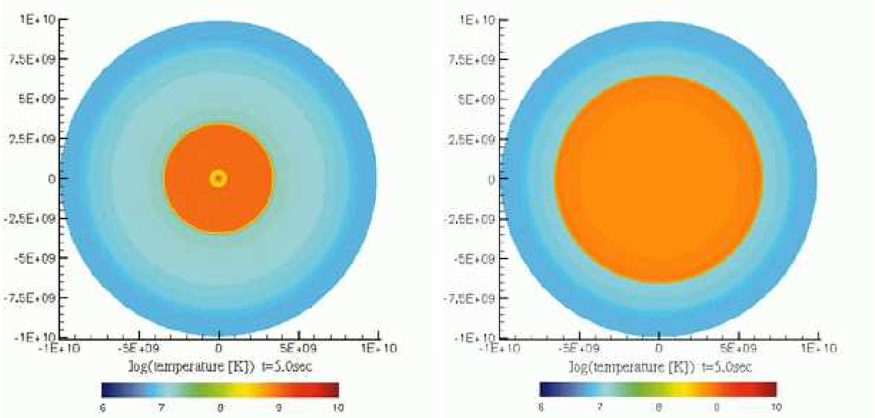

Figure 2: Temperature contours at $t = 5.0$ sec. *Left* model Sa. *Right* model Sb. The unit of a space scale is cm.

axis.

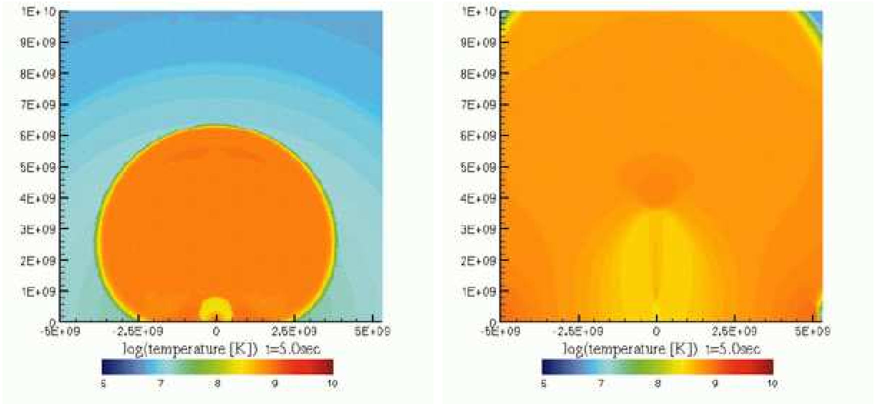

Figure 3: Temperature contours at $t = 5.0$ sec. *Right* model Sa. *Left* model Sb. Only the northern hemisphere is shown. The unit of a space scale is cm.

Table 1 shows derived synthesized elements of all models. The main difference can be seen between different energy deposition rates. This is quite natural because the particles in the models Sb and Ab experience enough high temperature to synthesize the heavy elements for longer period and the number of them is so much. There is no substantial difference between spherical and asymmetric models. We observed the region where nucle-

Table 2: Abundance of heavy elements in the ejecta for each model in units of $M_\odot$. All unstable nuclei produced in the ejecta are assumed to decay to the corresponding stable nuclei. The amount of ^{56}Ni is also shown in the last row.

Element	Model Sa	Model Sb	Model Aa	Model Ab
O	9.3E+0	8.8E+0	9.1E+0	8.5E+0
Mg	5.4E-1	5.0E-1	5.3E-1	4.9E-1
Si	2.4E-1	3.8E-1	2.4E-1	3.1E-1
S	3.3E-2	1.2E-1	3.4E-2	9.0E-2
Ar	6.6E-3	2.4E-2	7.7E-3	1.8E-2
Ca	4.5E-3	1.9E-2	5.6E-3	1.7E-2
Ti	1.2E-5	9.4E-4	8.3E-6	1.0E-3
Fe	1.4E-2	3.1E-1	8.0E-2	3.7E-1
^{56}Ni	6.1E-3	1.4E-1	2.7E-2	1.6E-1

osynthesis mainly occurs around the polar region in the case of asymmetric models.

These results suggest that a suddenly energy deposition is necessary for SN1998bw to explain the observed rich ^{56}Ni if ^{56}Ni is synthesized in the ejecta. On the contrary, there is a possibility to synthesize less heavy elements even if the explosion energy is very high $\sim 10^{52}$ erg. This explosion may correspond to the case of GRB011211 which had an afterglow with lime emissions of Mg, Si, S, Ar, Ca because our calculation shows less synthesized heavy metals in the case of model Sa and Aa.

Summary

Hydrodynamic calculations of the explosion in which total explosive energy is fixed to be 10^{52} erg are shown. Two types of initial density profile of the progenitor such as spherical and asymmetric models and two types energy deposition ways such as quick and moderate one are studied. Thus totally four cases are shown in this paper. The shock velocity is faster for the cases of the quick energy deposition and slower for the cases of the moderate energy deposition. The outflow becomes jet-like if the progenitor is asymmetric. Assuming nucleosynthesis mainly occurs in the outflow, the calculation of nucleosynthesis is also shown. A large amount of ^{56}Ni is synthesized for the cases of the quick energy deposition because the large explosive energy can

be converted to thermal energy by a strong shock effectively. But there is less dependence on the density structure of the progenitor.

Our results suggest that the explosive properties of hypernova SN1998bw which associate with GRB980425 can be explained by the quick formation of the outflow. The energy deposition rate may have some relations with observed duration of gamma-rays.

Acknowledgements

Hydrodynamic calculations are carried out on SX5 System at Cybermedia Center in Osaka University. A.M. acknowledges financial support by Japan Society for the Promotion of Science fellowship. This research has been supported in part by grants-in-aid by the Ministry of Education, Culture, Sports, Science and Technology of Japan (S14079202, S14102004, and S14740166).

References

[1] P. Meszaros, & M. J. Rees, ApJ **476** (1997) 232.

[2] S. E. Woosley, ApJ **405** (1993) 273.

[3] A. I. MacFadyen, & S. E. Woosley, ApJ **524** (1999) 262.

[4] K. Iwamoto, et al., Nature **395** (1998) 672.

[5] J. N. Reeves et al., A&A **403** (2003) 463.

[6] R. E. Rutledge & Sako M., MNRAS **339** (2003) 600.

[7] A. Mizuta, S. Yamada, & H. Takabe, ApJ **606** (2004) 804.

[8] S. E. Woosley, R. G. Eastman, & B. P. Schmidt, ApJ **516** (1999) 788.

[9] M. A. Aloy et al., ApJ **531** (1999) L119.

[10] K. Maeda et al., ApJ **565** (2002) 405.

[11] J. Pruet, S. E. Woosley, & R. D. Hoffman, ApJ **586** (2003) 1254.

[12] S. Nagataki, M. Hashimoto, K. Sato, & S. Yamada, ApJ **486** (1997) 1026.

[13] S. Nagataki, T. M. Shimizu, & K. Sato, ApJ **495** (1998) 413.

[14] M. Hashimoto, K. Nomoto, & T. Shigeyama, A&A **210** (1989) L5.

Towards gravitational wave signals from realistic core collapse supernova models

E. Müller[1], *M. Rampp*[1], *R. Buras*[1], *H.-T. Janka*[1], *D. H. Shoemaker*[2]

[1]Max-Planck-Institut für Astrophysik, Karl-Schwarzschild-Str. 1, D-85740 Garching, Germany
[2]LIGO Laboratory, 175 St. Albany Street, Massachusetts Institute of Technology, Cambridge, MA 02139, USA

Abstract

We have computed the gravitational wave signal from supernova core collapse using the presently most realistic input physics available. We start from state-of-the-art progenitor models of rotating and non-rotating massive stars, and simulate the dynamics of their core collapse by integrating the equations of axisymmetric hydrodynamics together with the Boltzmann equation for the neutrino transport including an elaborate description of neutrino interactions, and a realistic equation of state. Using the Einstein quadrupole formula we compute the quadrupole wave amplitudes, the Fourier wave spectra, the amount of energy radiated in form of gravitational waves, and the signal-to-noise ratios for the LIGO I and the tuned Advanced LIGO ("LIGO II") interferometers resulting both from non-radial mass motion and anisotropic neutrino emission.

The simulations demonstrate that the dominant contribution to the gravitational-wave signal is produced by neutrino-driven convection behind the supernova shock. For stellar cores rotating at the extreme of current stellar evolution predictions, the core-bounce signal is detectable ($S/N \gtrsim 7$) with LIGO II for a supernova up to a distance of ~ 5 kpc, whereas the signal from post-shock convection is observable ($S/N \gtrsim 7$) with LIGO II up to a distance of ~ 100 kpc, and with LIGO I to a distance of ~ 5 kpc. If the core is non-rotating its gravitational wave emission can be measured with LIGO II up to a distance of ~ 15 kpc ($S/N \gtrsim 8$), while the signal from the Ledoux convection in the deleptonizing, nascent neutron star can be detected up to a distance of ~ 10 kpc ($S/N \gtrsim 8$). Both kinds of signals are generically produced by convection in any core collapse supernova.

Summary of the paper by E. Müller, M. Rampp, R. Buras, H.-Th. Janka, and D.H. Shoemaker, 2004, *Astrophysical Journal* **603**, 221-230.